AFGL-TR-88-0280

AN ASSESSMENT OF THE APPLICATION OF *IN SITU* ION-DENSITY DATA FROM DMSP TO MODELING OF TRANSIONOSPHERIC SCINTILLATION

AD-A202 415

James A. Secan
Robert M. Bussey
Northwest Research Associates, Inc.
P.O. Box 3027
Bellevue, Washington 98009

15 September 1988
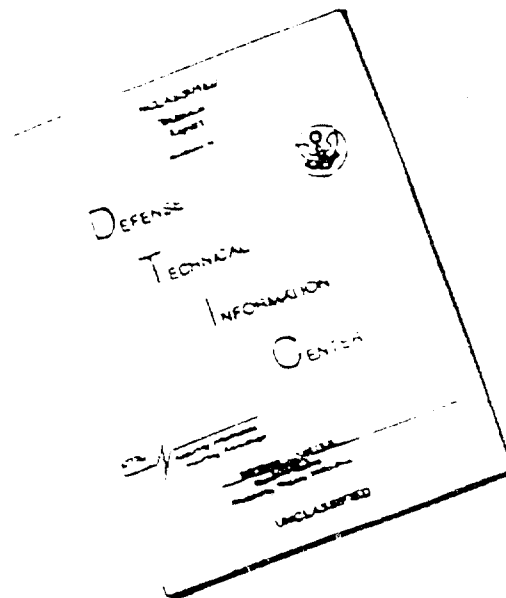
Scientific Report No. 2

Prepared for:

AIR FORCE GEOPHYSICS LABORATORY
AIR FORCE SYSTEMS COMMAND
UNITED STATES AIR FORCE
HANSCOM AFB, MASSACHUSETTS 01731-5000
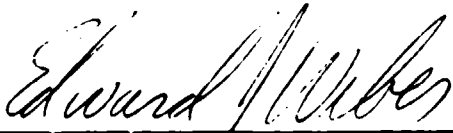
DTIC
ELECTE
DEC 1 9 1988
S   H   D

88 12 19010

DISCLAIMER NOTICE

THIS DOCUMENT IS BEST QUALITY AVAILABLE. THE COPY FURNISHED TO DTIC CONTAINED A SIGNIFICANT NUMBER OF PAGES WHICH DO NOT REPRODUCE LEGIBLY.

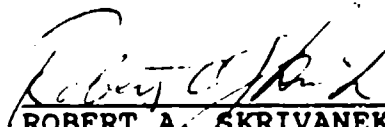"This technical report has been reviewed and is approved for publication"

EDWARD J. WEBER
Contract Manager

WILLIAM K. VICKERY
Acting Branch Chief

FOR THE COMMANDER

ROBERT A. SKRIVANEK
Division Director

REPORT DOCUMENTATION PAGE

1a. REPORT SECURITY CLASSIFICATION	1b. RESTRICTIVE MARKINGS
Unclassified	

2a. SECURITY CLASSIFICATION AUTHORITY	3. DISTRIBUTION/AVAILABILITY OF REPORT
	Approved for public release.
2b. DECLASSIFICATION/DOWNGRADING SCHEDULE	Distribution unlimited.

4. PERFORMING ORGANIZATION REPORT NUMBER(S)	5. MONITORING ORGANIZATION REPORT NUMBER(S)
NWRA-CR-88-R031	AFGL-TR-88-0280

6a. NAME OF PERFORMING ORGANIZATION	6b. OFFICE SYMBOL (If applicable)	7a. NAME OF MONITORING ORGANIZATION
Northwest Research Associates, Inc.	CR	Air Force Geophysics Laboratory

6c. ADDRESS (City, State, and ZIP Code)	7b. ADDRESS (City, State, and ZIP Code)
P.O. Box 3027 Bellevue, WA 98009	Hanscom AFB, MA 01731

8a. NAME OF FUNDING/SPONSORING ORGANIZATION	8b OFFICE SYMBOL (If applicable)	9. PROCUREMENT INSTRUMENT IDENTIFICATION NUMBER
		F19628-86-C-0195

8c. ADDRESS (City, State, and ZIP Code)	10. SOURCE OF FUNDING NUMBERS			
	PROGRAM ELEMENT NO.	PROJECT NO.	TASK NO.	WORK UNIT ACCESSION NO.
	62101F	4643	09	AI

11. TITLE (Include Security Classification)
An Assessment of the Application of In Situ Ion-density data from DMSP to modeling of Transionospheric Scintillation

12. PERSONAL AUTHOR(S)
Secan, James A., Robert M. Bussey

13a. TYPE OF REPORT	13b. TIME COVERED	14. DATE OF REPORT (Year, Month, Day)	15. PAGE COUNT
Scientific No. 2	FROM 87Sep15 TO 88Sep14	88Sep15	86

16. SUPPLEMENTARY NOTATION

17	COSATI CODES		18. SUBJECT TERMS (Continue on reverse if necessary and identify by block number)
FIELD	GROUP	SUB-GROUP	Ionosphere, Ionsopheric Scintillation, Radiowave Scintil-
04	0		lation, Defense Meteorology Satellite Program (DMSP),
20	14		

19. ABSTRACT (Continue on reverse if necessary and identify by block number)

Modern military communication, navigation, and surveillance systems depend on reliable, noise-free transionospheric radio frequency channels. They can be severely impacted by small-scale electron density irregularities in the ionosphere which cause both phase and amplitude scintillation. Basic tools used in planning and mitigation schemes are climatological in nature and thus may greatly over- and under-estimate the effects of scintillation in a given scenario. This report describes the second year of an investigation into the feasibility of using *in situ* observations of the ionosphere from the USAF DMSP satellite to calculate esti-mates of irregularity parameters which could be used to update scintillation models in near real-time. Methods for processing DMSP Scintillation Meter (SM) data and for calculating estimates of $C_k L$ from the SM data are described. Results of the analysis of DMSP SM data from a coordinated data-collection campaign run in January 1988 are presented.

20. DISTRIBUTION/AVAILABILITY OF ABSTRACT	21. ABSTRACT SECURITY CLASSIFICATION
☐ UNCLASSIFIED/UNLIMITED ☐ SAME AS RPT ☐ DTIC USERS	Unclassified
22a. NAME OF RESPONSIBLE INDIVIDUAL	22b. TELEPHONE (Include Area Code)	22c. OFFICE SYMBOL
Edward Weber		AFGL/LIS

DD FORM 1473, 84 MAR   83 APR edition may be used until exhausted.   SECURITY CLASSIFICATION OF THIS PAGE
All other editions are obsolete.

TABLE OF CONTENTS

LIST OF FIGURES

LIST OF TABLES

PREFACE

This report describes the work completed during the second year of a three-year investigation into the feasibility of using *in-situ* observations of the ionosphere from the DMSP SSIES sensors to calculate parameters which characterize ionospheric scintillation effects. Work during this year focused on a coordinated data-collection campaign conducted in January 1988. During these campaigns, the AFGL Airborne Ionospheric Observatory (AIO) and the EISCAT radar, located in northern Norway, collected data during near-overhead passes of the DMSP F8 satellite. The results of analysis of the SSIES Scintillation Meter (SM) density data collected by F8 on those passes are presented in this report.

This work is part of a larger effort with an overall objective of providing the USAF Air Weather Service with the capability of observing ionospheric scintillations, and the plasma density irregularities which cause the scintillations, in near real-time and updating models of ionospheric scintillation with these observations.

1. Introduction

Many modern military systems used for communications, command and control, navigation, and surveillance depend on reliable and relatively noise-free transmission of radiowave signals through the earth's ionosphere. Small-scale irregularities in the ionospheric density can cause severe distortion, known as radiowave scintillation, of both the amplitude and phase of these signals. A basic tool used in estimating these effects on systems is a computer program, WBMOD, based on a single-scatter phase-screen propagation model and a number of empirical models of the global morphology of ionospheric density irregularities. An inherent weakness of WBMOD is that the irregularity models provide median estimates for parameters with large dynamic ranges, which can lead to large under- and over-estimation of the effects of the ionospheric irregularities on a system.

One solution to this problem, at least for near real-time estimates, is to update the WBMOD irregularity models with observations of the various parameters modeled. One proposed source for these observations is from the *in situ* plasma density monitor to be flown on the Defense Meteorology Satellite Program (DMSP) satellites. This study is designed to assess the applicability of this data set to real-time updates of the WBMOD models. There are two primary objectives:

(1)   Develop and refine techniques for generating estimates of parameters which characterize ionospheric scintillation from *in situ* observations of the ionospheric plasma from the DMSP SSIES sensors.

(2)   Determine if the parameters calculated from the SSIES data can be used to determine the scintillation effects on a transionospheric radiowave signal.

This report describes the results obtained during the second year of the study. The focus during this year was on collecting and processing SSIES data from the DMSP F8 satellite for two intervals in January 1988 during which the AFGL Airborne Ionospheric Observatory (AIO), an AFGL UHF-beacon scintillation monitor, and the EISCAT incoherent scatter radar were making measurements in the vicinity of Tromso, Norway.

1

2. Background

The propagation model used in the WBMOD program (based on weak-scatter phase-screen theory[1]) characterizes the ionospheric electron density irregularities which cause scintillation via eight independent parameters[2]:

(1)   a: The irregularity axial ratio along the direction of the ambient geomagnetic field.

(2)   b: The irregularity axial ratio perpendicular to the direction of the ambient geomagnetic field.

(3) δ: The angle between sheet-like irregularity structures and geomagnetic L shells.

(4) h_p: The height of the equivalent phase screen above the earth's surface.

(5) $\underline{v}_d$: The *in situ* irregularity drift velocity.

(6) α_o: The outer scale of the irregularity spectrum.

(7)   q: The slope of a power-law distribution which describes the one-dimensional power density spectrum (PDS) of the irregularities.

(8) $C_k L$: The height-integrated strength parameter.

The first three parameters (a, b, and δ) and the direction of the ambient geomagnetic field specify the propagation geometry, while the last three (α_o, q, and $C_k L$) specify the spectral characteristics of the irregularities.

It may be possible to obtain estimates for the values of three of these parameters from the DMSP SSIES sensors: $\underline{v}_d$ (from the SSIES Ion Drift Meter (DM)), and q and $C_k L$ (from the SSIES Ion Scintillation Meter (SM)). In this study, we will focus on the estimation of $C_k L$ from this data set and consider q and $\underline{v}_d$ only in terms of the effects of uncertainties in these parameters on the estimates of $C_k L$. Of the eight parameters, $C_k L$ varies the most as a function of location and time, and has the most profound effect on the accuracy of estimates of scintillation levels made by the WBMOD model.

In the phase-screen propagation theory used in WBMOD[2], the $C_k L$ parameter is actually the product of two parameters: C_k, the three-dimensional spectral "strength" of the electron density irregularities at a scale size of 1 km* (related to the structure constant used in classical turbulence theory); and L, the thickness of the irregularity layer. The models in WBMOD were obtained from analysis of phase scintillation data from the WIDEBAND and HiLat satellites, which will provide estimates of the height-integrated value of $C_k L$ rather than indepen-

---

*   The cited reference develops the theory in terms of an earlier definition of the strength parameter, C_s, which is defined at a scale size of 2π meters. It is related to C_k according to the equation $C_s = (2\pi/1000)^{q+2} C_k$.

uent measures of C_k and L. Because of this, the model was developed for C_kL rather than for C_k and L separately.

The calculation of an estimate of the C_kL parameter from topside *in situ* ion density observations requires two operations. First, an estimate of C_k at the satellite altitude is made from a finite-length time series of density measurements. Second, the estimate of C_k is converted to an estimate of C_kL in some fashion which will account for both the thickness of the irregularity layer and the variation of C_k, or $<\Delta N_e^2>$, within the layer.

The data set from which the estimates of these parameters are to be obtained will be collected by three instruments in the DMSP SSIES (Special Sensor for Ions, Electrons, and Scintillation) sensor package. This data set will contain the following *in situ* observations:

(1) High time-resolution (24 samples/sec) measurements of the ion density and measurements of the ion density irregularity PDS at high fluctuating frequencies from the Ion Scintillation Meter (SM)[3].

(2) Measurements of the horizontal and vertical cross-track ion drift velocities from the Ion Drift Meter (DM)[3].

(3) Measurements of the ion and electron temperatures, the densities of O+ and the dominant light ion (H+ or He+), and the horizontal ram ion drift velocity from the ion Retarding Potential Analyzer (RPA)[4].

The basic data of this set are the high time-resolution density data from the SM which will be used to generate estimates of the irregularity PDS. The drift velocity measurements from the DM and RPA will be used in calculating an estimate of C_k from parameters obtained from the PDS. and the other measurements from the RPA will be used in calculating C_kL from C_k.

In the first year of this project, techniques for calculating estimates of C_kL from the SSIES data set were developed, and parametric studies were conducted to determine the uncertainties in the final C_kL estimates due to uncertainties in the parameters and procedures used to calculate the estimates. Since the first SSIES sensor package was not flown until mid-1987. these studies were conducted using simulated SM density data sets and phase scintillation data from the Wideband satellite. The results of these studies were reported in Scientific Report 1 for this project[5] and will be summarized in this report where pertinent.

The second phase, which was begun during this year, will focus on how well these techniques work using data from the DMSP F8 and F9 spacecraft. There will be two investigations conducted during this phase, (1) an assessment of the validity of the basic assumptions made in order to calculate an estimate of C_kL from a C_k measurement made at altitudes of 800 to 850 km. and (2) an analysis of C_kL values calculated for selected DMSP orbits. The basis for the

first investigation will be one, or possibly more, coordinated data collection campaigns in which a wide range of near-coincident ionospheric measurements will be made in conjunction with DMSP overflights.

3. Validation of Procedures Used to Calculate q and T_1.

The two basic parameters derived from the ion density data for calculating C_kL are the slope (q) and 1Hz intercept (T_1) of a linear least-squares fit in log(frequency) and log(power spectral density (PSD)) to the power-density spectrum (PDS). In the first report for this project[5], it was found that the following procedures provided the best estimates of q and T_1:

a. Detrend the density data by removing a background trend calculated from either (1) a low-pass (Butterworth) filter on the entire data set, or (2) a quadratic least-squares fit to each 512-point data segment.

b. Window the detrended data using a 30% split-bell cosine window function.

c. Calculate an estimate of the PDS from an FFT of the detrended, windowed data.

d. Smooth the PDS estimate using a 5-point, centered smoothing function with binomial weights.

e. Calculate estimates of q and T_1 ´ ᵢ. a linear least-squares fit to log(PSD) versus log(frequency) over the frequen ge 0.2 to 7.0 Hz.

The various parameters in this processing procedure were establish by analysis of sets of simulated SM density data which had been generated for a wide range of values of q. While we were careful to not introduce any *a priori* bias into the analysis due to the way in which the simulation data sets were generated, we wanted to validate the procedures using actual observations.

The main difficulty in assessing the accuracy of the various procedures using "real" data is that the values for q and T_1 are not known. One could, however, assess the relative effects of changing various parameters in these procedures, such as the size of the window or the type of detrending, by designating the results obtained from one configuration of these parameters as "truth" and comparing the results obtained using other configurations. As there were no SSIES SM data available at the time of the initial study, a sample of phase scintillation data collected at Poker Flat, Alaska, from the Wideband satellite was used to validate these procedures. This analysis showed that the relative differences between results obtained from various parameter configurations were similar to those found in the analysis of the simulation data sets, so we were fairly confident that the selected procedures were valid.

As a final check, this validation procedure was repeated with a randomly selected sample of SSIES SM data. Figure 1 shows the raw (upper plot) and detrended (lower plot)

5
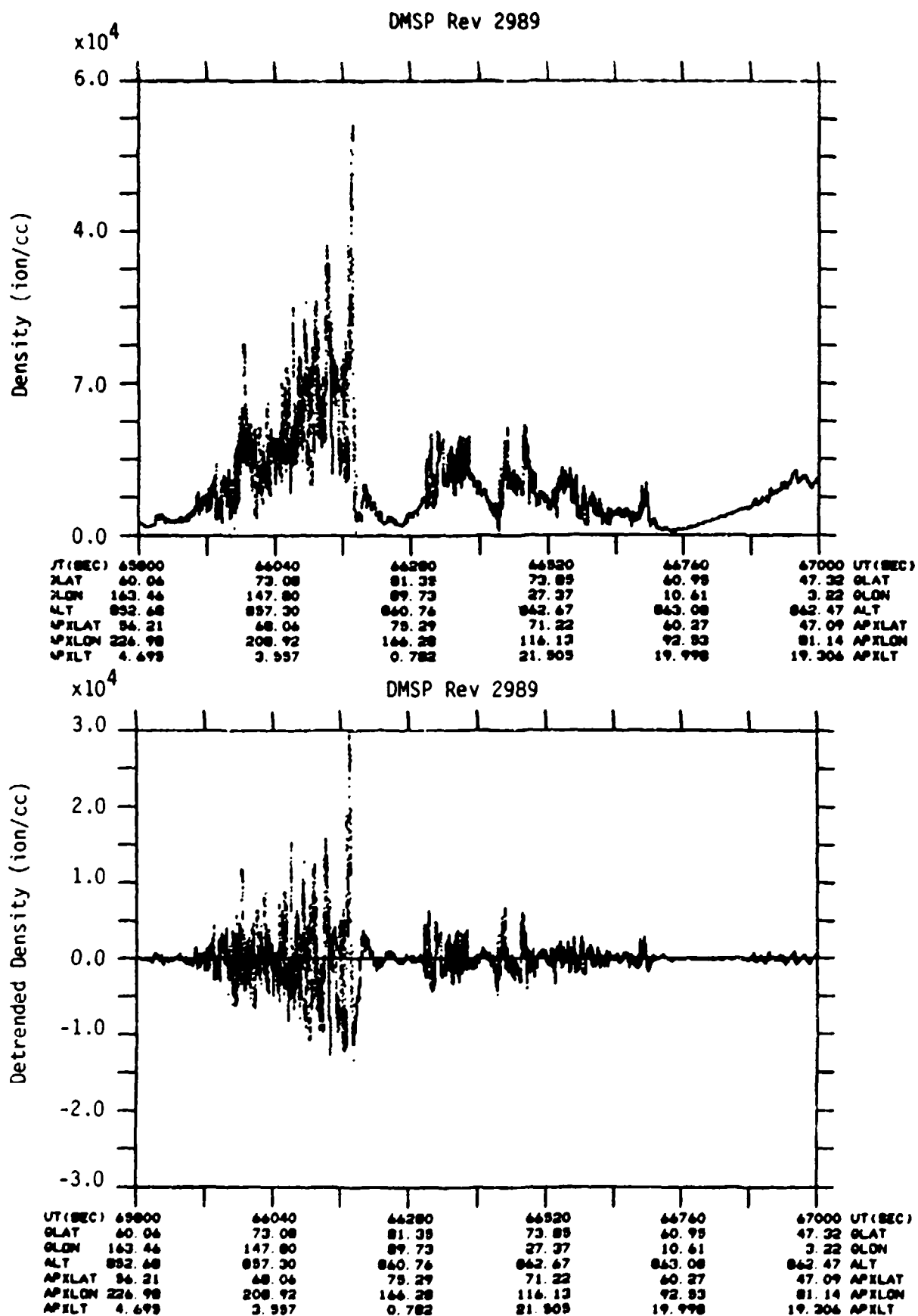
Figure 1. DMSP SM sensor ion density data from a 20 minute section of Rev 2989. Upper plot is the raw density record; lower plot is the detrended density obtained by removing a trend generated from a low-pass filter with a cutoff frequency of 0.0234375Hz.

6

SSIES SM ion density data from satellite F8, Rev 2898, collected over the northern auroral/polar region. The detrender used was the same as that employed in processing the Poker Flat/Wideband data, but in this case a 42.66667-second (0.0234375Hz) detrend cut-off was used. This was selected to correspond to twice the size of the data window (21.3333 seconds) to remove any detrender effects from the frequency range covered by the PDS.

A total of 120 T_1/q analyses were taken from this data set and used in the validation procedure. Figure 2 shows plots of Δq and $\Delta \log(T_1)$ as functions of window severity for each of the five smoothing cases (no smoothing through 9-point smoothing) for the data in Figure 1. The same behavior is shown in these plots as was found in analysis of both the simulation data sets and the Wideband phase data set (see Figures 2 and 7 in Scientific Report No. 1[5]), i.e., the loss (gain) in $\Delta \log(T_1)$ due to windowing (smoothing), and the trends in Δq and $\Delta \log(T_1)$ as functions of window severity and smoother length. The variances for each data point for the various cases were also similar to those for the simulation and phase data sets. Figure 3 presents the results of the detrender study for this data set. The four curves show the results using a linear detrend (L), a quadratic detrend (Q), an end-match/remove-mean detrend (E), and a low-pass filter detrend (F). Again, the results are very similar to those obtained using the other data sets (see Figures 6 and 8 in Scientific Report No. 1[5]).

A final issue which could not be resolved until data were available from the SM sensor was the selection of the frequency range over which the PDS would be fit. The desire is to fit to as much of the spectrum as possible in the kilometer scale-size regime, but to avoid biasing the fit with breaks in the spectrum (at the outer scale-size and at any high-frequency "freezing-scale" size), or by attempting to fit across an artificial break caused by a "noise floor" in the data. The PDS plots in Figure 4, taken from a section of Rev 2961, show clear examples of a low-frequency break at about 0.3 Hz (a scale size of roughly 25km) and a possible high-frequency break in the PDS in the upper-right plot (time 68105) at about 5 Hz (roughly 1.5km scale size). While no rigorous analysis was made to determine the best fit range during this stage in the project, a large number of spectra were manually reviewed to identify a reasonable fit range. The straight-line segments overlaying the spectra in Figure 4 show the range finally selected, 0.3 to 5.0 Hz. We plan to revisit this issue next year as the low-frequency roll-off seen in Figure 4, at what may be an outer scale, will have an effect on the accuracy of any $C_k L$ values calculated from spectra containing such a feature.
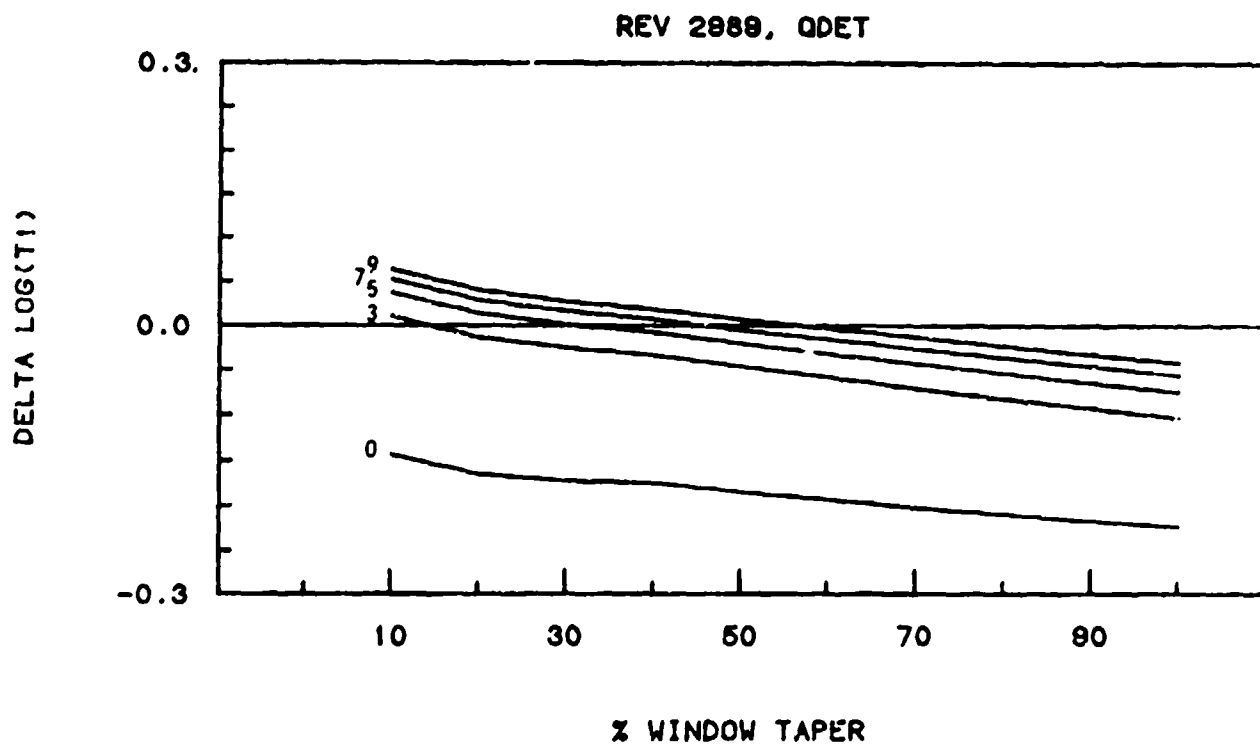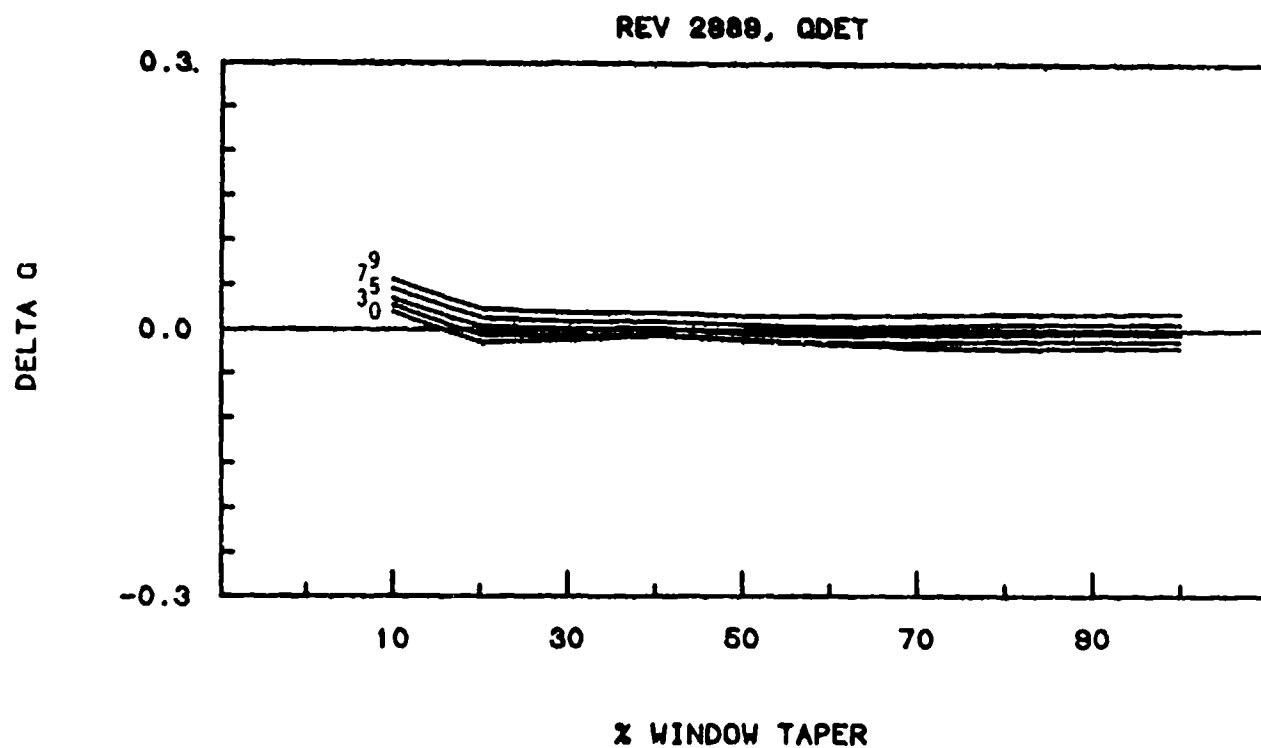
Figure 2. Effects of windows and smoothing on data from Rev 2989. All data sets were detrended using a quadratic detrender. Numbers indicate the length of the smoothing function in data points covered.

8

REV 2989, 5PT SMOOTH
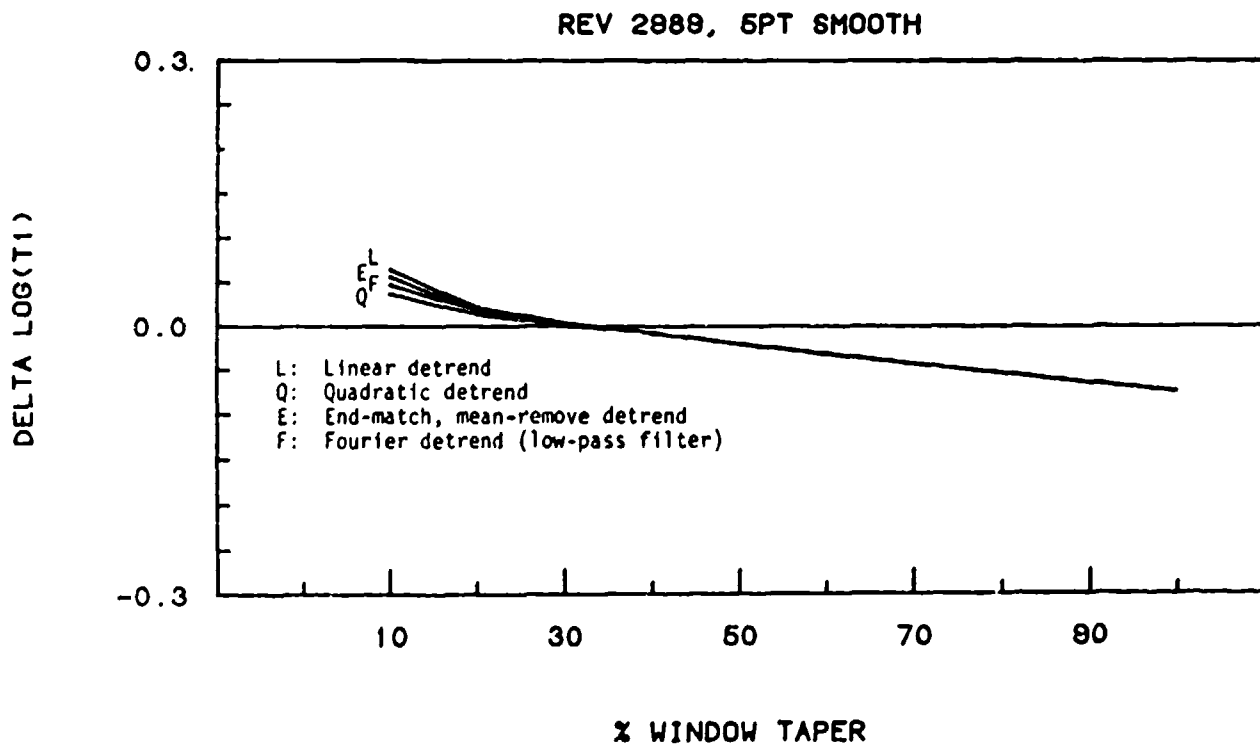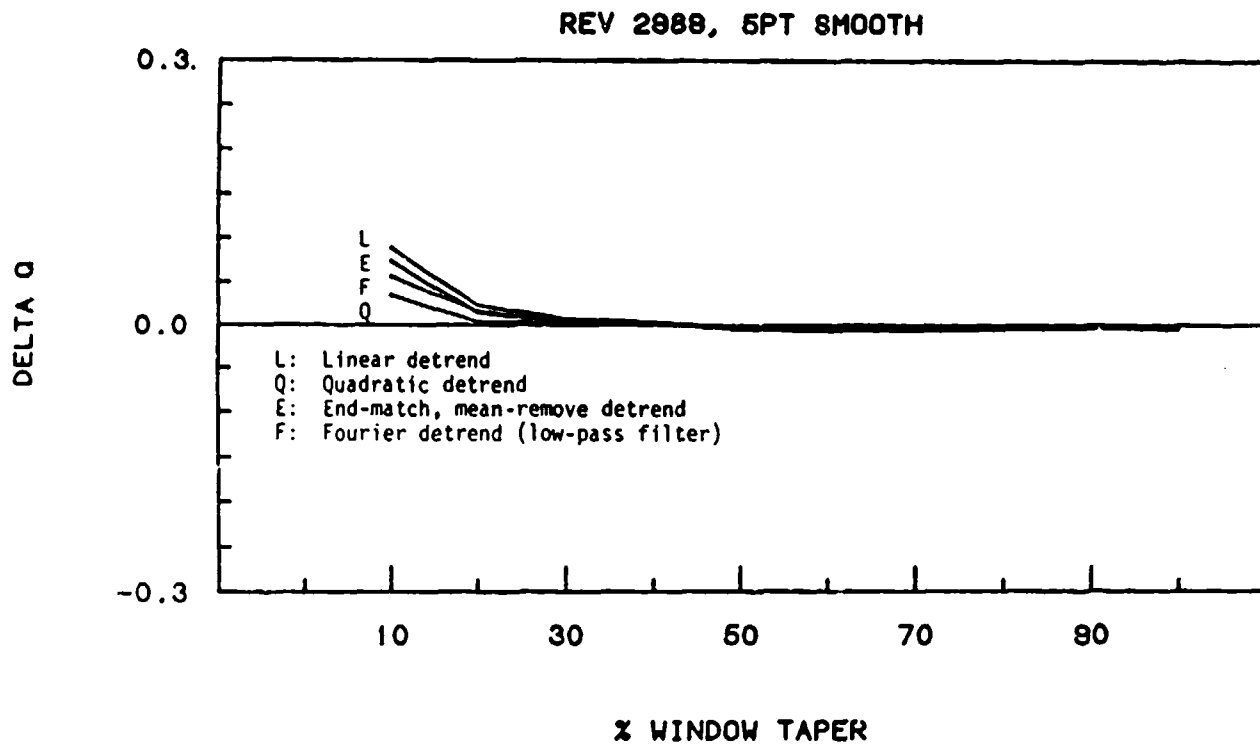
REV 2989, 5PT SMOOTH

Figure 3. Detrender effects from analysis of data from Rev 2989. A five-point smoother was used in all cases.

9
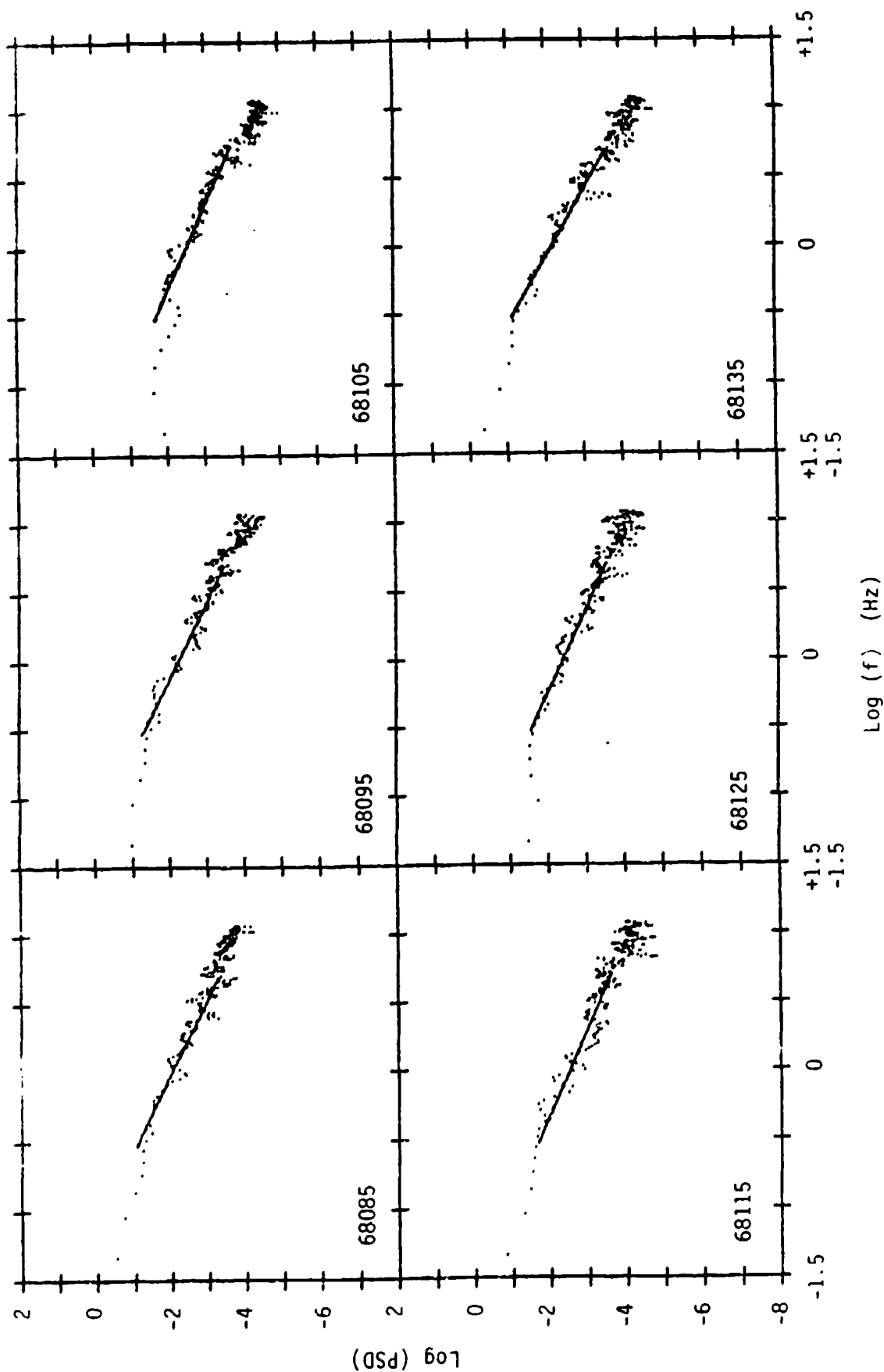
Figure 4. Spectra from a one-minute segment of the detrended data from Figure 1. The data sets were windowed with a 30% cosine taper, and the spectra were smoothed with a five-point smoothing function. The straight-line segments are the results of least-squares fits to the spectra from which values of T_1 and q are derived.

4. Analysis of SSIES/AIO/EISCAT Campaign Data.

Most of the work during the past year was directed at analysis of the SSIES SM data collected during a coordinated data-collection campaign conducted during January 1988 in the vicinity of the EISCAT incoherent radar facility located in northern Norway. This section will describe the mechanics of the campaign, the procedures developed for processing the SSIES Scintillation Meter (SM) and Drift Meter (DM) data collected during the campaign, and the preliminary results obtained from the analysis.

4.1 Campaign Description.

The primary objective of the SSIES/AIO/EISCAT campaign was to make near-coincident observations of the state of the ionosphere and of a radio signal propagating through the ionosphere in order to assess the validity of using information from the SSIES SM sensor to characterize and quantize the effects of scintillation on a transionospheric radio transmission. The concept was to use estimates of the scintillation parameters C_kL and q derived from the SSIES SM density data to calculate estimates of the level of phase and amplitude scintillation to be expected on a specific transionospheric satellite communications link, and then to compare these to the scintillation levels actually observed on that link.

The following data were collected during this campaign:

a. From the DMSP F8 satellite:

    (1) *In-situ* observations of the total ion density (N_i) at a data rate of 24 samples/sec from the SSIES SM sensor.

    (2) *In-situ* observations of the horizontal (u_h) and vertical (u_v) cross-track components of the ion drift velocity at a data rate of 6 samples/sec from the SSIES DM (Drift Meter) sensor.

    (3) *In-situ* observations of precipitating electrons and ions at a data rate of one energy spectrum per second from the SSJ/4 sensor.

b. From the AFGL Airborne Ionospheric Observatory (AIO):

    (1) Phase and amplitude records of a 250MHz radio transmission from an AFSAT satellite (#7225).

11

(2) All-sky photometer images at three wavelengths (4278Å, 5577Å, and 6300Å) at a data rate of (at least) one image per wavelength per minute from the All-Sky Imaging Photometer (ASIP).

(3) Ionospheric soundings at a data-rate of approximately one sounding every two-to-three minutes from the Digisonde.

c. From the EISCAT incoherent radar:

(1) Electron density profiles along a near-meridian-plane scan.

(2) Electron and ion temperature profiles along a near-meridian-plane scan.

(3) Ion drift velocity profiles along a near-meridian-plane scan.

AFGL/LIS is coordinating the analysis of the various AIO and EISCAT data sets and the data from the DMSP SSJ/4 sensor. Analysis of data from the various SSIES sensors is NWRA's responsibility. (Note: We had hoped to process data from the SSIES Retarding Potential Analyzer (RPA) sensor to obtain observations of the ion temperature and the ratio of the number density of $O+$ ions to $H+$ (or $He+$) ions, both of which would have been used in the calculation of $C_k L$. Unfortunately, this instrument failed prior to the first campaign period.)

One data set was collected during each day of the campaign (8-9 and 15-18 January 1988). The DMSP F8 satellite is in a nominal dawn-dusk orbit which, during the two campaign collection intervals, passed the satellite near the EISCAT facility at around 1830UT. The observing plan was to have the AIO fly a north-south pattern configured so that the ionospheric penetration point of the AIO-AFSAT radio link passed near the DMSP orbit track, and for the EISCAT facility to conduct north-south meridian scans roughly aligned with the DMSP track at the time of the overpass.

4.2 Analysis of the SSIES Campaign Data.

The objective of the analysis of the SSIES data taken during this campaign is to produce estimates of the level of phase and amplitude scintillation observed on the AIO-AFSAT radio link. This is done in four stages: (1) convert the raw telemetry data into break-free time series of (a) the *in-situ* ion density and (b) the *in-situ* ion drift velocity, (2) calculate estimates of C_k and q from the ion density data, (3) calculate estimates of C_k' n C_k using models and observations of the ionospheric height profile, and (4) calculate estimates of the values of S_4 and σ_ϕ for the AIO-AFSAT link using the $C_k L$ and q values derived from the SSIES observations and the propagation theory from the WBMOD model[1],[2]. The processing required in

12

each of these stages is described in the following sections. During this year, we have completed stages 1a (density data) and 2 for all six near-overhead passes and have completed preliminary work for stages 3 and 4 using only model information for the $C_k L$ calculation. We will complete these stages in the next year as soon as we receive profile data from the EISCAT radar and scintillation information from the AIO-AFSAT link.

Table 4-01. Time Periods for SSIES Analysis.

Date	Rev No.	Full Set Start	End	Analysis Set Start	End
08 Jan 88	2862	18:21:30	18:46:30	18:36:30	18:41:30
09 Jan 88	2876	18:09:30	18:34:30	18:24:30	18:29:30
15 Jan 88	2961	18:37:00	19:02:00	18:51:30	18:56:30
16 Jan 88	2975	18:25:00	18:50:00	18:39:00	18:44:00
17 Jan 88	2989	18:12:00	18:37:00	18:27:00	18:32:00
18 Jan 88	3003	17:59:30	18:24:30	18:15:30	18:20:30

Table 4-01 lists the time periods covered by the SSIES data analysis for each of the six near-overhead passes. The first set of numbers for each pass indicate the total span of the ion density time series processed for the pass (25 minutes of data centered on the time at which the DMSP satellite reached its northern-most latitude), and the second set indicates the time period for which the scintillation processing was done (5 minutes of data centered on a time interval identified by AFGL/LIS). Plots of the geometry for each pass (showing the relative positions of the DMSP track, the AIO track, the nearest-coincident penetration point of the AIO-AFSAT link, and the EISCAT radar scan track) and the results of the analyses described in the following sections for each of the six passes are located in Appendix A.

4.2.1 Stage 1: Converting Telemetry Data to Density Data.

Data from the SSIES sensor were collected at the Air Force Global Weather Central (AFGWC) and, with the exception of data for 15 January, was placed on save tapes for further processing at NWRA. Data for 15 January were later provided by Dr. Fred Rich (AFGL/LIS). Table 4-02 summarizes the SSIES data collected during the campaign which are currently available at NWRA.

13

As indicated in this table, the data were provided to NWRA in two quite different physical and logical formats. The AFGWC-format tapes are copies of file SSP*IESPREPFILE, which is formatted according to AFGWC's circular file format[6]. The copies are made using the UNISYS COPY utility, which writes the file to tape in blocks of 1792 36-bit words. The

---

Table 4-02. Raw SSIES Data Available at NWRA.

Date	Time	Format[1]
08 Jan 88	1632-2359 UT	AFGWC
09 Jan 88	0000-2359 UT	AFGWC
10 Jan 88	0000-0436 UT	AFGWC
15 Jan 88	0520-1640 UT	AFGWC
	1557-2103 UT	AFGL
16 Jan 88	0509-2359 UT	AFGWC
17 Jan 88	0000-0452 UT	AFGWC
	1801-2359 UT	AFGWC
18 Jan 88	0000-2359 UT	AFGWC
19 Jan 88	0000-0427 UT	AFGWC

[1] The format entry indicates the format of the tape on which the data currently reside. Details of these formats are given in the text.

AFGL-format tape contains unformatted-binary records written to tape in blocks of 1087 60-bit words. While both tapes contain the raw SSIES data frames and an ephemeris record once per minute, the format of both types of data and the contents of the ephemeris records are different.

Processing the SSIES SM data from raw tapes to break-free records of ion density is a multi-step process which, at times, can be somewhat more manual-intensive than was originally envisioned. A number of problems were encountered in converting the raw SM telemetry in c ion density measurements, which required the development of tools for editing the data in both raw and processed forms to facility the production of break-free (and discontinuity-free) data sets (see Appendix B for a discussion of these problems). After working with the data from several passes, the following scheme was developed for routine processing to convert telemetry voltages to ion density:

1. Convert the format of a raw data tape file into a disk data file. Separate utilities were required for the AFGWC and AFGL format tapes to unpack and reformat them.

2. Extract the SM and DM data from of the disk file, along with the ephemeris data and other miscellaneous data from the SSIES data frames required for processing (or making sense of) the SM or DM data, and load it into a file designed for interactive editing (an SMDM file) and an ephemeris file (an EPHEM file). This step used the unpacking and decoding stages of the code developed for processing the data at AFGWC[7], modified as necessary to generate the desired output files. Again, separate processors are required for the AFGWC and AFGL formats, but the output files from this step are identical.

3. Edit the SM data to remove or alleviate problems such as those described in Appendix B which were identified during the previous step.

4. Generate a file (an SMDEN file) containing total ion density calculated from the raw SM data in the edited SMDM file. This step uses code from the SM processing stage of the AFGWC software, modified to (1) access the SMDM files, and (2) incorporate new processing algorithms to deal with some of the problems identified in Appendix B. This is typically an iterative process in which new errors/problems are encountered which require further editing of the raw data.

5. When a final SMDEN file has been built, this is then edited to remove discontinuities introduced by the V_{bias} problem described in Appendix B and any other blatantly erroneous data (such as those shown in Figure B-02d). Breaks in the data, due to either removal of status flags or deletion of bad data segments, are then filled in by linear interpolation between the last good data on either side of the break.

The results of this processing stage are shown in Figures A-xxb (full 25-minute data set) and A-xxc (5-minute analysis data set) for the six passes, where xx is 01-06 corresponding to Revs 2862, 2876, 2961, 2975, 2989, and 3003, respectively.

4.2.2 Stage 2: Calculate Estimates of C_k and q.

The second stage of processing, calculating estimates for C_k and q, follows the processing guidelines developed in the first year of the project. Once the SM telemetry data has been converted to density records, this stage can be run (and rerun as necessary) fairly quickly, as little human intervention is required. The steps in this stage are as follows:

1. Detrend the density data by removing a trend record generated by a low-pass Butterworth filter with a 0.046875 Hz cutoff frequency. The cutoff frequency is set to the inverse of the time span of the data sample size used in generating the power density spectra (21.33333... seconds).

2. Step through the data, selecting 512-point data sets centered on ten-second time intervals. Apply a 30% split-bell cosine window to each data set.

3. Generate power density spectra (PDS) for overlapping 512-point data samples selected at 10-second intervals throughout the data set. Each data set is windowed with a 30% split-bell cosine taper prior to passing it to an FFT. The resulting PDS is then smoothed using a 5-point smoothing function with binomial weights.

4. Generate estimates of T_1 and q by least-squares fit of a linear segment to each PDS over a frequency range of 0.3 to 5.0 Hz in log(frequency) and log(PSD).

5. Calculate estimates of C_k from T_1 and q using velocity data from the EPHEM file built in step 1b.

The results of this processing stage are shown in Figures A-xxd (detrended density data), A-xxe (density data trend), A-xxf (q), and A-xxg (C_k) for the six passes.

4.2.3 Stage 3: Calculate Estimates of $C_k L$.

The plan is to calculate estimates of $C_k L$ from C_k in two ways: (1) using only those observations available in the DMSP data set with models for the parameters required which have not been observed, and (2) using all ionospheric data collected during the campaign, in particular the ionospheric profile data from the EISCAT radar scans. In both cases, an estimate is made of the effective layer thickness, L_{eff}, which is multiplied times the C_k estimate from stage 3 in the processing to obtain an value for $C_k L$. The data from EISCAT have not yet been made available for this part of the processing, so we will describe only the processing done to calculate $C_k L$ using DMSP data and models.

As mentioned earlier, it was hoped that we would have the full set of SSIES instruments working during the campaign, but the RPA sensor died during the month of December 1987. The data from this sensor were to be used to calculate the *in-situ* ion temperature, T_i, and the ratio of the number density of O+ to the number density of the dominant light ion (usually H+). The model we will use to calculate the plasma density distribution in the topside ionosphere was designed to use these data, if available, to refine internal models of the ion temper-

16

ature and ion species distribution[8]. The loss of these data is not crucial to this experiment, but it would have allowed us to determine how useful (or possibly critical) these data might be for converting C_k to a representative estimate of $C_k L$.

With the loss of the RPA, the only data used in generating the profiles from which L_{eff} is calculated are observations of the total ion density from the SM sensor. The calculation of $C_k L$ for each of the C_k estimates from stage 3 was done as follows:

1. An average density value was calculated from the density trend generated in stage 2 (step 1) for the 21-1/3 second data interval for which the C_k estimate is valid.

2. A field-line trace is made from the satellite altitude down to 350km, and model values for the F2-layer critical frequency ($f_o F2$) and height ($h_m F2$) are calculated from the ITS78 climatological model[9].

3. The ITS78 values for $f_o F2$ and $h_m F2$ are iteratively adjusted until the topside profile model fits through the average density value calculated from the SM density trend at the altitude of the satellite. The fitting procedure used is described in detail in [8] (Section 3.2).

4. An estimate of L_{eff} is calculated from this profile using the equation

$$L_{eff} = \frac{\int_{h_b}^{h_s} N_e^2(h)\, dh}{N_e^2(h_s)} \qquad [4-01]$$

where h_s is the satellite altitude and h_b is the (modeled) base of the irregularity layer. In these calculations it is assumed that the irregularity layer extends one scale height below the peak of the F2 layer (i.e., $h_b = h_m F2 - H$, where H is the plasma scale-height at $h_m F2$).

5. The estimate for $C_k L$ is then calculated from

$$C_k L = C_k\, L_{eff} \qquad \cdot \qquad [4-02]$$

17

The results of this processing stage are shown in Figures A-xxh (C_kL) and A-xxi (L_{eff}) for the six passes.

4.2.4 Stage 4: Calculate Estimates of S_4 and σ_ϕ.

The calculation of S_4 and σ_ϕ is made using a modified version of the propagation model in the WBMOD ionospheric scintillation model[1][2]. Besides the estimates of C_kL and q, this model requires information defining the link geometry (AIO and AFSAT locations and AIO velocity), system parameters (radio frequency and time period over which σ_ϕ is calculated), environment parameters (date, time, sunspot number, and K_p), values for the irregularity axial ratios (a and b), and values for the *in-situ* drift velocity of the irregularities. If values for a, b, or the drift velocity are not provided, the analysis code will use models for these parameters from WBMOD to calculate estimates. In the calculations reported here, we have used model values for the drift velocity[10] and a 20:1 rod model for the shape of the irregularities (i.e., a = 20 and b = 1). All calculations use a value of 250MHz for the AIO/AFSAT link radio frequency, and the σ_ϕ values given are calculated for an 80-second integration interval.

While calculating estimates of S_4 and σ_ϕ using the C_kL and q values calculated in the previous stages is relatively straightforward, calculating estimates of what we expect to find in the AIO-AFSAT scintillation data complicates the issue considerably. There are two complicating issues here - one concerning the static geometry of the experimental setup (i.e., the relative locations and times at which the various instruments were collecting data) , and the other concerning the dynamic geometry (i.e., the relative velocities of the various instruments with respect to the ionospheric irregularities). Neither of these issues is insurmountable, but both must be handled carefully to insure a valid comparison between the SSIES and AIO/AFSAT data sets.

The first issue is a typical problem for any experiment in which several instruments are attempting to make coincident measurements of the ionosphere, particularly when one instrument is on a satellite, the other is on an aircraft, and the ionosphere being probed is in the very dynamic auroral zone. We wish to identify those times when the AIO/AFSAT raypath was propagating through a section of the ionosphere which had been probed by the DMSP SSIES sensors, or, in more formal terms, we wish to map the DMSP SSIES observations into the frame defined by the AIO/AFSAT observations. An accurate job of matching density features from the SSIES observations with scintillation features in the AIO/AFSAT observations will require access to both data records. At this time we do not have access to the AIO/AFSAT records, so we have identified those times when the raypath ionospheric penetration point

18

passed closest (in both time and space) to the F2-region track* of the DMSP satellite, and will calculate estimates of S_4 and σ_ϕ from the SM density data for this time of nearest approach and for the two ten-second C_kL calculation periods prior to and after this time.

The second issue is somewhat more difficult to resolve, although, fortunately, it will affect the σ_ϕ calculation only. The level of phase scintillation observed on a particular link will be a sensitive function of the velocity of the ionospheric irregularities causing the scintillation with respect to the raypath. For a link involving a low-orbiting satellite, the scanning motion of the raypath through the irregularities due to the orbital motion of the satellite is usually dominant over the *in-situ* drift velocity of the irregularities, and one can assume (with varying degrees of validity) that the irregularities are not moving with respect to the rest of the system. However, for a slowly changing receiver-transmitter geometry, such as is the case for the AIO/AFSAT link, the bulk of the phase scintillation is due to the drift motion of the irregularities which must be either observed or modeled.

In this experiment, we do have observations of the *in-situ* drift velocity of the ionospheric ions at the DMSP altitude from the Drift Meter (DM) and the RPA sensors. The DM sensor provides the horizontal and vertical cross-orbit-track components of the velocity, and the RPA provides an estimate of the component in the along-orbit direction. One can then assume that the electrostatic potential which is driving this drift maps down field lines, and calculate an estimate of the drift velocity in the F2 region. There are, however, problems with this. As stated earlier, the RPA sensor died in December 1987, so these data were not available. In addition, there are difficulties with the DM sensor data. Previous checks of the DM velocity data uncovered what appears to be an offset in the sensor orientation with respect to the satellite velocity vector (i.e., the sensor is not normal to this vector as required by the sensor design), which results in contamination of the two cross-track components by the velocity of the satellite with respect to the ionospheric plasma (see [7] Volume Va; Rich, private communication; and Heelis, private communication). In addition, the data from this sensor become less reliable when the density is low (as it is in most of the cases under study) which is manifested in an increased scatter in the data. Due to dwindling resources for this project year, we did not want to tackle this problem in its entirety until next year. We do, however, need to include the effects of the plasma drift in the σ_ϕ calculations, so we will use the drift velocity model from the WBMOD scintillation code[10]. We have also included an estimate of the aircraft velocity in the relative velocity calculations, although we used only a simple north-south velocity model

---

* Defined as the trace of the point in the F2 region which maps ups the local field line to the DMSP satellite.

which can be made more realistic in the next year when we add the observed drift velocities from the DM sensor.

In summary, the values we will present in the following section for S_4 and σ_ϕ should be viewed as first-order estimates, i.e., if the AIO/AFSAT raypath actually passed through the sections of the ionosphere we have assumed at the times we have assumed, and if the actual drift velocity of the irregularities is near to the velocities generated by our model, these values should be accurate to within roughly 10-20%. If the situation is markedly different, however, the values for σ_ϕ may be as much as 60-120% off[5].

4.3 Discussion of Results.

As can be seen by a casual examination of the data plots in Appendix A, we were fortunate in this campaign in that we have data sets from both magnetically quiet (9 and 16 January) and active (8, 15, 17, and 18 January) periods. The solar fluxes are beginning to recover from the latest solar minimum, as indicated by a 90-day mean sunspot number ranging from 40 to 45 and the daily number ranging from 57 to 90 over the campaign interval. This translates into more solar-produced ionospheric plasma, which is important for the production of well-defined polar-cap patches if these patches are indeed plasma detached from the mid-latitude sunlit ionosphere equatorward of the dayside convection "throat" and swept into the polar cap convection pattern[11]. There are several features in these six passes across the northern polar cap which could possibly be such patches, most notably the feature in Rev 2961 between times 67980 and 68050 which may be a patch in the process of merging into the auroral region.

The primary objective of this particular study, however, is not to go "patch catching," but to assess the potential for using the SSIES SM sensor data for making quantitative estimates of the effects of ionospheric irregularities on transionospheric radio signals. The data for all six passes have been processed as described previously, and we will discuss the results obtained to date for each individual pass. (The plots of total density, C_kL, and q from Appendix A (Figures A-xxb, h, and g) are repeated as Figures 5-10 in this section for convenience.)

(Note: It became apparent in reviewing these data sets that in order to make sense of some of the features we will need to look at both the SSIES DM drift data and high time-resolution particle precipitation data from the SSJ/4 sensor to better define the environment in which the features are imbedded. This is a major task item for the next year of this project.)

The data from this pass, shown in Figure 5, is representative of moderately disturbed conditions (six of the preceding eight K_p values were between 4- and 4+). Several structures which could be polar cap patches can be seen in the density plot in Figure 5 prior to time 67140 with a lower-density irregularity region from that time to time 67260. Both C_kL and q are relatively uniform to about time 67110, when C_kL ⊦ gins to decrease, q increases, and both become less uniform. It is tempting to identify the first, higher-density, region prior to time 67140 as plasma from polar-cap patches and the second, lower-density, region between times 67140 and 67250 as locally-produced auroral-zone plasma, but without information on the convection and precipitation patterns this is purely conjecture.

The time of near-coincidence with the AIO/AFSAT raypath is indicated with an arrow labeled AIO in Figure 5, and the calculated estimates for S_4 and σ_ϕ for the SM data from this time and the two 10-second periods on either side of this time are given in Table 3.

Table 3. Propagation Analysis for Rev 2862 (8 January 1988).

AIO/AFSAT Time: 18:39:30 UT
Penetration Point Latitude: 68.62   Longitude: 108.65

Time	Apex Latitude	Longitude	C_kL	q	S_4	σ_ϕ
67150	69.33	106.66	2.39×10^{31}	1.70	0.28	1.70
67160	68.93	105.50	5.54×10^{30}	2.05	0.14	1.32
67170	68.51	104.39	2.82×10^{31}	1.69	0.30	1.82
67180	68.10	103.31	2.74×10^{31}	1.66	0.30	1.73
67190	67.68	102.29	4.96×10^{30}	1.95	0.13	1.09

SSN: 57 $\overline{SSN}$: 40.6
K_p: 3 ΣK_p: 28

There is a small patch of enhanced irregularities very near to the identified coincident point, with calculated values for S_4 of 0.30 inside the patch and 0.14 outside and values for σ_ϕ of about 1.8 radians in the patch and 1.1-1.3 radians outside.

Figure 5. Results from the analysis of SSIES SM sensor density data for Rev 2862 on 08 January 1988: (A) Total ion density, (B) $C_k L$, (C) q.

4.3.2 Rev 2876, 9 January 1988.

This particular pass was during a fairly quiet period (the two preceding K_p values were both 0 +), and this is reflected in the quiet nature of the density and irregularity data in Figure 6. There are no patch-like structures present, and the auroral zone is well north of the AIO/AFSAT coincident point. The corresponding scintillation parameter values for this case (Table 4) are fairly low, with S_4 between 0.03 and 0.07 and σ_ϕ between 0.07 and 0.24 radians.

Table 4. Propagation Analysis for Rev 2876 (9 January 1988).

AIO/AFSAT Time: 18:27:10 UT
Penetration Point Latitude: 68.22   Longitude: 108.27

Time	Apex Latitude	Longitude	C_kL	q	S_4	σ_ϕ
66410	69.01	108.79	1.64×10^{30}	1.52	0.07	0.20
66420	68.60	107.65	4.94×10^{29}	2.34	0.04	0.24
66430	68.18	106.56	1.99×10^{29}	2.13	0.03	0.12
66440	67.76	105.51	2.58×10^{29}	1.46	0.03	0.07
66450	67.34	104.50	5.27×10^{29}	1.25	0.04	0.09

SSN: 62 $\overline{SSN}$: 40.9
K_p: 1 ΣK_p: 14 +

Figure 6. Results from the analysis of SSIES SM sensor density data for Rev 2876 on 09 January 1988: (A) Total ion density, (B) C_kL, (C) q.

24

4.3.3 Rev 2961, 15 January 1988.

The data on this day (Figure 7) were collected during the most disturbed day of the month (four K_p values of 6+ or higher during the preceding 24 hours), although the most severe disturbance ended roughly nine hours prior to the pass. The structure in the pass is similar to that in Rev 2862, with a patch-like structure between times 67980 and 68050 and lower-density auroral-zone structure between times 68050 and 68175. The single, isolated patch in this data set is very interesting in that the character of the irregularity structure in the poleward half of the patch is quite different from that in the equatorward half. Our current conjecture is that this patch has recently convected into the auroral precipitation zone, and that the equatorward half of the patch is now connected to an auroral E-layer with much higher plasma density than the polar E-layer under the poleward half of the patch. Recent computer simulations are beginning to show that the presence (or lack of) an enhanced E-region will affect the growth and vertical mapping of ionospheric irregularities[12]. (A more detailed analysis of this patch is being pursued further under the auspices of the Defense Nuclear Agency.)

The scintillation parameters for the AIO/AFSAT coincident point are in Table 5. This is a fairly disturbed case, with S_4 between 0.4 and 0.5 (nearing strong-scatter conditions), and σ_ϕ values ranging from 2 to 5 radians.

Table 5. Propagation Analysis for Rev 2961 (15 January 1988).

AIO/AFSAT Time: 18:54:45 UT
Penetration Point Latitude: 69.17   Longitude: 107.82

Time	Apex Latitude	Longitude	C_kL	q	S_4	σ_ϕ
68065	70.07	104.32	2.99×10^{31}	2.11	0.31	3.84
68075	69.68	103.13	5.02×10^{31}	2.16	0.40	5.37
68085	69.27	101.96	8.38×10^{31}	1.82	0.49	4.21
68095	68.86	100.85	5.34×10^{31}	1.79	0.40	3.22
68105	68.44	99.76	3.56×10^{31}	1.60	0.33	2.02

SSN: 90   SSN: 43.1
K_p: 3- ΣK_p: 42+

Figure 7. Results from the analysis of SSIES SM sensor density data for Rev 2961 on 15 January 1988: (A) Total ion density, (B) C_kL, (C) q.

4.3.4 Rev 2975, 16 January 1988.

These data, shown in Figure 8, were taken on a relatively quiet day and are quite similar to the data from Rev 2876. The AIO/AFSAT coincident point was well equatorward of the auroral zone, as is reflected in the very low scintillation values in Table 6, with S_4 of about 0.02 (essentially zero) and σ_ϕ between 0.1 and 0.2 radians.

Table 6. Propagation Analysis for Rev 2975 (16 January 1988).

AIO/AFSAT Time: 18:42:00 UT
Penetration Point Latitude: 70.04   Longitude: 110.?5

Time	Apex Latitude	Longitude	$C_k L$	q	S_4	σ_ϕ
67300	70.71	109.58	3.55×10^{28}	2.78	0.01	0.20
67310	70.33	108.28	8.69×10^{28}	2.32	0.02	0.17
67320	69.94	107.04	1.44×10^{29}	1.67	0.02	0.10
67330	69.54	105.82	3.10×10^{29}	1.82	0.03	0.17
67340	69.14	104.68	3.65×10^{29}	1.46	0.04	0.13

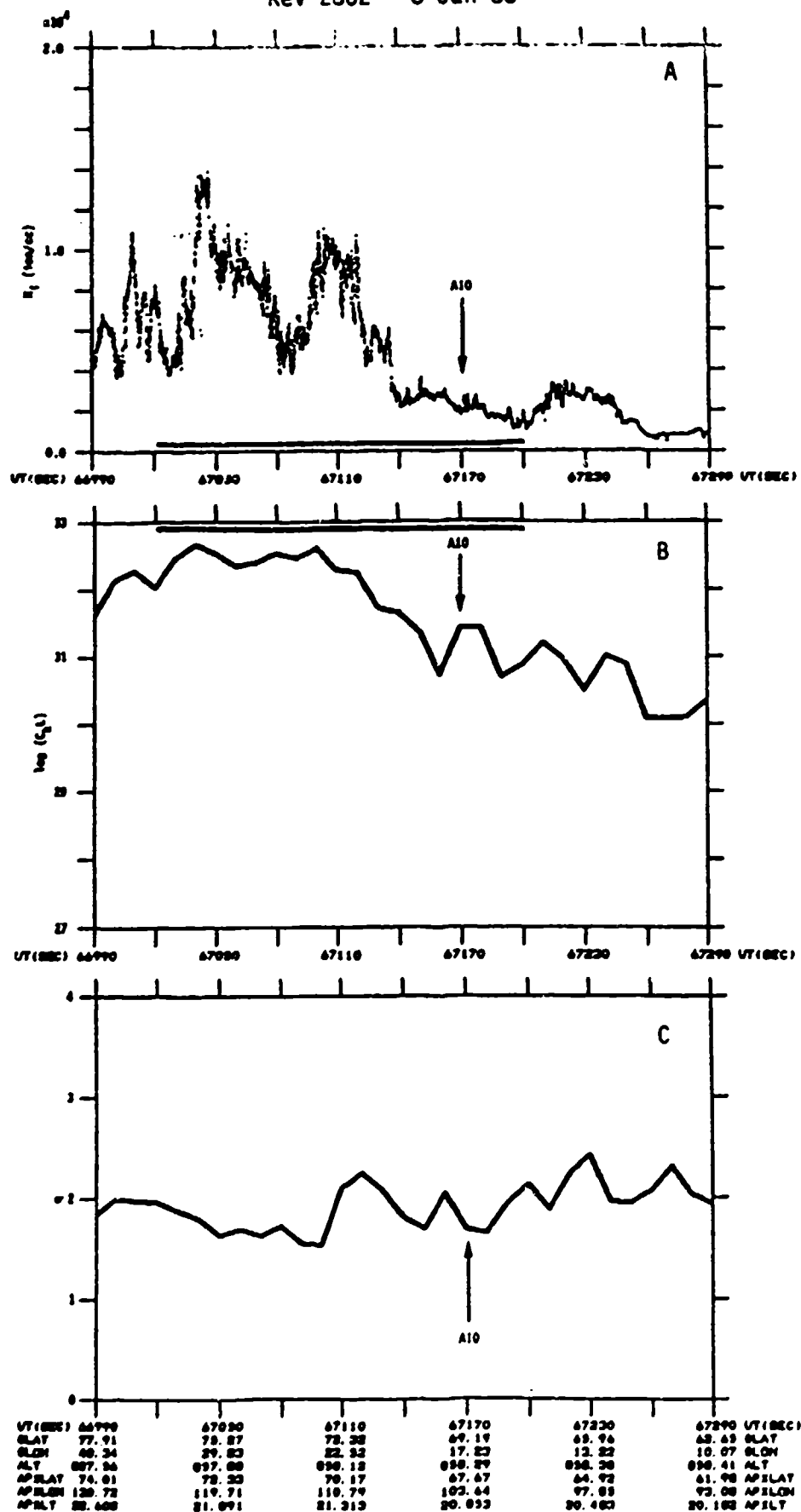SSN: 83 $\overline{\text{SSN}}$: 43.6
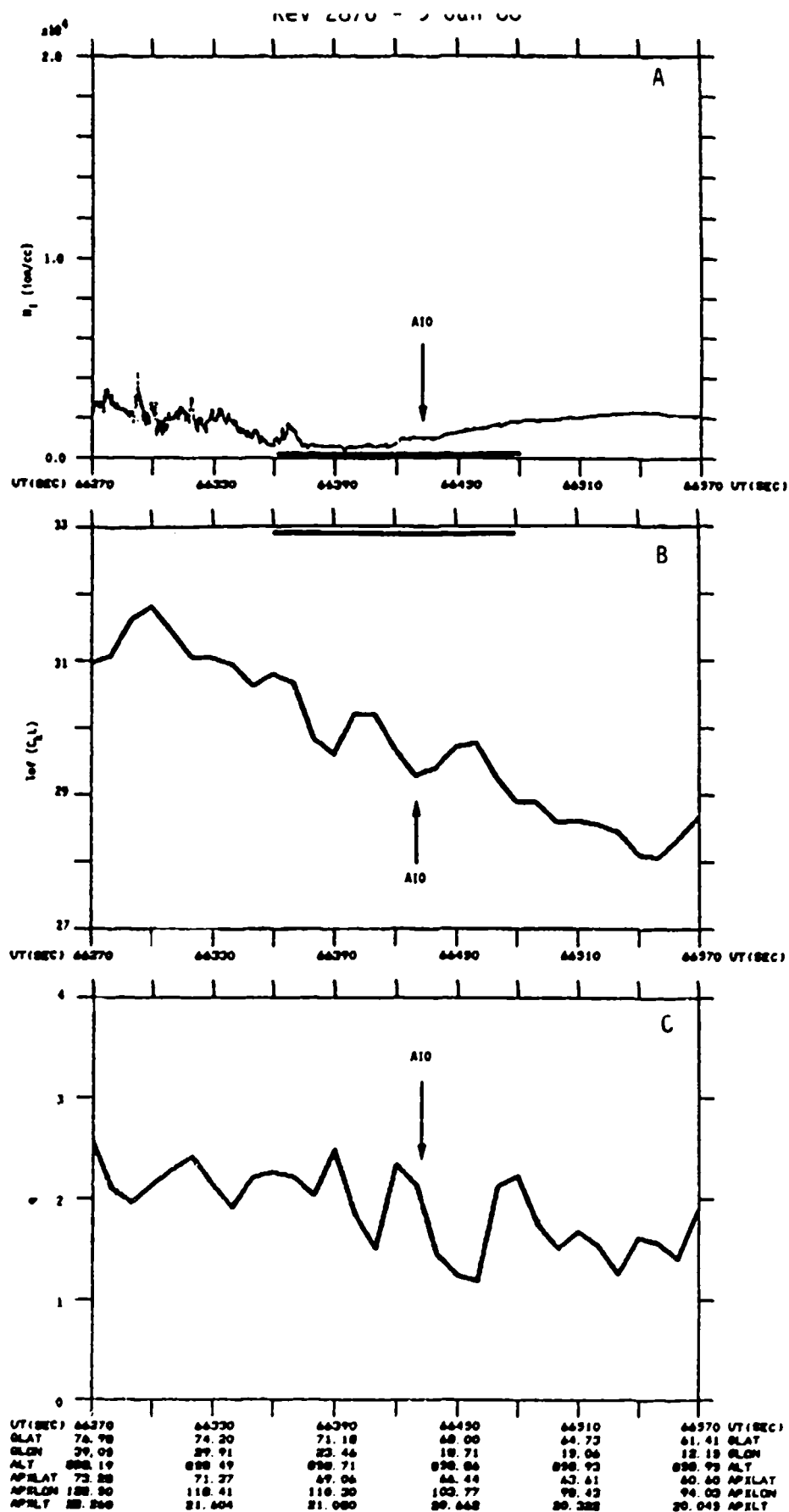K_p: 1- ΣK_p: 12 +

Figure 8. Results from the analysis of SSIES SM sensor density data for Rev 2975 on 16 January 1988: (A) Total ion density, (B) $C_k L$, (C) q.

4.3.5 Rev 2989, 17 January 1988.

Although taken during a quieter period than the data from Rev 2961, the data from this pass (Figure 9) are more uniformly disturbed throughout the section of the pass near Tromso. Again, one can identify possible polar cap patches, but there is less difference in the density structure of the patches and that in the auroral zone. The C_kL values are very uniform throughout much of this data set, essentially constant from time 66510 to the point where the satellite left the auroral region, while q is constant only to time 66650. This may be another manifestation of the behavior of the topside plasma structure when there is a strong underlying E-region. The scintillation parameters in Table 7 are also fairly uniform, with S_4 values between 0.3 and 0.4 and σ_ϕ values between 4.3 and 5.3 radians.

Table 7. Propagation Analysis for Rev 2989 (17 January 1988).

AIO/AFSAT Time: 18:30:05 UT
Penetration Point Latitude: 68.56   Longitude: 108.69

Time	Apex Latitude	Longitude	C_kL	q	S_4	σ_ϕ
66585	69.42	108.54	4.06×10^{31}	2.60	0.39	5.23
66595	69.02	107.38	3.66×10^{31}	2.48	0.36	4.26
66605	68.60	106.27	2.88×10^{31}	2.66	0.34	4.78
66615	69.19	105.19	1.62×10^{31}	2.80	0.27	4.32
66625	67.77	104.16	2.75×10^{31}	2.61	0.33	4.38

SSN: 72 $\overline{SSN}$: 43.8
K_p: 2+ ΣK_p: 13

29

Figure 9. Results from the analysis of SSIES SM sensor density data for Rev 2989 on 17 January 1988: (A) Total ion density. (B) C_kL, (C) q.

30

4.3.6 Rev 3003, 18 January 1988.

The data from this pass (Figure 10) are very similar to that from Rev 2989, the main differences being the location of the equatorward boundary of the auroral zone and the higher variability in the q parameter. The values for C_kL and the scintillation parameters near the AIO/AFSAT coincident point, however, are a bit higher for this pass (Table 8), with S_4 between 0.4 and 0.5 and σ_ϕ between 3.3 and 5.7 radians.

Table 8. Propagation Analysis for Rev 3003 (18 January 1988).

AIO/AFSAT Time: 18:18:15 UT
Penetration Point Latitude: 67.14   Longitude: 105.70

Time	Apex Latitude	Longitude	C_kL	q	S_4	σ_ϕ
65875	67.87	107.39	3.11×10^{31}	2.59	0.24	4.91
65885	67.44	106.37	1.22×10^{32}	1.81	0.43	3.33
65895	67.01	105.39	1.65×10^{32}	2.10	0.50	5.69
65905	66.57	104.45	9.14×10^{31}	2.31	0.39	5.66
65915	66.13	103.53	6.58×10^{31}	1.68	0.33	2.05

SSN: 68 $\overline{SSN}$: 44.18
K_p: 5- ΣK_p: 18 +

31

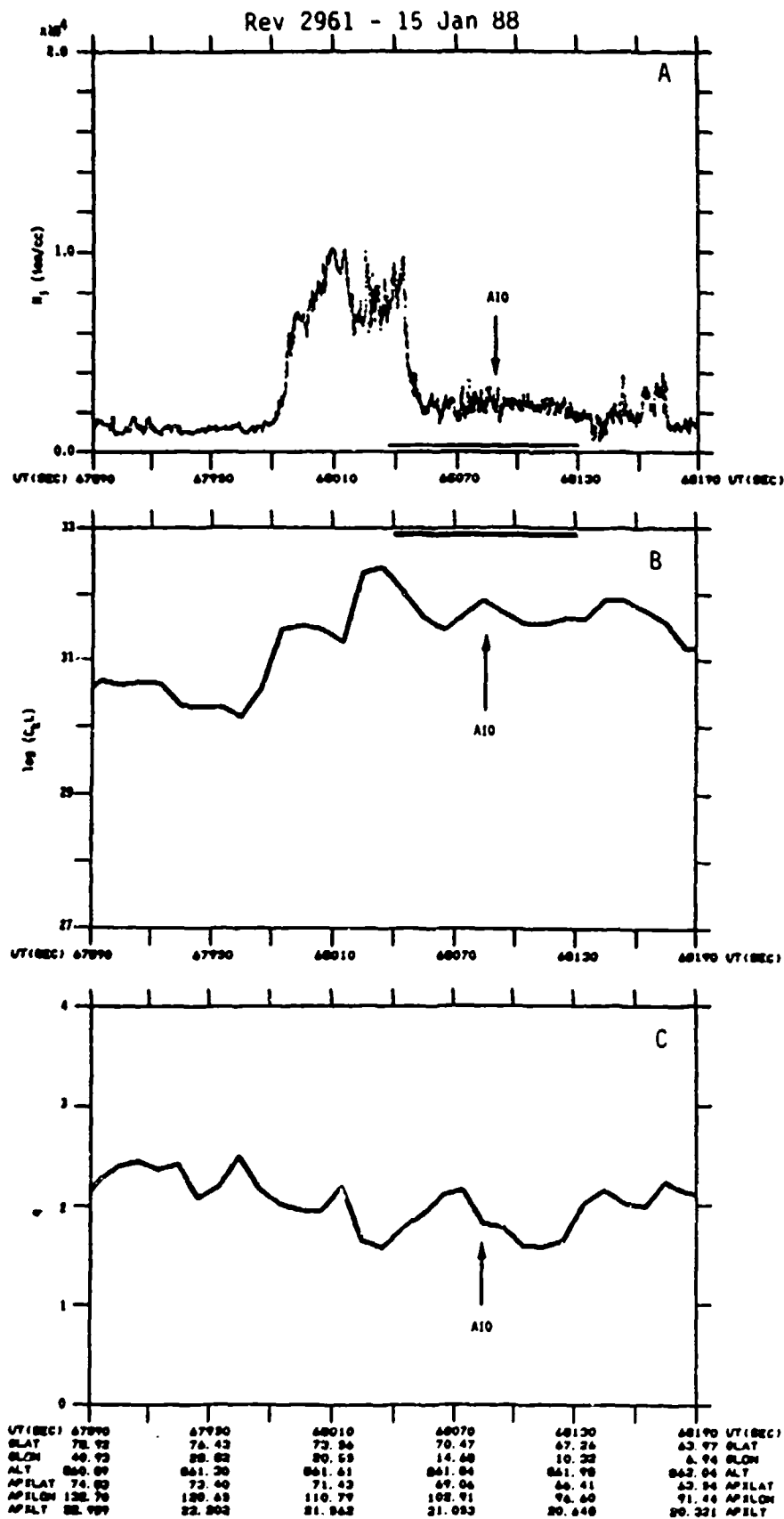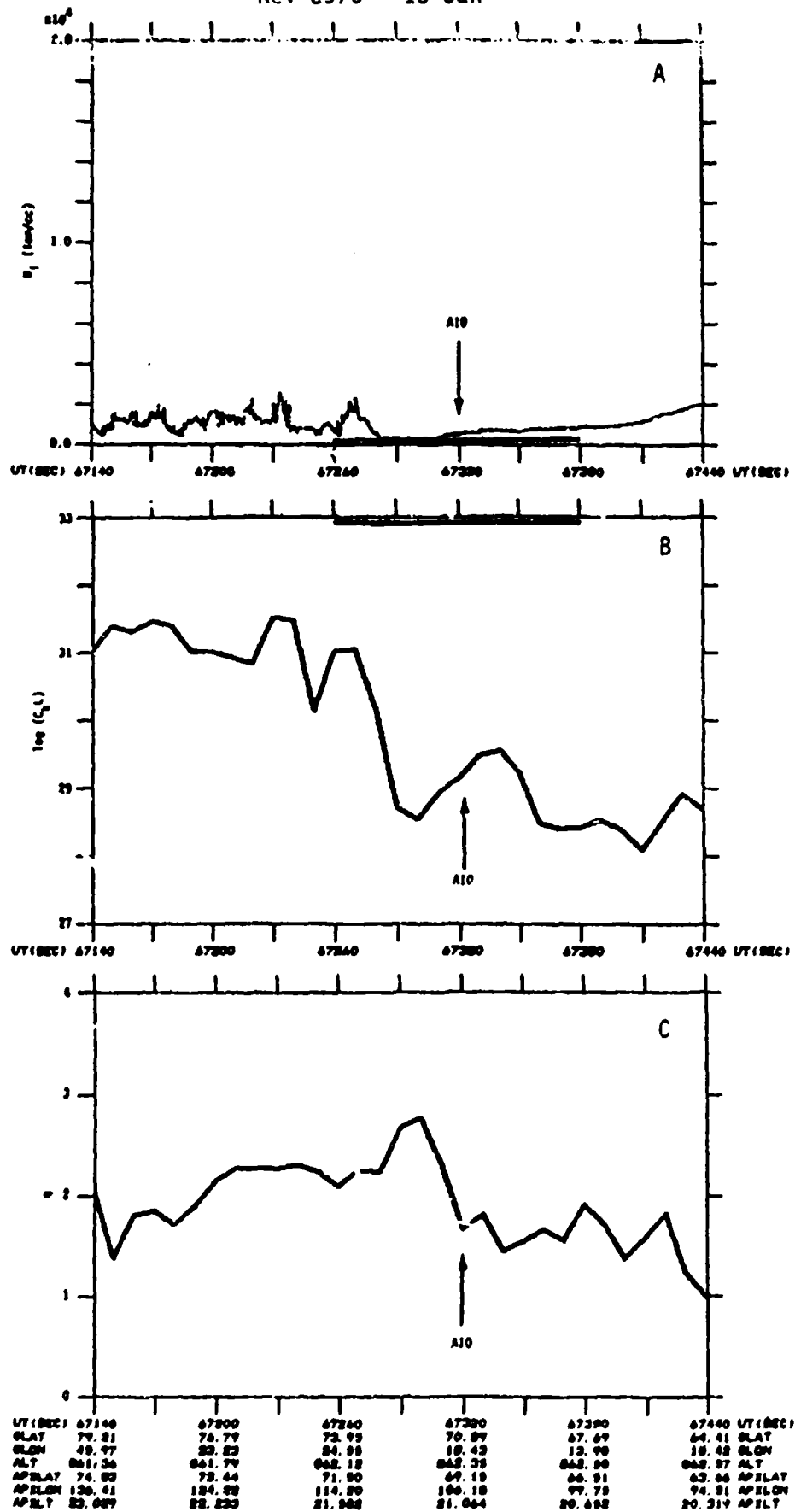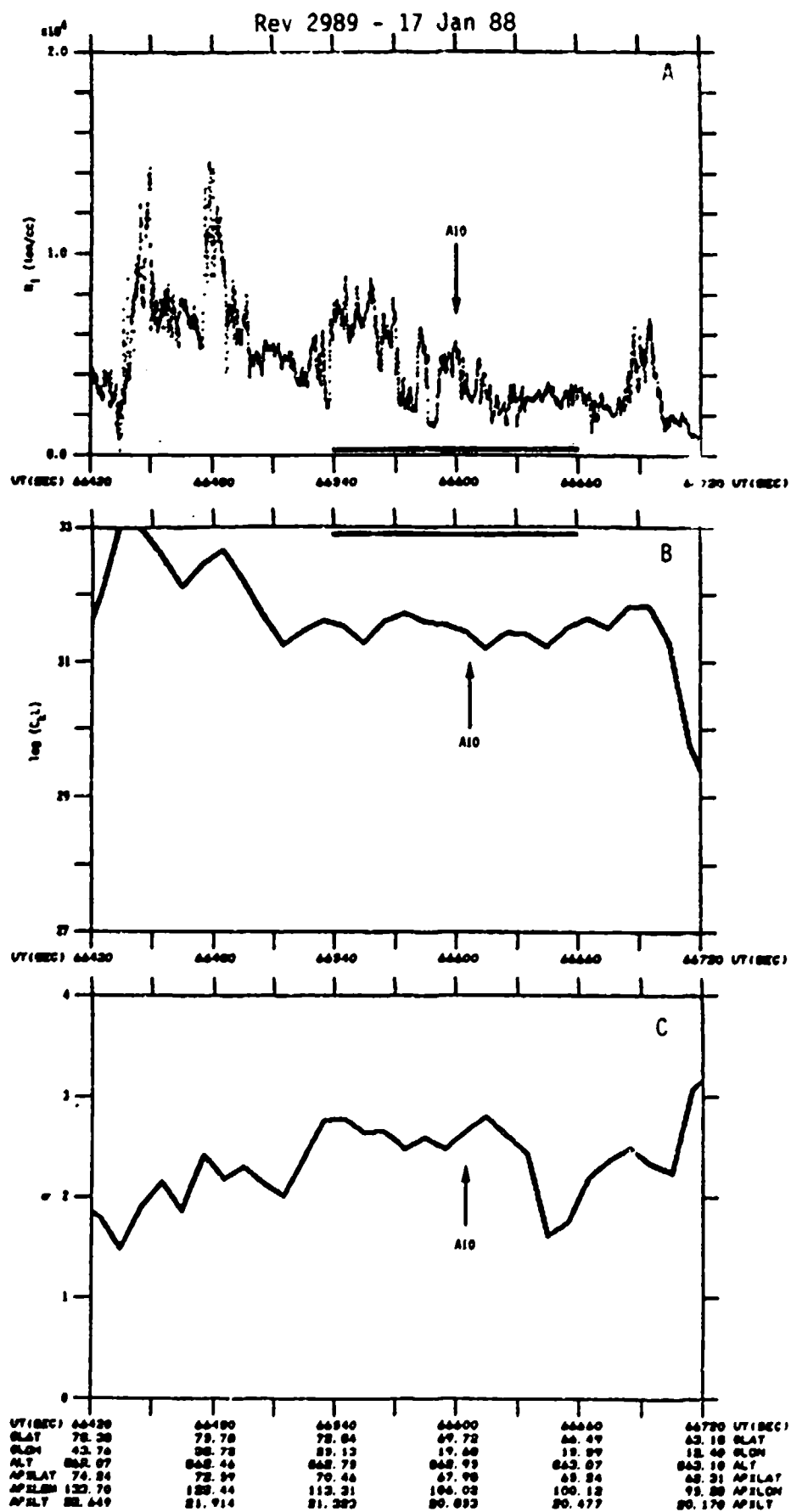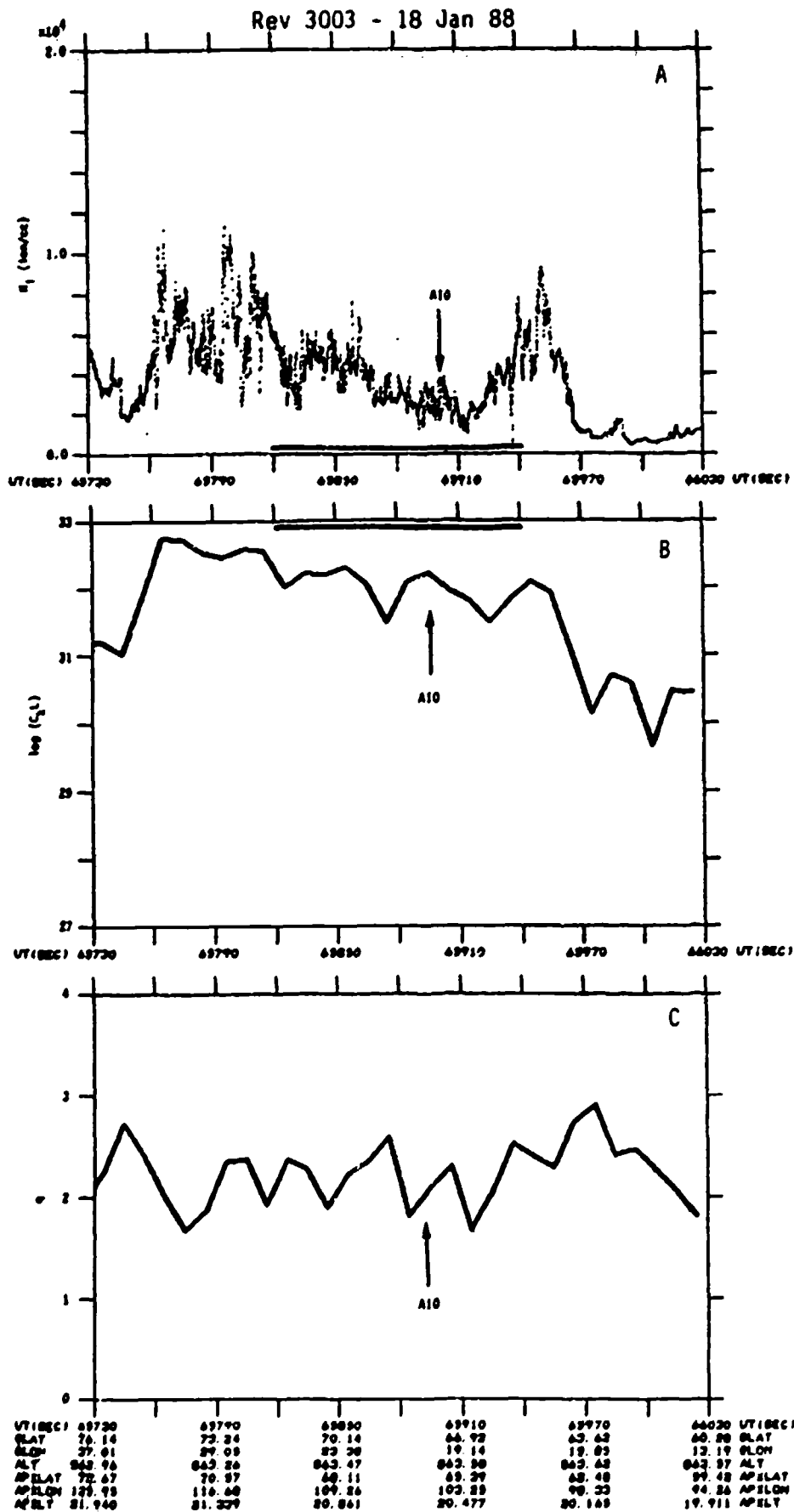Figure 10. Results from the analysis of SSIES SM sensor density data for Rev 3003 on 18 January 1988: (A) Total ion density, (B) C_kL, (C) q.

5. Conclusion.

During the year covered by this report, we have completed preliminary processing of the DMSP SSIES Scintillation Meter data collected as part of the SSIES/AIO/EISCAT coordinated data collection campaign conducted during January 1988. Data from sections of six passes near Tromso, Norway, have been processed, and predictions have been made of the level of amplitude and phase scintillation on the radio link between the AIO aircraft and an AFSAT satellite based on spectral strength (C_kL) and slope (q) parameters calculated from the SM ion density data. A large body of data-processing software was developed to aid in the reduction and analysis of the data. This software, and the procedures for using it, have been designed so that they may be easily used for processing data from future campaigns.

In the next year of this project, analysis of the data from this campaign would continue with the following tasks:

(1) Conduct a side-by-side comparison of the SM density data to the amplitude and phase records from the AIO/AFSAT radio link to aid in mapping the results of the SM data analysis into the AIO/AFSAT geometry.

(2) Process the SSIES DM plasma drift data and the SSJ/4 particle precipitation data for each of the passes and establish the location of major structures and boundaries in the plasma convection and auroral precipitation patterns, both of which are important facets of the physics underlying the irregularities observed in the SM data and the scintillation observed on the AIO/AFSAT link.

(3) Compare the EISCAT and Digisonde observations of the ionospheric plasma density profile to the model profile used to calculate L_{eff}. Recalculate any C_kL values for cases in which the model did not adequately reproduce the observations.

REFERENCES

[1]   Fremouw, E.J. and Lansinger, J.M., A Computer Model for High-Latitude Phase Scintillation Based on WIDEBAND Satellite data From Poker Flat, DNA Report 5685F. Defense Nuclear Agency, Washington, DC, February 1981.

[2]   Rino, C.L., "A Power Law Phase Screen Model for Ionospheric Scintillation, 1. Weak Scatter," Radio Sci., 14, 1135-1145, 1979.

[3]   Holt, B.J., Drift Scintillation Meter, AFGL-TR-84-0103, Air Force Geophysics Laboratory, Hanscom AFB, MA, March 1984, ADA142523.

[4]   Greenspan, M.E., P.B. Anderson, and J.M. Pelagatti, Characteristics of the Thermal Plasma Monitor (SSIES) for the Defense Meteorological Satellite Program (DMSP) Spacecraft S8 Through S10, AFGL-TR-86-0227, Air Force Geophysics Laboratory, Hanscom AFB, MA, October 1986, ADA176924.

[5]   Secan, J.A., An Assessment of the Application of In Situ Ion-Density Data From DMSP to Modeling of Transionospheric Scintillation, Scientific Report No. 1, AFGL-TR-87-0269, Air Force Geophysics Laboratory, Hanscom AFB, MA, September 1987, ADA188919.

[6]   DMSP Block 5D2 Special Sensor Data Processing System Data Base Specification, Air Force Global Weather Central (SDMS), Offutt AFB, NE, May 1985.

[7]   Secan, J.A. and Bussey, R.M., DMSP SSIES Flight Data Processor System Documentation, NWRA-CR-87-R011, Volumes I-V, Northwest Research Associates, Inc., Bellevue, WA, 1987.

[8]   Secan, J.A. Development of Techniques for the Use of DMSP SSIE Data in the AWS 4D Ionosphere Model, AFGL-TR-85-0107(I), Air Force Geophysics Laboratory, Hanscom AFB, MA, April 1985, ADA176412.

[9]   Barghausen, A.F., J.W. Finney, L.L. Proctor, and L.D. Schulz, Predicting Long-Term Operational Parameters of High-Frequency Sky-Wave Telecommunications Systems. ESSA Technical Report ERL 110 - ITS 78, U.S. Government Printing Office, 1969.

[10]   Secan, J.A. and E.J. Fremouw, Improvement of the Scintillation-Irregularity Model in WBMOD, DNA Report DNA-TR-81-241, Defense Nuclear Agency, Washington. DC, 1983.

[11] Weber, E.J., R.T. Tsunoda, J. Buchau, R.E. Sheehan, D.J. Strickland, W. Whiting, and J.G. Moore, "Coordinated Measurements of Auroral Zone Plasma Enhancements," J. Geophys. Res., 90, 6497-6513, 1985.

[12] Keskinen, M.J. "E-Region Effects on F-Layer Structure With Magnetospheric Coupling," presented at the HiLat/Polar BEAR Science Team Meeting, Springfield, MD, 26-27 July 1988.

Appendix A. Plots of SSIES Campaign Data.

This appendix contains plots of the total ion density data collected from the SSIES SM sensor in the six near-overhead passes during the January 1988 SSIES/AIO/EISCAT/AFSAT data collection campaign and a number of scintillation parameters calculated from these data. Included for each pass is the following:

(1) A diagram which shows the relationships in time and location between data collected from the SSIES sensors, the AIO sensors (ionosonde, photometers, and AFSAT receiver), and the EISCAT radar.

(2) A plot of the total ion density from the SM sensor for a 25-minute segment of the DMSP orbit centered on the highest latitude reached in that orbit.

(3) A plot of the total ion density for a 5-minute segment roughly centered on the time at which all-sky photometer images were taken (denoted the AIO time period).

(4) A plot of the detrended ion density data (21.33...-sec detrend period) for the AIO time period.

(5) A plot of the ion density trend for the AIO time period (note - the detrended data was generated by subtracting the trend shown in this plot from the data shown in the total ion density plot).

(6) A plot of the spectral slope parameter (q) for the AIO time period calculated from fits to power-density spectra (PDS) extracted from the detrended density data. The data processing used a 30% cosine window, a seven-point PDS smoother, and a fit over the range 0.5 to 3.0 Hz to determine q and T_1 (see processing details in Appendix B.)

(7) A plot of the C_k estimates calculated from q and T_1 for the AIO time period.

(8) A plot of the $C_k L$ estimates calculated for the AIO time period.

(9) A plot of the effective layer thickness parameter (L_{eff}) used to convert C_k to $C_k L$.

EXPERIMENT GEOMETRY
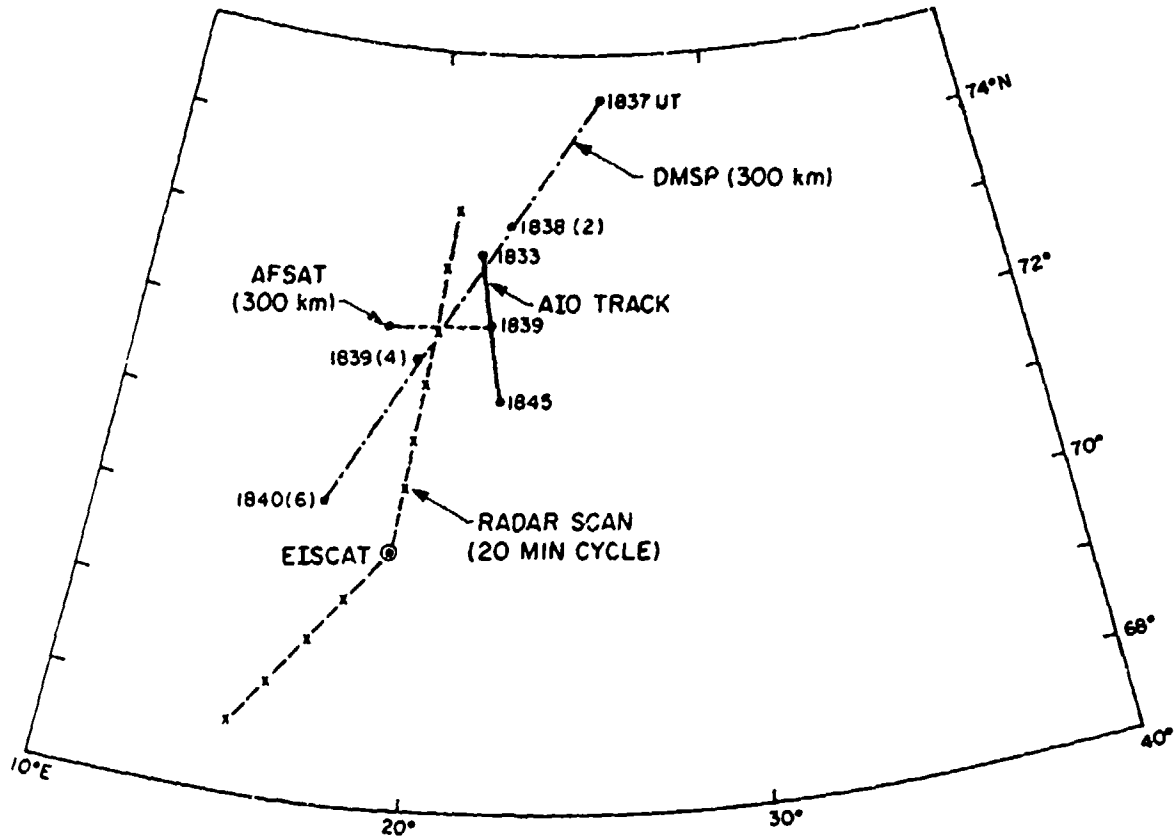
Figure A-01a. Experiment geometry for Rev 2862 on 8 January 1988. Solid line is the Airborne Ionospheric Observatory aircraft ground track, dot-dashed line is the DMSP track mapped down to 300km, and the dash-x line is the EISCAT scan ground track. The location of the 300km penetration point of the AIO-AFSAT line-of-sight for 1839 UT is plotted. Locations are in geographic coordinates and all times are UT.

AIO Time Period: 18:36:30 to 18:41:30

K_p: 3 ΣK_p: 28

SSN: 57

Average SSN: 38.0 (7-day)   40.6 (90-day)
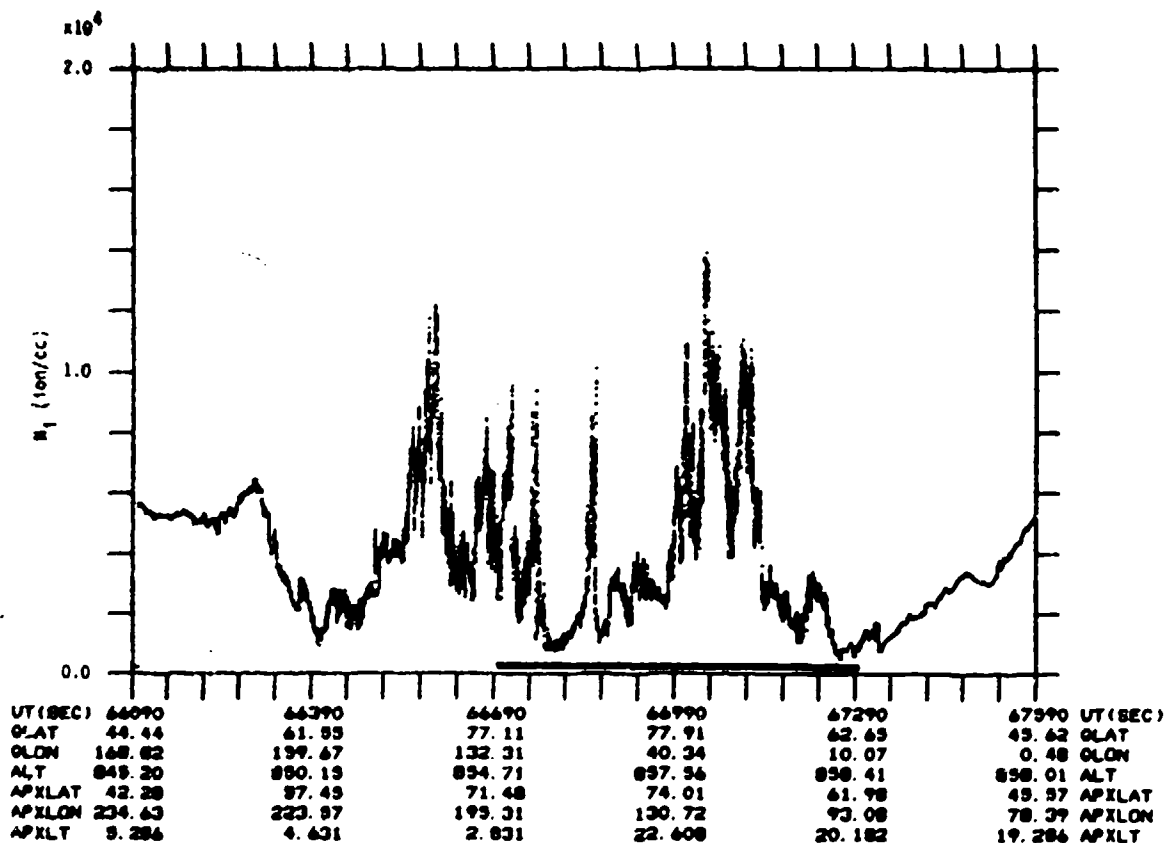
Figure A-01b. Total ion density, entire polar cap section of Rev 2862 (8 Jan 88). The heavy line indicates AIO-EISCAT section of pass.
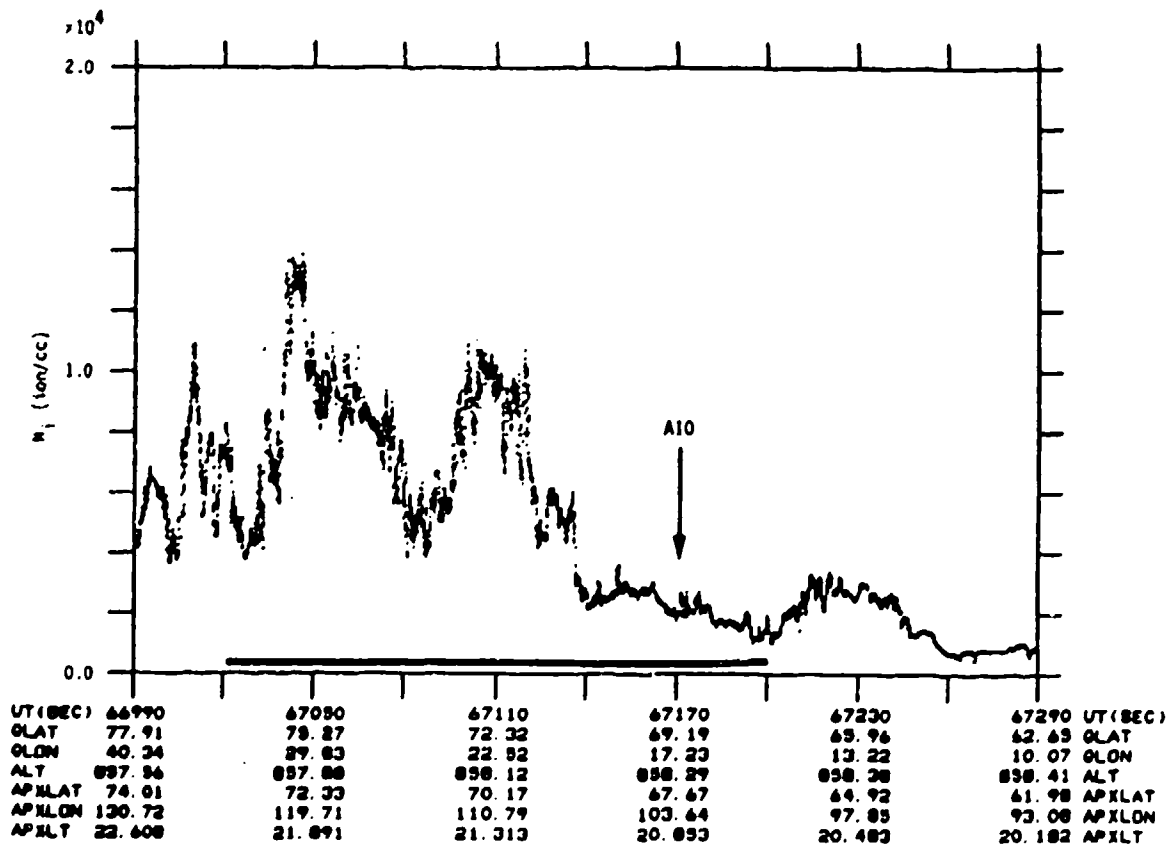
Figure A-01c. Total ion density, AIO-EISCAT section of Rev 2862 (8 Jan 88). The heavy line indicates section of pass shown in Figure A-01a; arrow indicates point of nearest spatial/temporal coincidence with AIO observations.
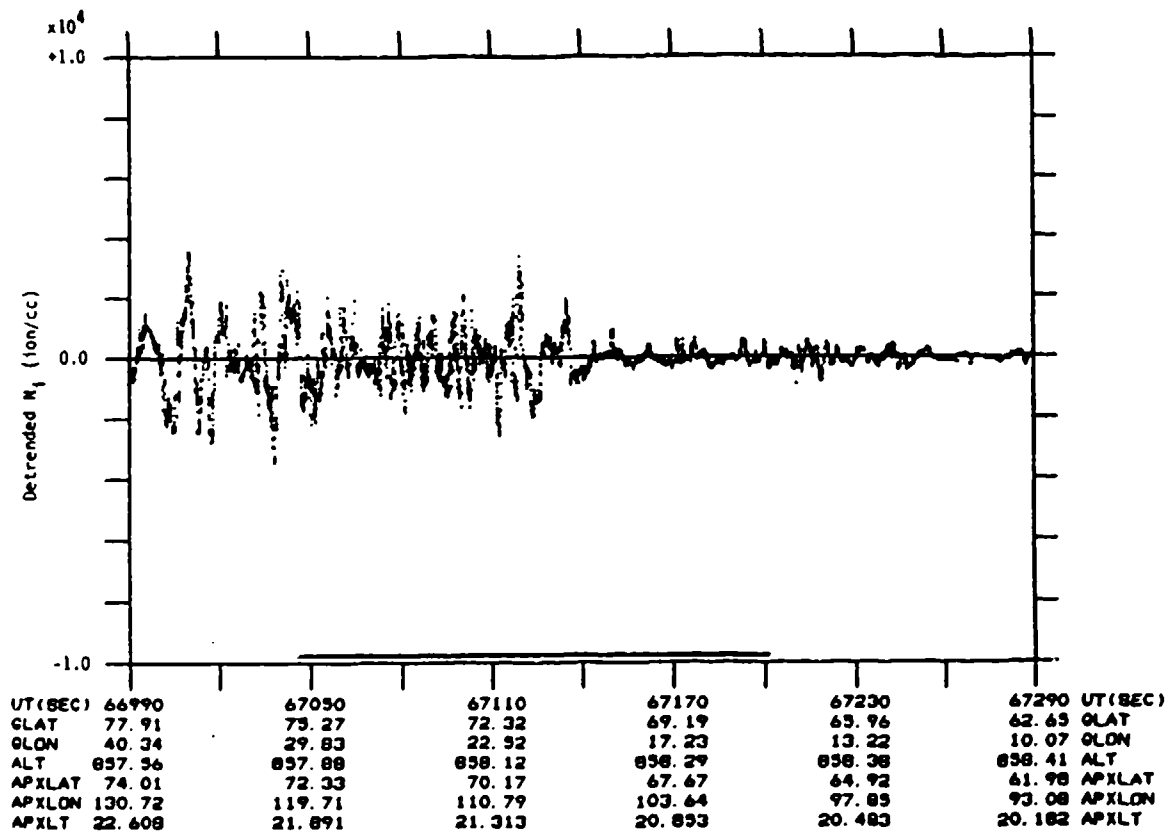
Figure A-01d. Detrended ion density for AIO-EISCAT section of Rev 2862 (8 Jan 88). Detrender cutoff frequency of was 0.046875 Hz.
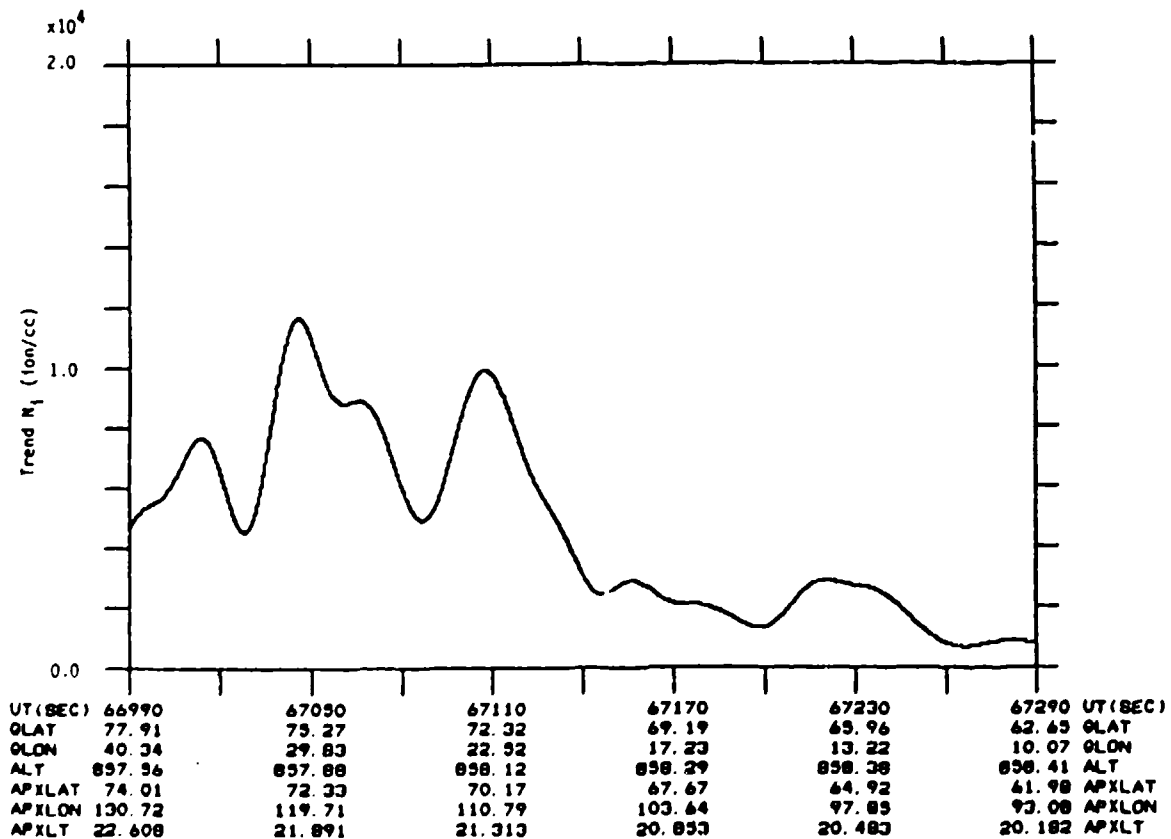
Figure A-01e. Ion density trend for AIO-EISCAT section of Rev 2862 (8 Jan 88). Detrender cutoff frequency of was 0.046875 Hz.

A-4
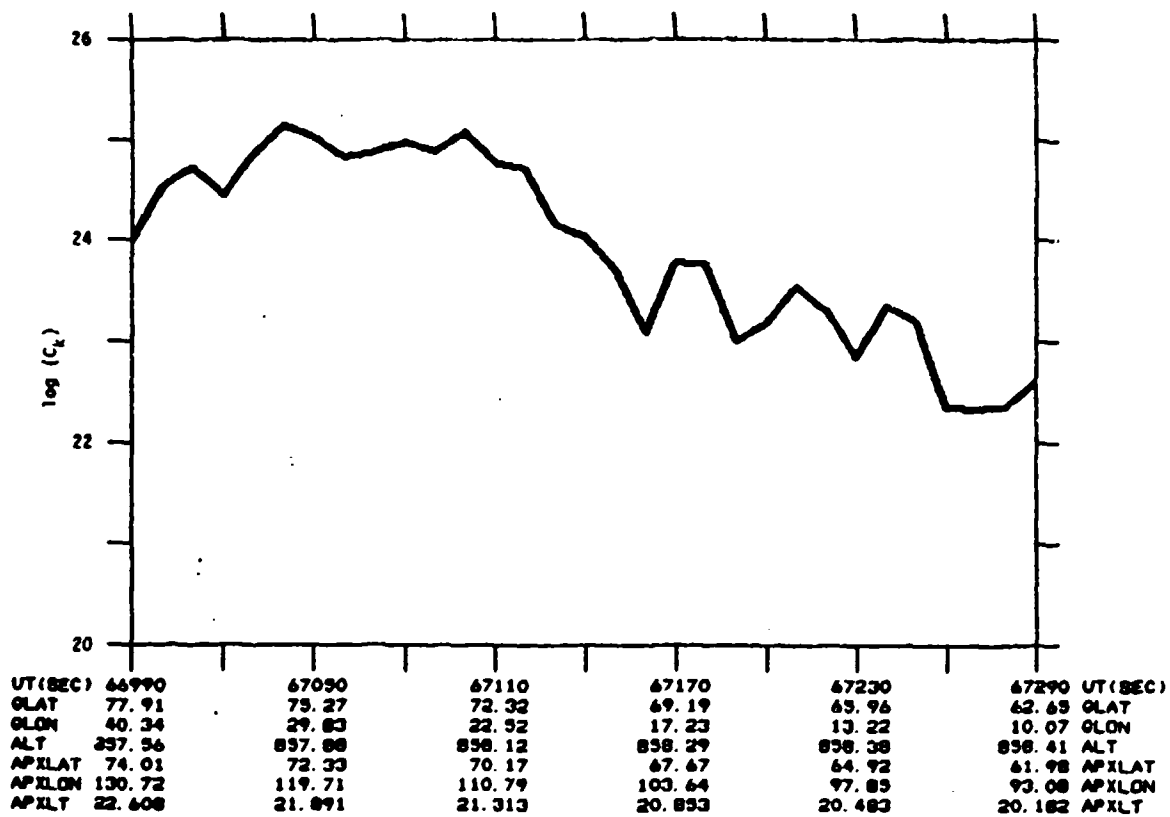
Figure A-01f. Results of C_k analysis for AIO-EISCAT section of Rev 2862 (8 Jan 88).

UT(SEC)	66990	67090	67110	67170	67230	67290	UT(SEC)
GLAT	77.91	75.27	72.32	69.19	65.96	62.65	GLAT
GLON	40.34	29.83	22.52	17.23	13.22	10.07	GLON
ALT	857.56	857.88	858.12	858.29	858.38	858.41	ALT
APXLAT	74.01	72.33	70.17	67.67	64.92	61.98	APXLAT
APXLON	130.72	119.71	110.79	103.64	97.85	93.08	APXLON
APXLT	22.608	21.891	21.313	20.893	20.483	20.182	APXLT
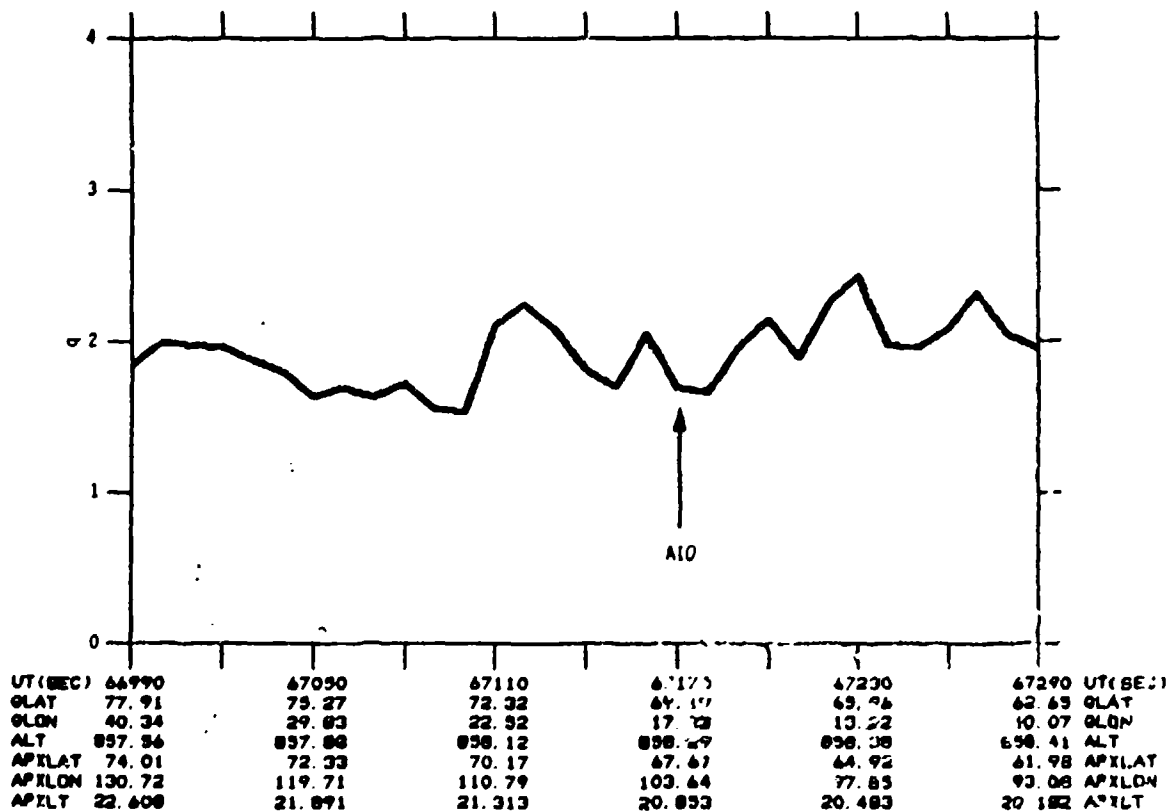
Figure A-01g. Spectral slope (q) for AIO-EISCAT section of Rev 2862 (8 Jan 88).

UT(SEC)	66990	67090	67110	67170	67230	67290	UT(SEC)
GLAT	77.91	75.27	72.32	69.19	65.96	62.65	GLAT
GLON	40.34	29.83	22.52	17.23	13.22	10.07	GLON
ALT	857.56	857.88	858.12	858.29	858.38	858.41	ALT
APXLAT	74.01	72.33	70.17	67.67	64.92	61.98	APXLAT
APXLON	130.72	119.71	110.79	103.64	77.85	93.08	APXLON
APXLT	22.608	21.891	21.313	20.893	20.483	20.182	APXLT

A-5

UT(SEC)	66990	67050	67110	6717C	67230	67290	UT(SEC)
GLAT	78.43	75.92	73.10	70.09	66.99	63.82	GLAT
GLON	40.82	30.08	22.61	17.20	13.12	9.92	GLON
ALT	857.56	857.88	858.12	858.29	858.38	858.41	ALT
APXLAT	74.01	72.33	70.17	67.68	64.93	62.00	APXLAT
APXLON	130.78	119.73	110.76	103.56	97.78	93.07	APXLON
APXLT	22.612	21.892	21.310	20.847	20.478	20.181	APXLT

** LOCATIONS TRACED DOWN TO AN ALTITUDE OF 350KM ***

Figure A-01h. C_kL for AIO-EISCAT section of Rev 2862 (8 Jan 88).

UT(SEC)	66990	67050	67110	67170	67230	67290	UT(SEC)
GLAT	78.43	75.92	73.10	70.09	66.99	63.82	GLAT
GLON	40.82	30.08	22.61	17.20	13.12	9.92	GLON
ALT	857.56	857.88	858.12	858.29	858.38	858.41	ALT
APXLAT	74.01	72.33	70.17	67.68	64.93	62.00	APXLAT
APXLON	130.78	119.73	110.76	103.56	97.78	93.07	APXLON
APXLT	22.612	21.892	21.310	20.847	20.478	20.181	APXLT

** LOCATIONS TRACED DOWN TO AN ALTITUDE OF 350KM ***
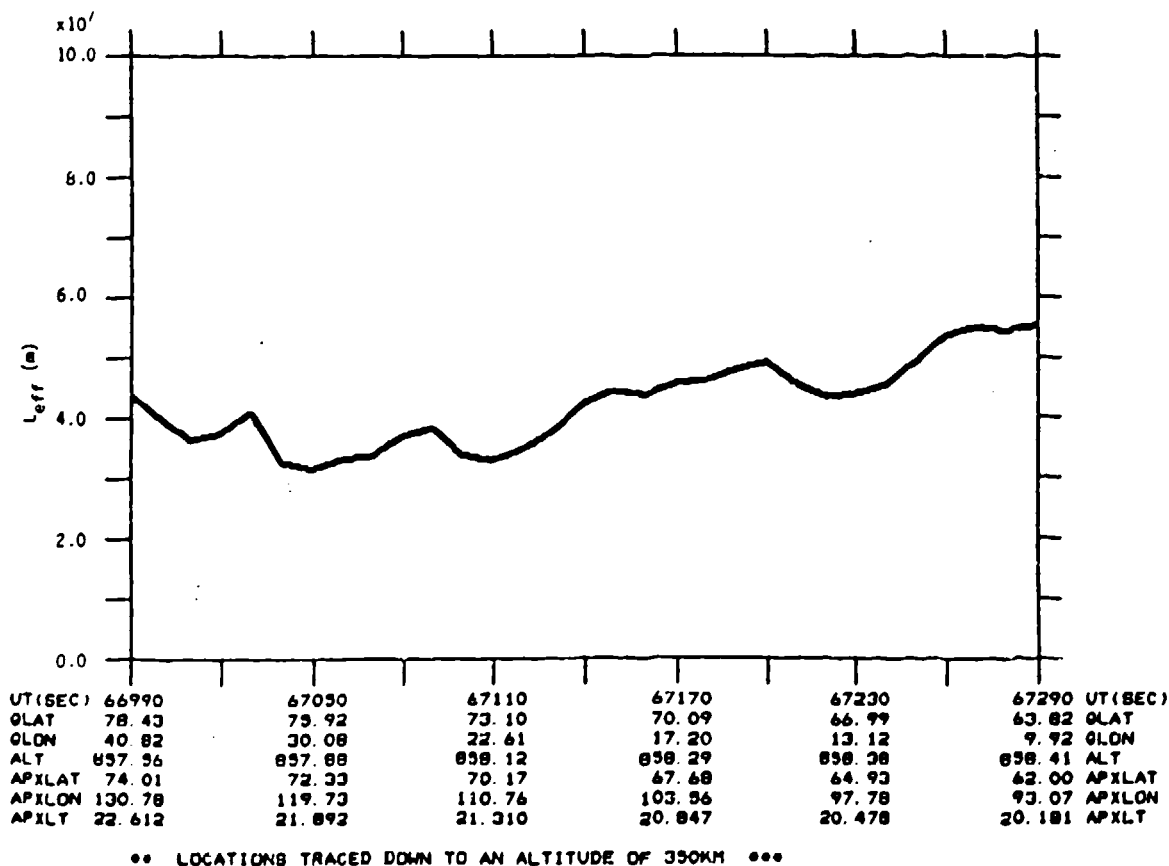
Figure A-01i. Effective layer thickness (L_{eff}) used to convert C_k to C_kL for AIO-EISCAT section of Rev 2862 (8 Jan 88).

A-6

EXPERIMENT GEOMETRY
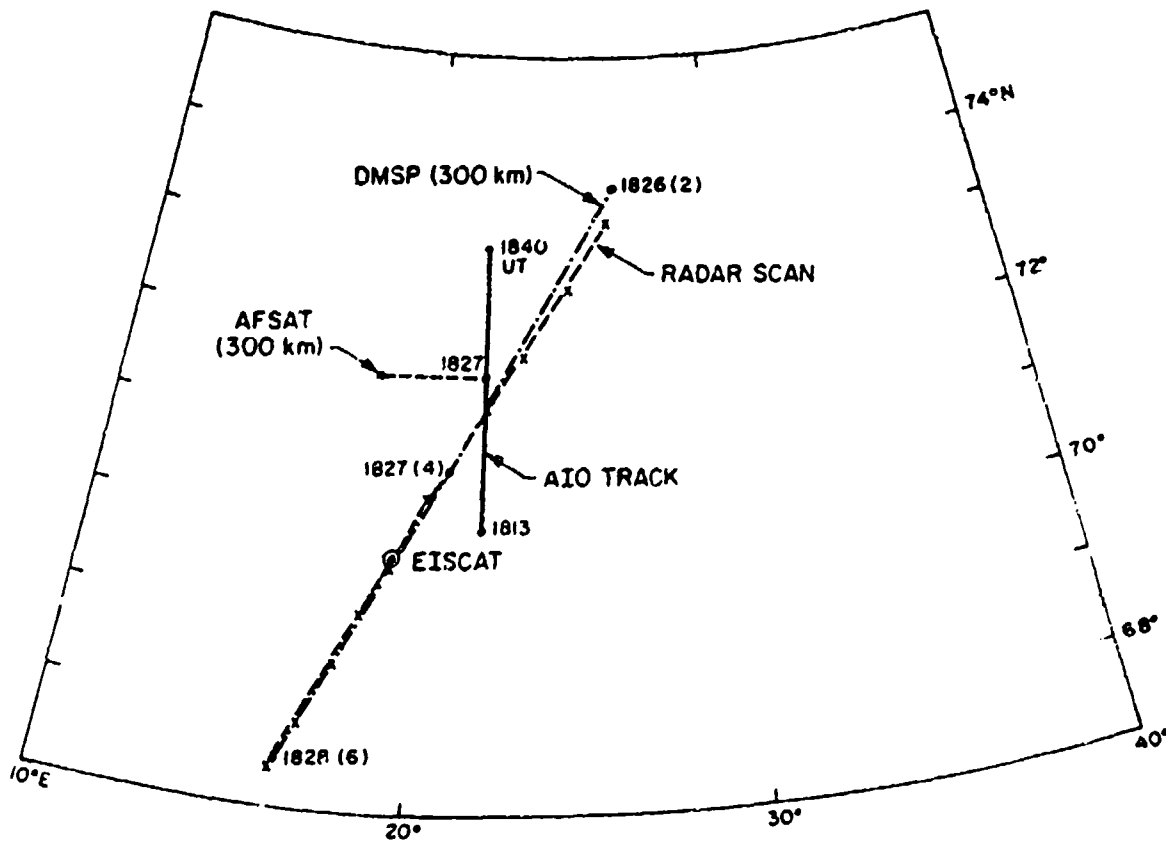
Figure A-02a. Experiment geometry for Rev 2876 on 9 January 1988. Solid line is the Airborne Ionospheric Observatory aircraft ground track, dot-dashed line is the DMSP track mapped down to 300km, and the dash-x line is the EISCAT scan ground track. The location of the 300km penetration point of the AIO-AFSAT line-of-sight for 1827 UT is plotted. Locations are in geographic coordinates and all times are UT.

AIO Time Period: 18:24:30 to 18:29:30

K_p: 1 ΣK_p: 14 +

SSN: 62

Average SSN: 42.4 (7-day)   40.9 (90-day)
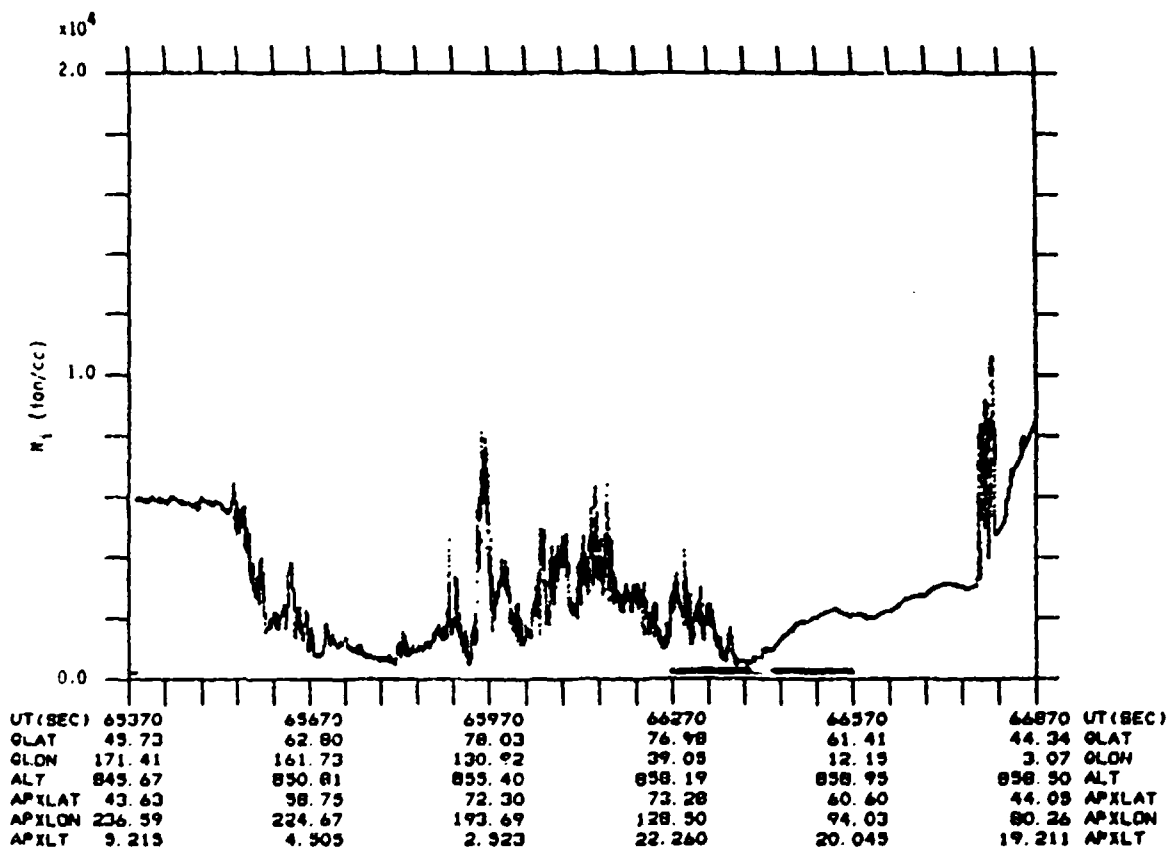
Figure A-02b. Total ion density, entire polar cap section of Rev 2876 (9 Jan 88). The heavy line indicates AIO-EISCAT section of pass.
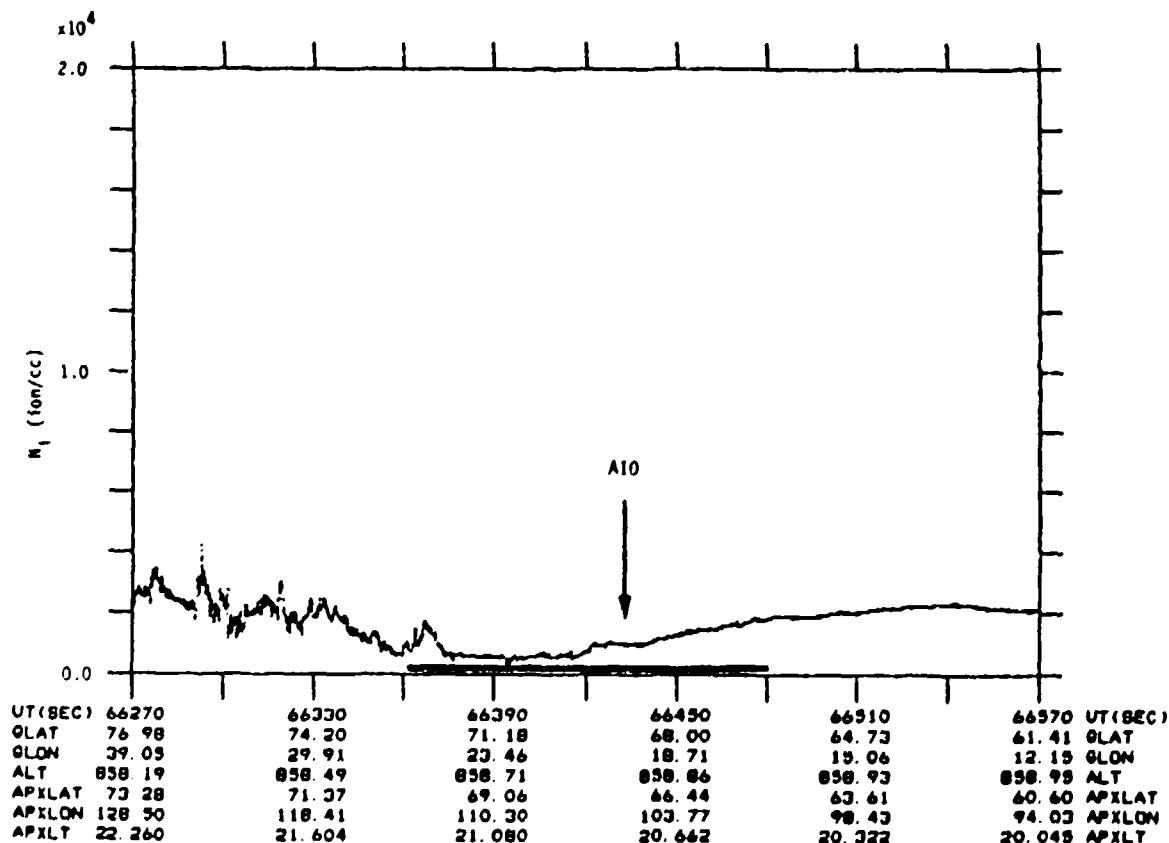
Figure A-02c. Total ion density, AIO-EISCAT section of Rev 2876 (9 Jan 88). The heavy line indicates section of pass shown in Figure A-02a; arrow indicates point of nearest spatial/temporal coincidence with AIO observations.

A-8
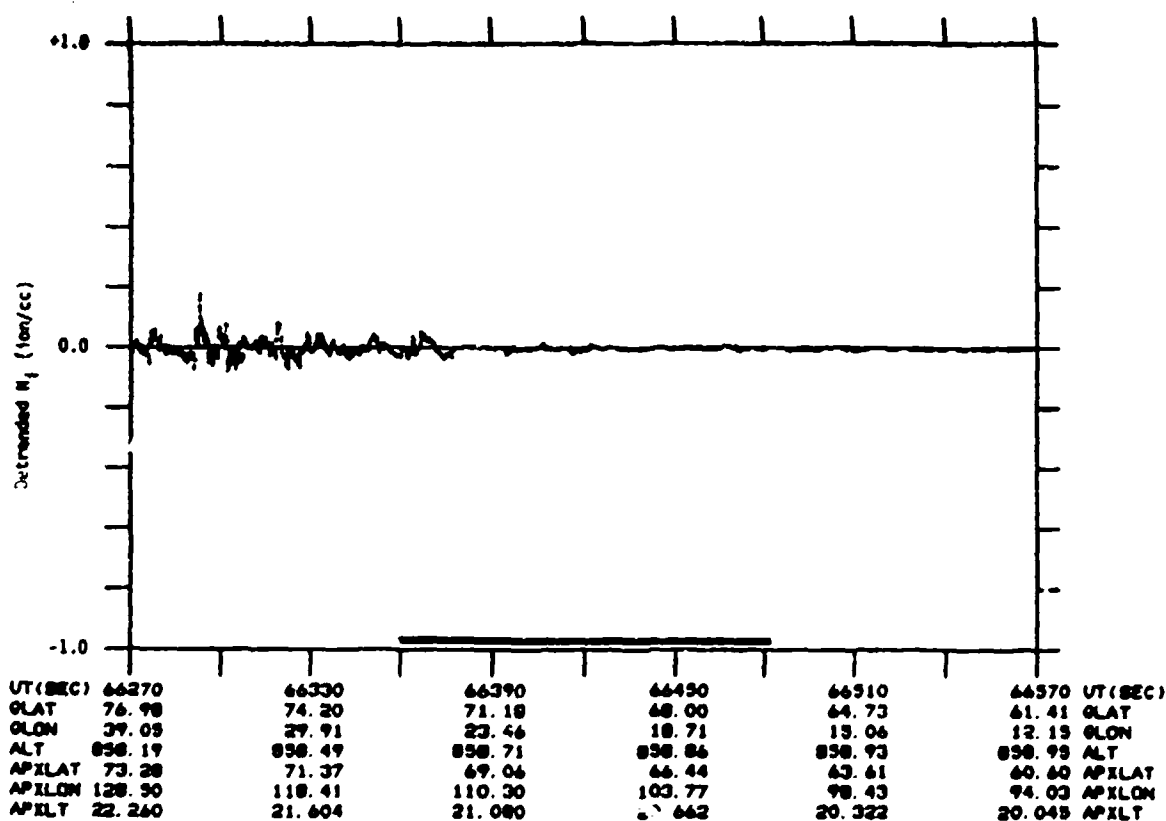
Figure A-02d. Detrended ion density for AIO-EISCAT section of Rev 2876 (9 Jan 88). Detrender cutoff frequency was 0.046875 Hz.

Figure A-02e. Ion density trend for AIO-EISCAT section of Rev 2876 (9 Jan 88). Detrender cutoff frequency was 0.046875 Hz.

A-9

UT(SEC)	66270	66330	66390	66450	66510	66570	UT(SEC)
GLAT	76.58	74.20	71.18	68.00	64.73	61.41	GLAT
GLON	39.05	29.91	23.46	18.71	15.06	12.15	GLON
ALT	858.19	858.49	858.71	858.86	858.93	858.95	ALT
APXLAT	73.28	71.37	69.06	66.44	63.61	60.60	APXLAT
APXLON	128.50	118.41	110.30	103.77	98.43	94.03	APXLON
APXLT	22.260	21.604	21.080	20.662	20.322	20.045	APXLT

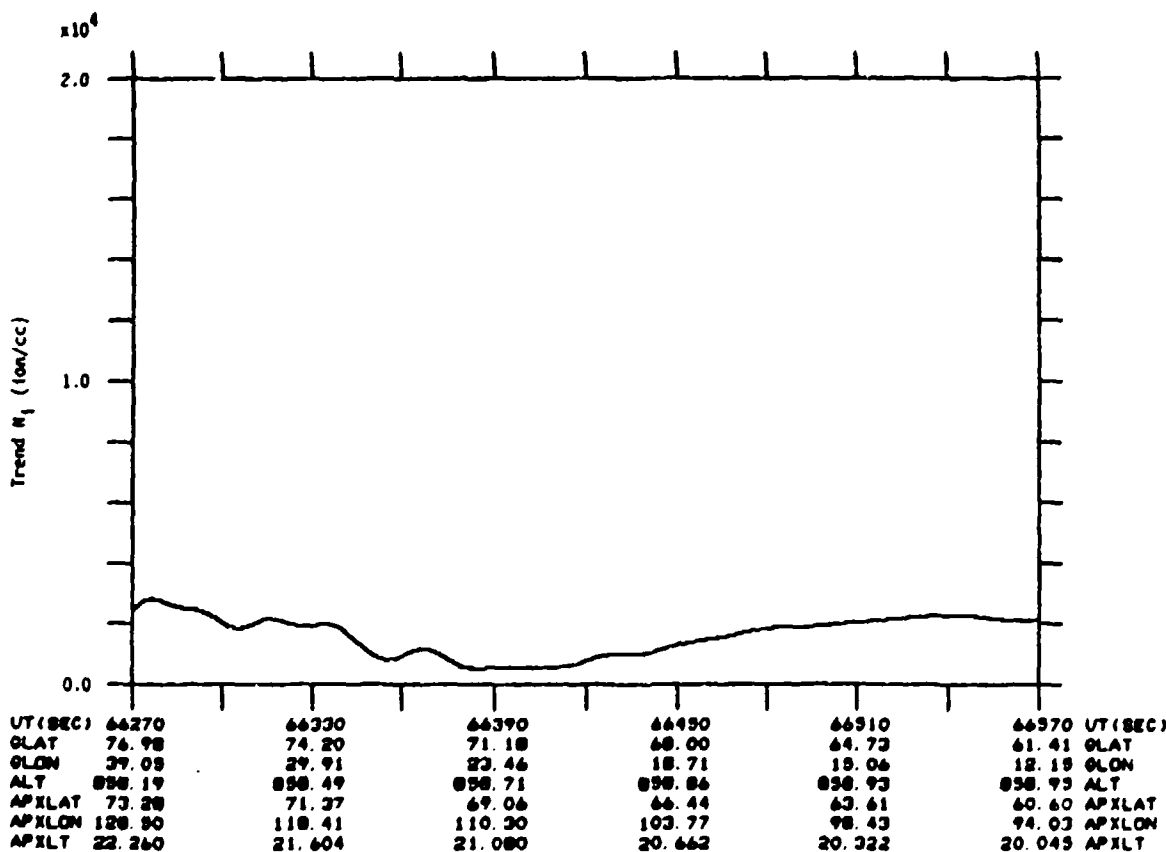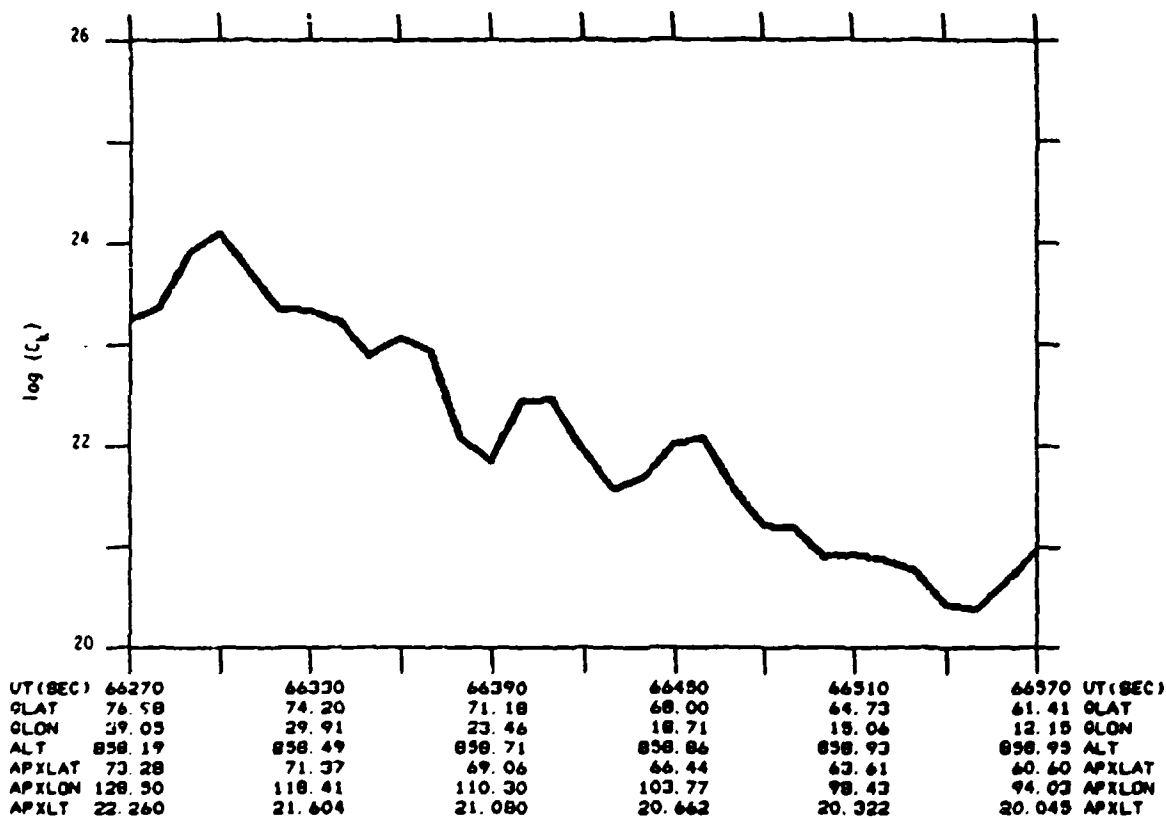Figure A-02f. Results of C_k analysis for AIO-EISCAT section of Rev 2876 (9 Jan 88).

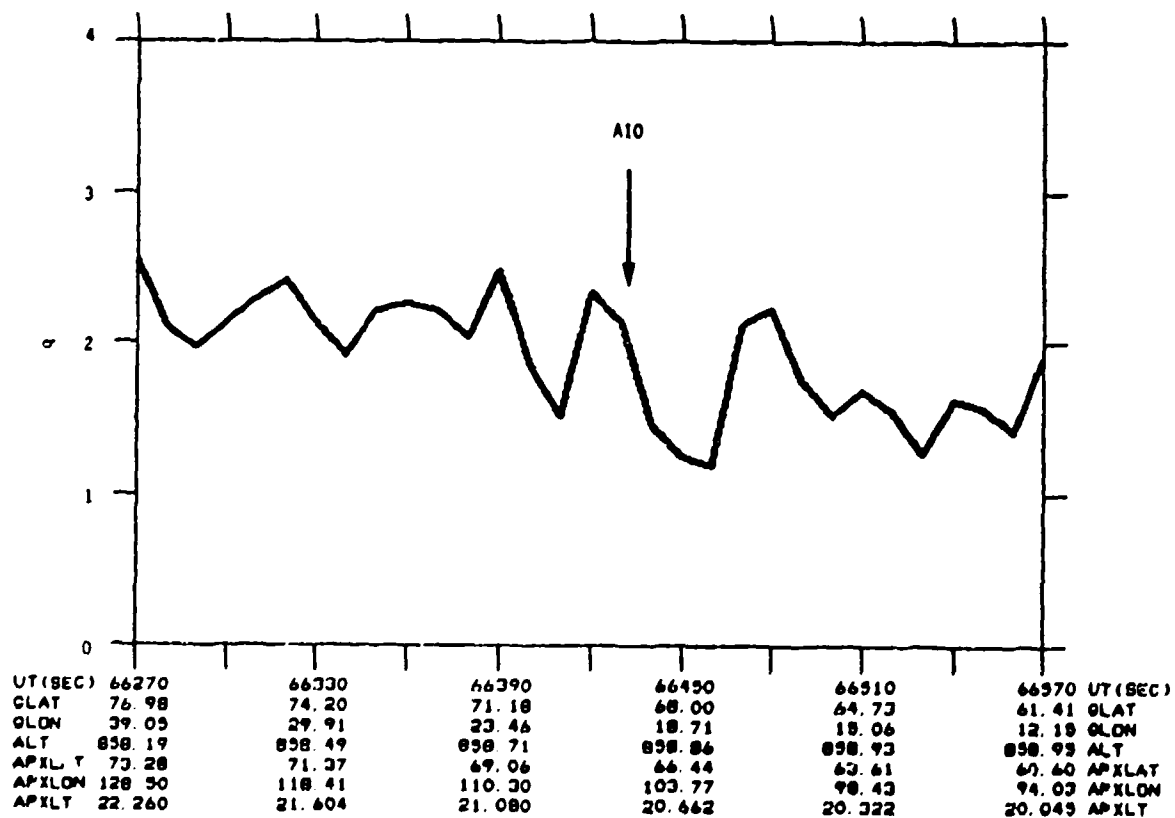| UT(SEC)	66270	66330	66390	66450	66510	66570	UT(SEC)
GLAT	76.98	74.20	71.18	68.00	64.73	61.41	GLAT
GLON	39.05	29.91	23.46	18.71	15.06	12.19	GLON
ALT	858.19	858.49	858.71	858.86	858.93	858.93	ALT
APXLAT	73.28	71.37	69.06	66.44	63.61	60.60	APXLAT
APXLON	128.50	118.41	110.30	103.77	98.43	94.03	APXLON
APXLT	22.260	21.604	21.080	20.662	20.322	20.049	APXLT

Figure A-02g. Spectral slope (q) for AIO-EISCAT section of Rev 2876 (9 Jan 88).
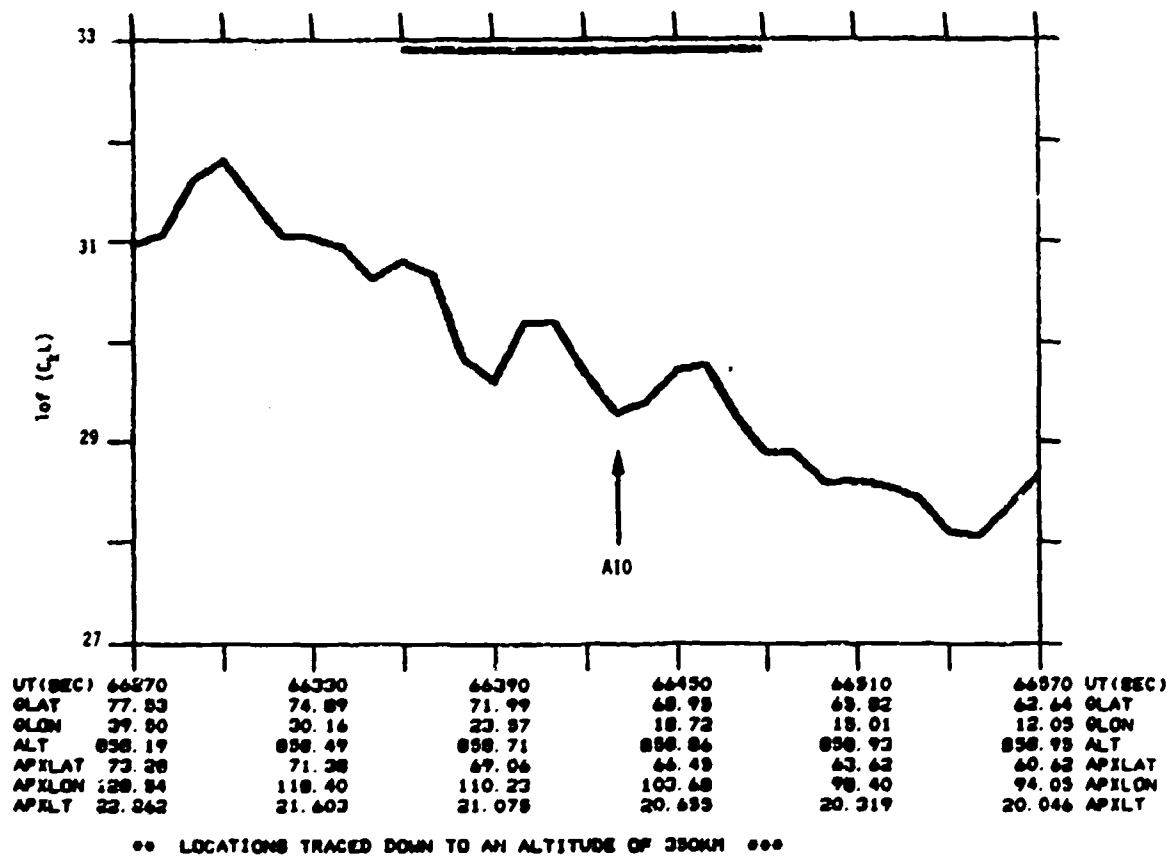
Figure A-02h. C_kL for AIO-EISCAT section of Rev 2876 (9 Jan 88).
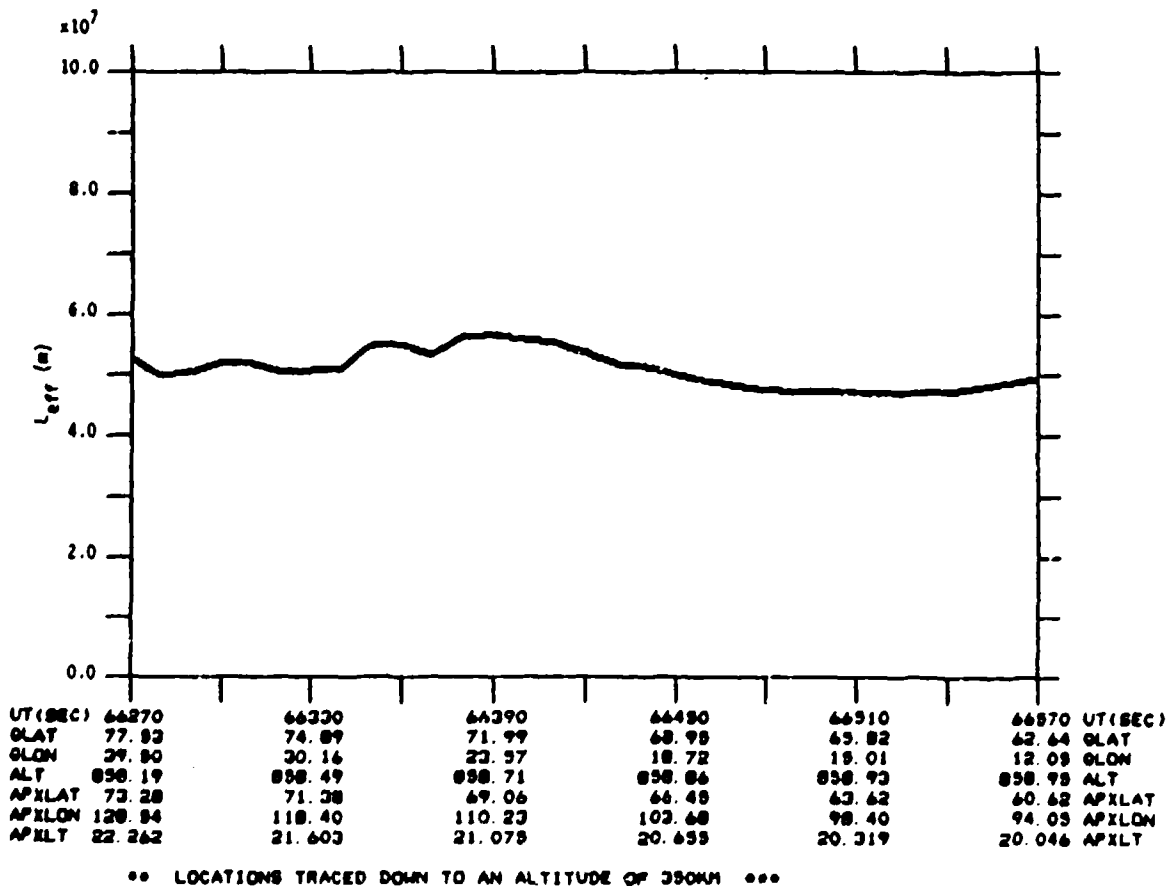
Figure A-02i. Effective layer thickness (L_{eff}) used to convert C_k to C_kL for AIO-EISCAT section of Rev 2876 (9 Jan 88).

A-11

EXPERIMENT GEOMETRY
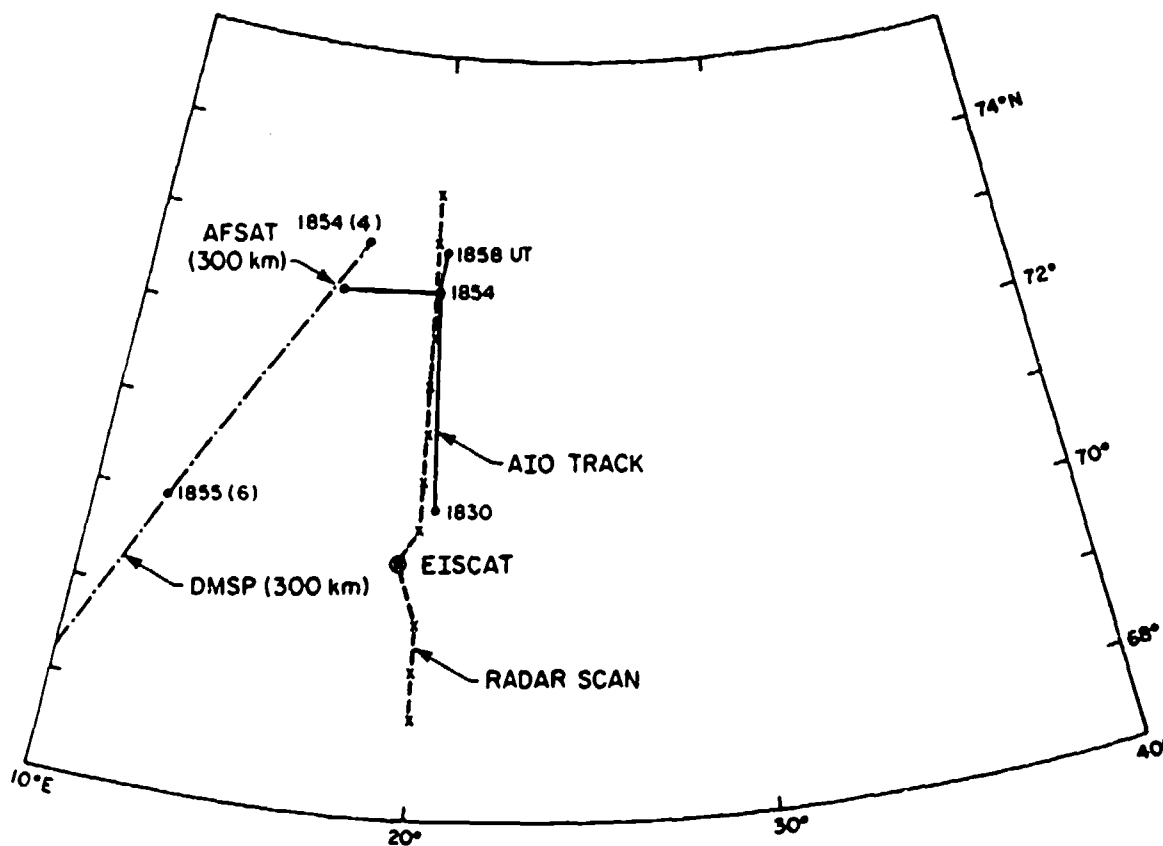
Figure A-03a. Experiment geometry for Rev 2961 on 15 January 1988. Solid line is the Airborne Ionospheric Observatory aircraft ground track, dot-dashed line is the DMSP track mapped down to 300km, and the dash-x line is the EISCAT scan ground track. The location of the 300km penetration point of the AIO-AFSAT line-of-sight for 1854 UT is plotted. Locations are in geographic coordinates and all times are UT.

AIO Time Period: 18:51:30 to 18:56:30

K_p: 3. ΣK_p. 42 +

SSN: 90

Average SSN: 75.6 (7-day)   43.1 (90-day)
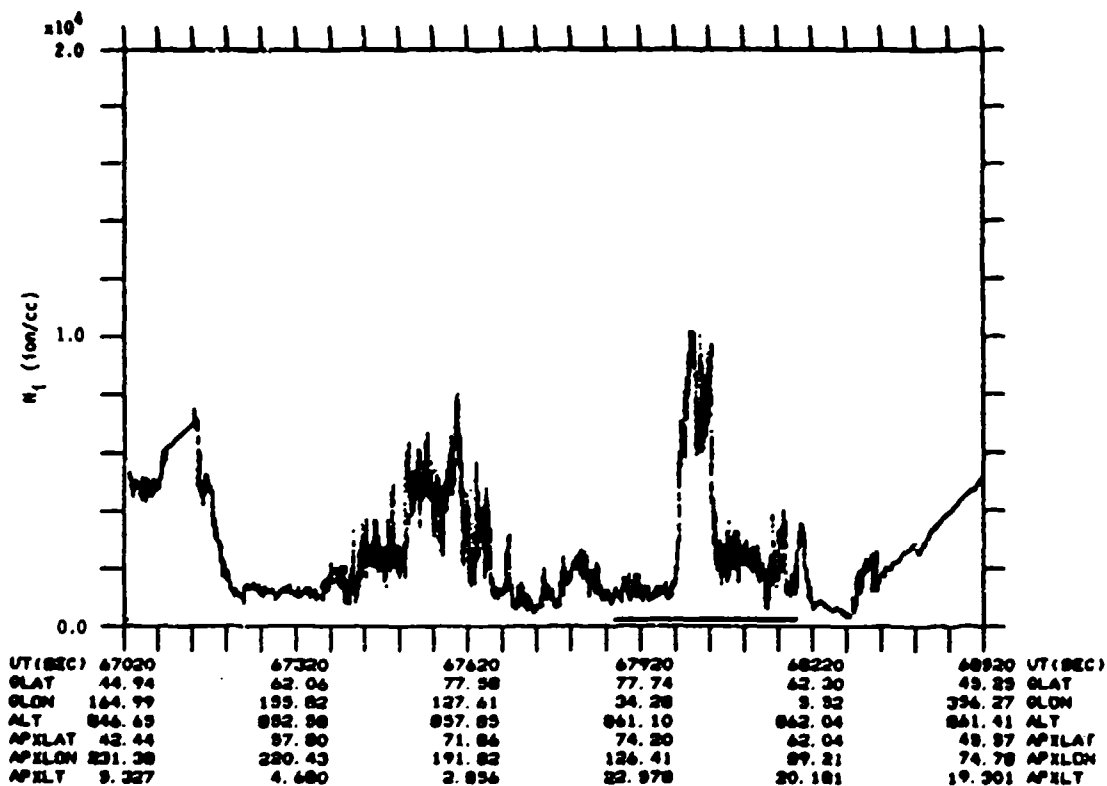
Figure A-03b. Total ion density, entire polar cap section of Rev 2961 (15 Jan 88). The heavy line indicates AIO-EISCAT section of pass.
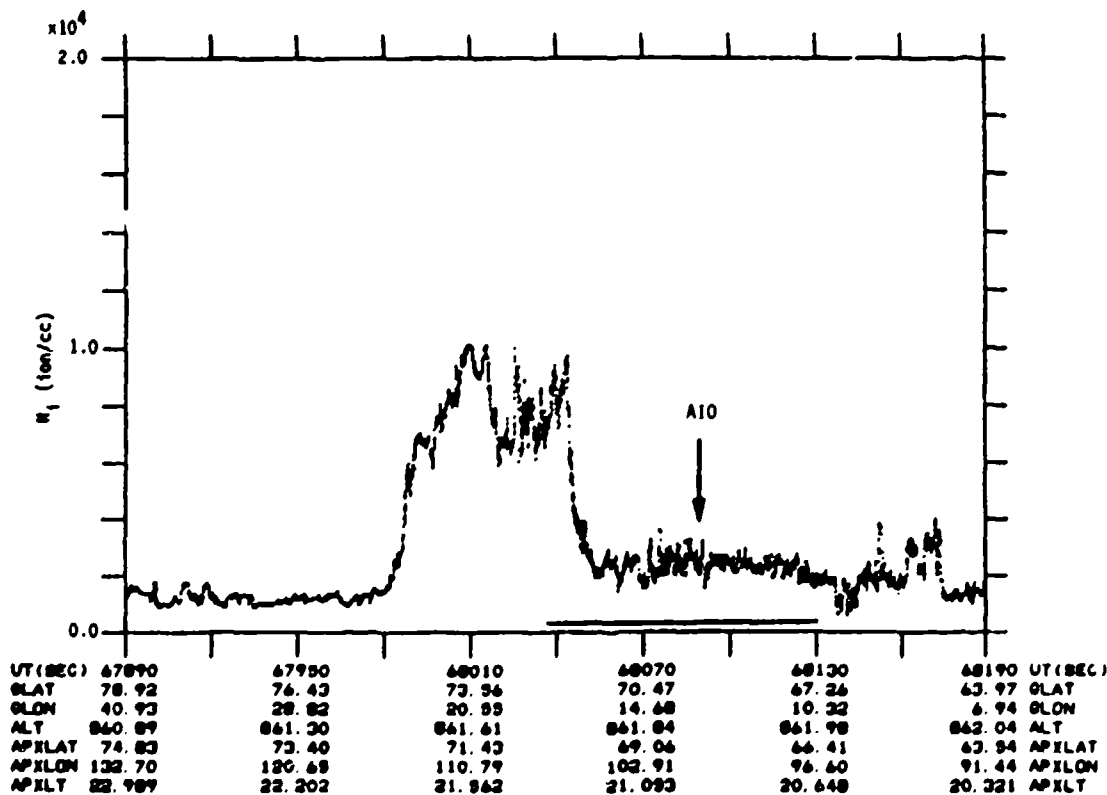
Figure A-03c. Total ion density, AIO-EISCAT section of Rev 2961 (15 Jan 88). The heavy line indicates section of pass shown in Figure A-03a; arrow indicates point of nearest spatial/temporal coincidence with AIO observations.
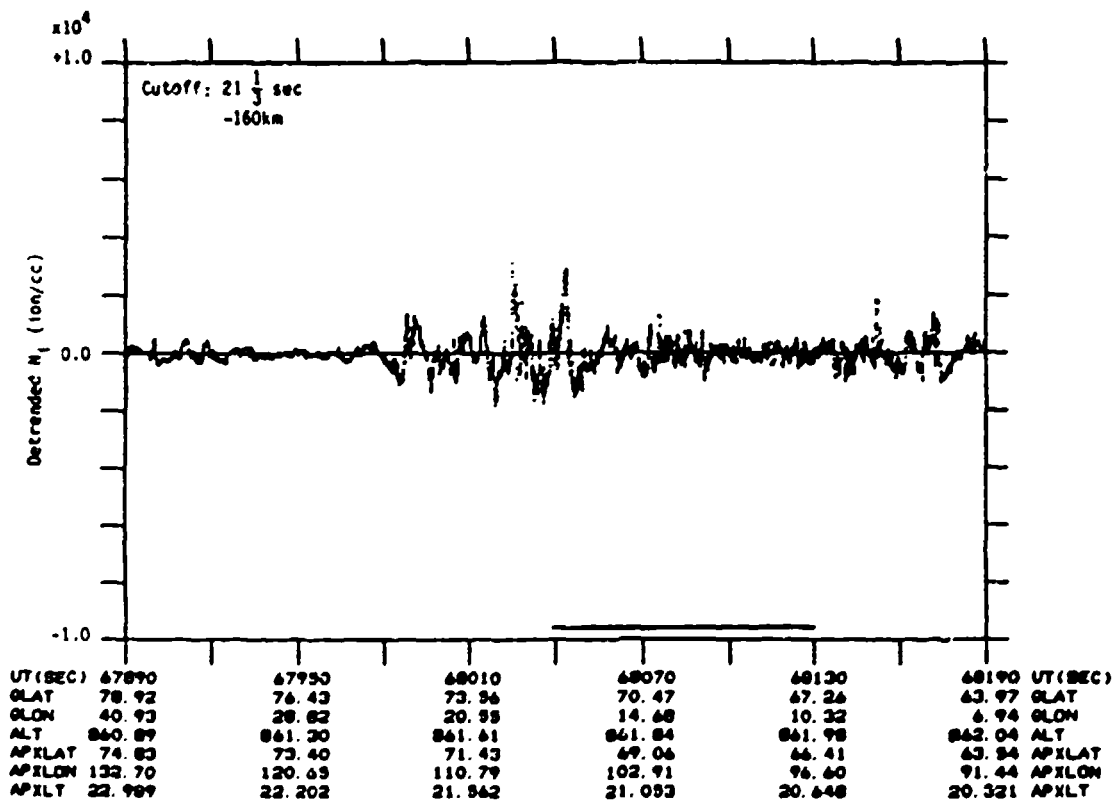
Figure A-03d. Detrended ion density for AIO-EISCAT section of Rev 2961 (15 Jan 88). Detrender cutoff frequency was 0.046875 Hz.
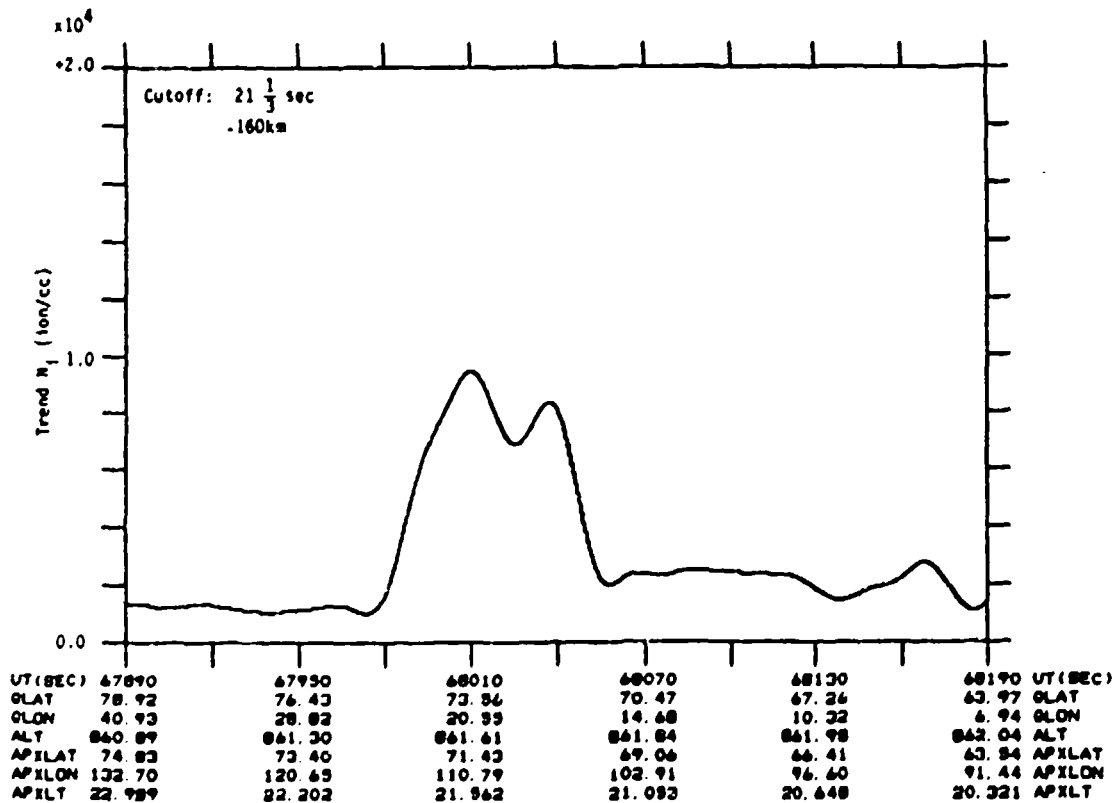
Figure A-03e. Ion density trend for AIO-EISCAT section of Rev 2961 (15 Jan 88). Detrender cutoff frequency was 0.046875 Hz.
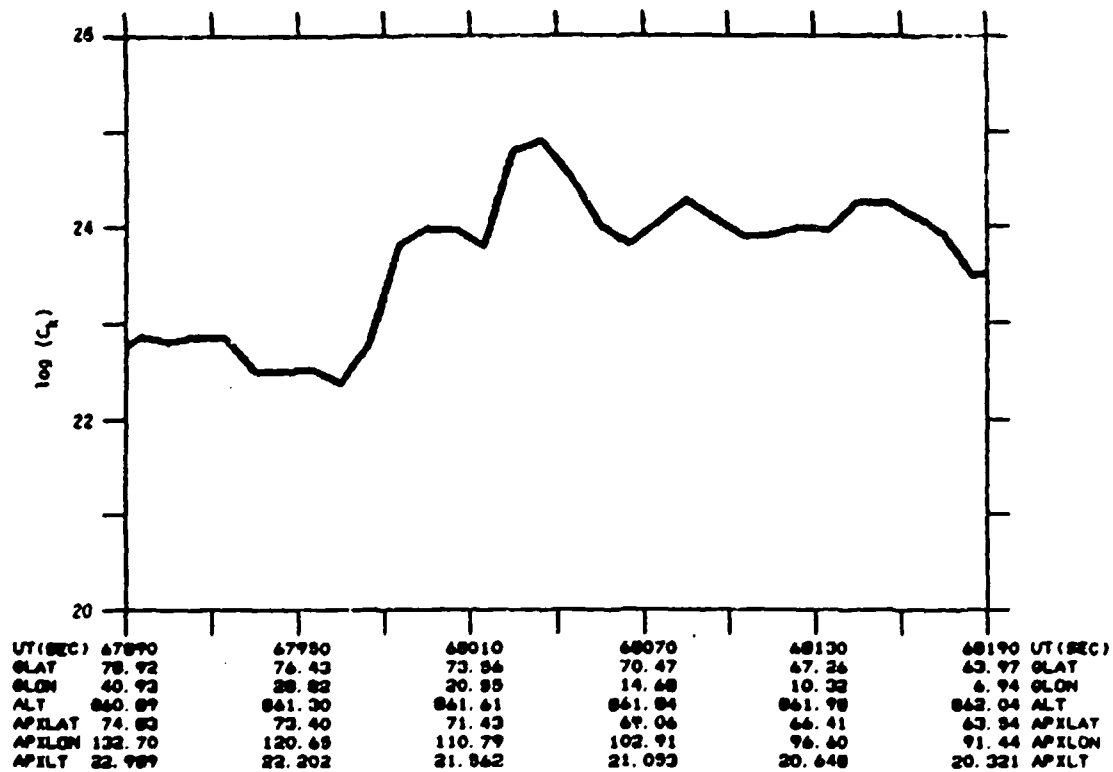
Figure A-03f. Results of C_k analysis for AIO-EISCAT section of Rev 2961 (15 Jan 88).

Figure A-03g. Spectral slope (q) for AIO-EISCAT section of Rev 2961 (15 Jan 88).

Figure A-03h. C_kL for AIO-EISCAT section of Rev 2961 (15 Jan 88).

| UT(SEC)	67890	67950	68010	68070	68130	68190	UT(SEC)
GLAT	79.41	77.04	74.29	71.33	68.25	65.09	GLAT
GLON	41.42	29.04	20.58	14.58	10.14	6.71	GLON
ALT	860.89	861.30	861.61	861.84	861.98	862.04	ALT
APXLAT	74.84	73.41	71.44	69.07	66.42	63.56	APXLAT
APXLON	132.79	120.72	110.81	102.87	96.33	91.41	APXLON
APXLT	22.995	22.206	21.562	21.049	20.643	20.319	APXLT

Figure A-03i. Effective layer thickness (L_{eff}) used to convert C_k to C_kL for AIO-EISCAT section of Rev 2961 (15 Jan 88).

A-16

EXPERIMENT GEOMETRY
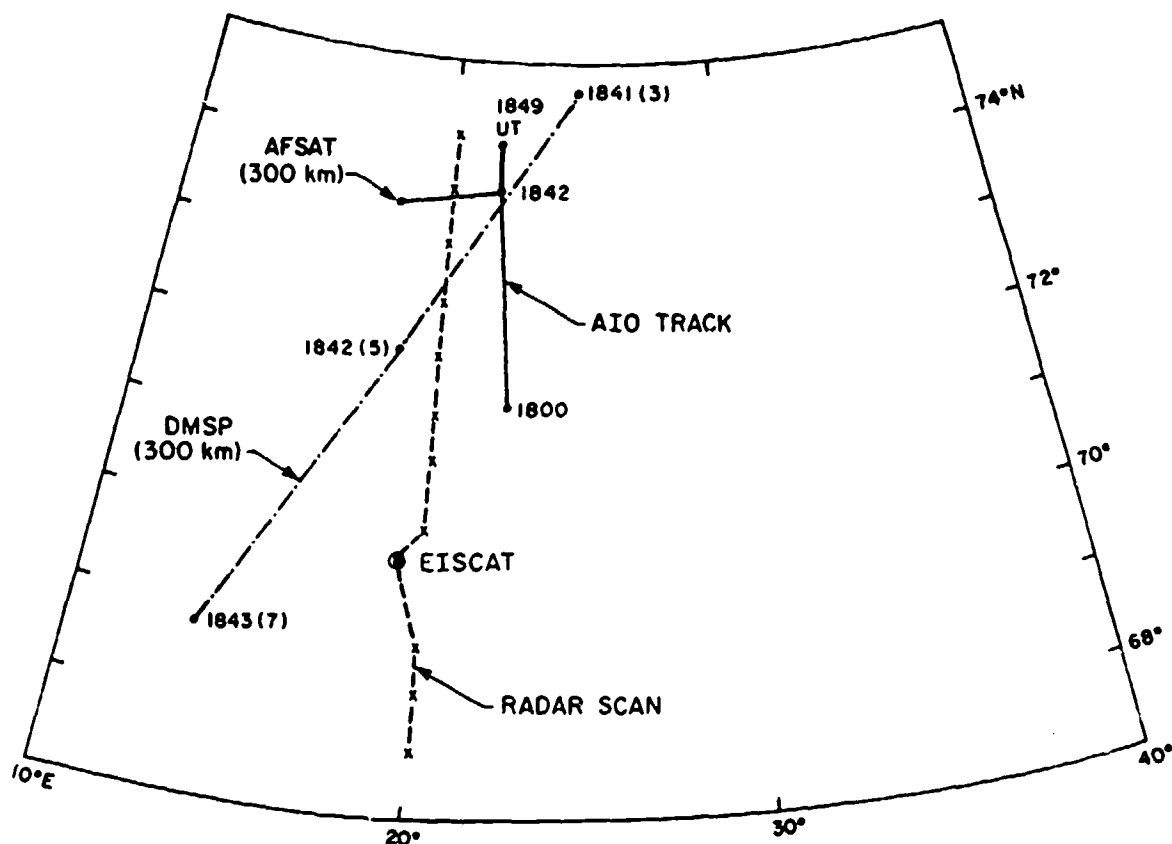
Figure A-04a. Experiment geometry for Rev 2975 on 16 January 1988. Solid line is the Airborne Ionospheric Observatory aircraft ground track, dot-dashed line is the DMSP track mapped down to 300km, and the dash-x line is the EISCAT scan ground track. The location of the 300km penetration point of the AIO-AFSAT line-of-sight for 1842 UT is plotted. Locations are in geographic coordinates and all times are UT.

AIO Time Period: 18:39:00 to 18:44:00

K_p: 1- ΣK_p: 12+
SSN: 83
Average SSN: 78.6 (7-day)   43.6 (90-day)
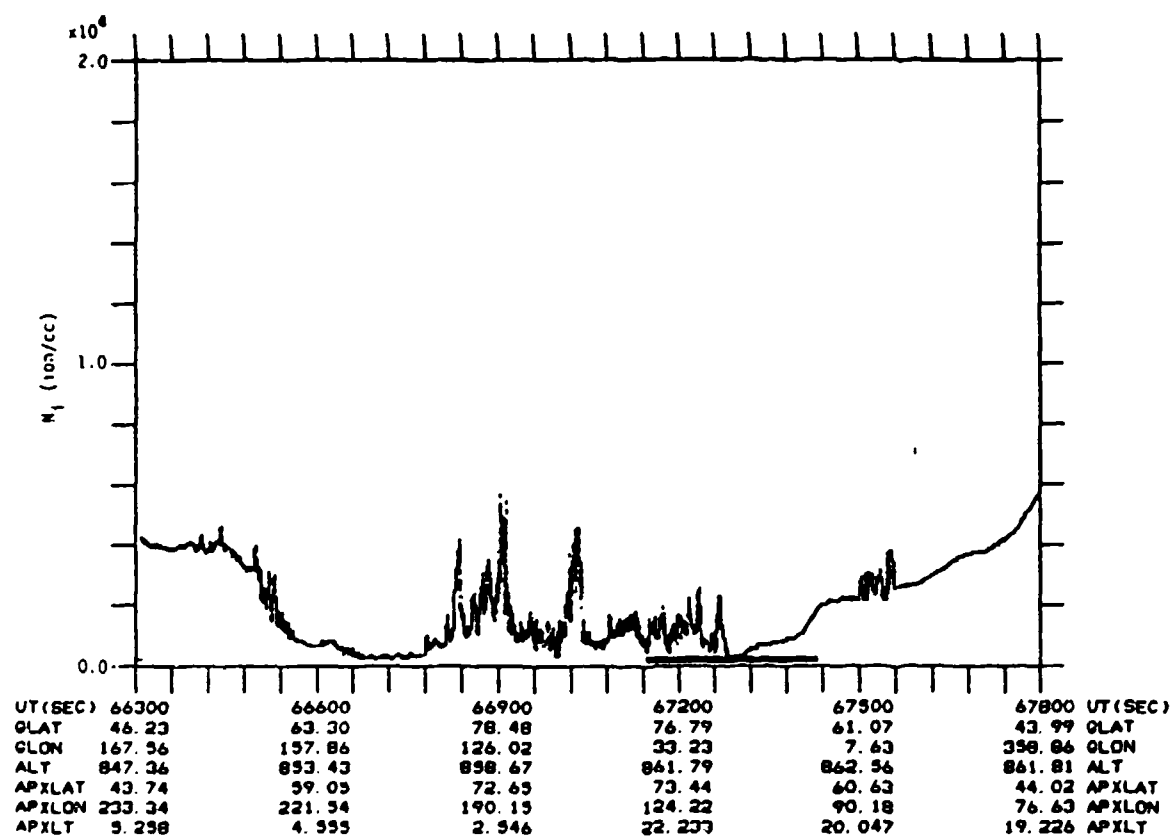
Figure A-04b. Total ion density. entire polar cap section of Rev 2975 (16 Jan 88). The heavy line indicates AIO-EISCAT section of pass.

UT(SEC)	66300	66600	66900	67200	67500	67800	UT(SEC)
GLAT	46.23	63.30	78.48	76.79	61.07	43.99	GLAT
GLON	167.56	157.86	126.02	33.23	7.63	358.86	GLON
ALT	847.36	853.43	858.67	861.79	862.56	861.81	ALT
APXLAT	43.74	59.05	72.65	73.44	60.63	44.02	APXLAT
APXLON	233.34	221.54	190.15	124.22	90.18	76.63	APXLON
APXLT	5.298	4.555	2.546	22.233	20.047	19.226	APXLT
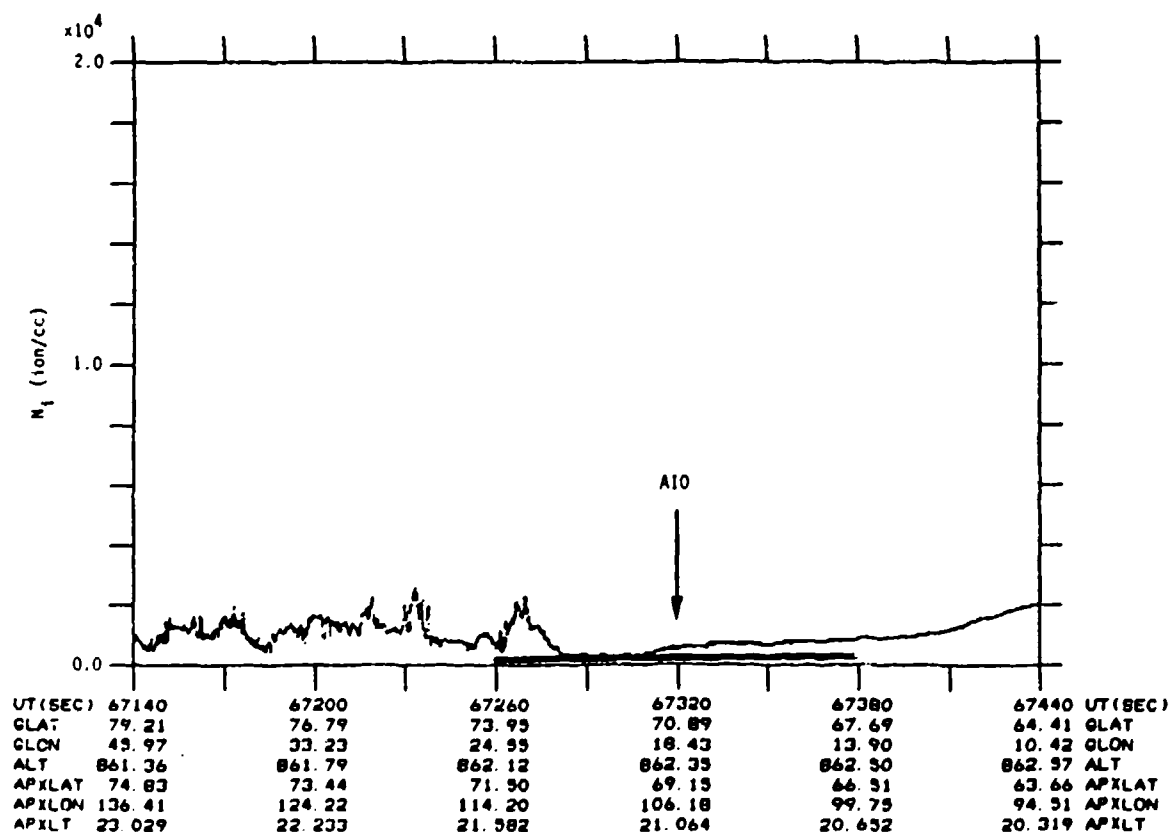
Figure A-04c. Total ion density, AIO-EISCAT section of Rev 2975 (16 Jan 88). The heavy line indicates section of pass shown in Figure A-04a; arrow indicates point of nearest spatial/temporal coincidence with AIO observations.

UT(SEC)	67140	67200	67260	67320	67380	67440	UT(SEC)
GLAT	79.21	76.79	73.93	70.89	67.69	64.41	GLAT
GLON	45.97	33.23	24.55	18.43	13.90	10.42	GLON
ALT	861.36	861.79	862.12	862.35	862.50	862.97	ALT
APXLAT	74.83	73.44	71.50	69.15	66.51	63.66	APXLAT
APXLON	136.41	124.22	114.20	106.18	99.75	94.51	APXLON
APXLT	23.029	22.233	21.582	21.064	20.652	20.319	APXLT

Figure A-04d. Detrended ion density for AIO-EISCAT section of Rev 2975 (16 Jan 88). Detrender cutoff frequency was 0.046875 Hz.
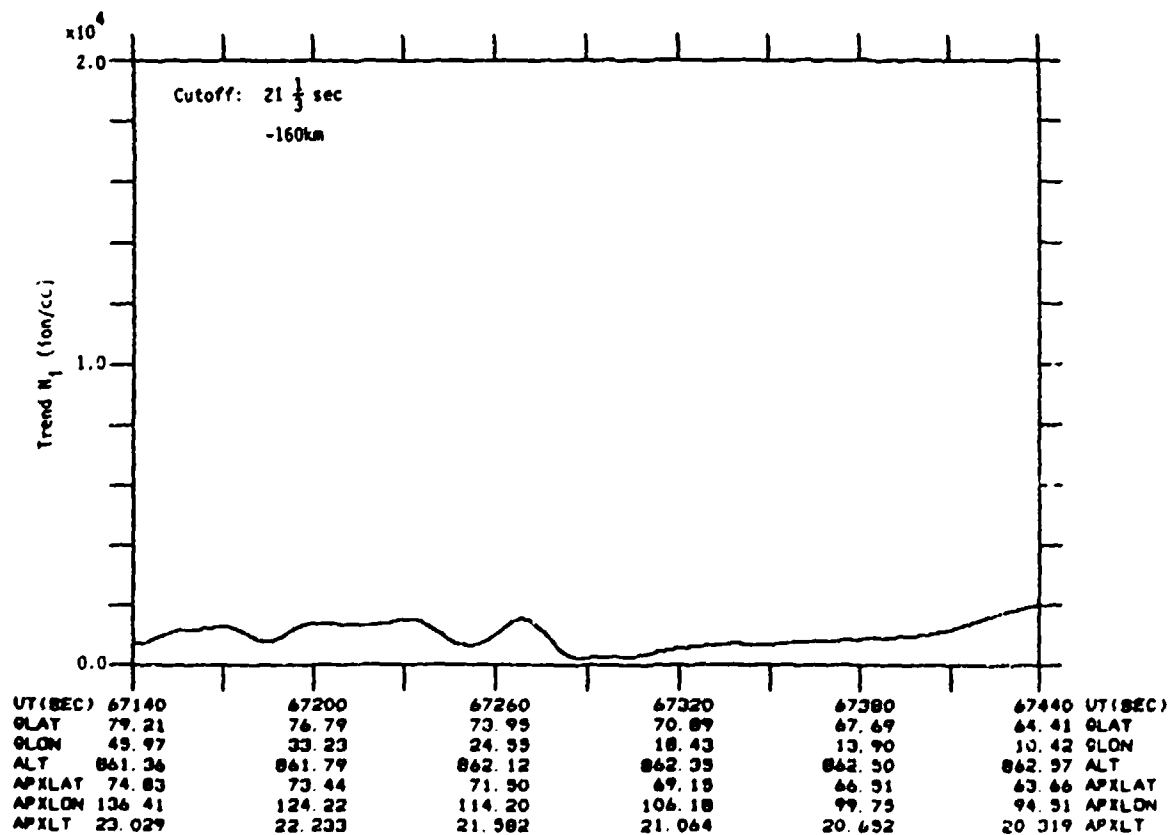
Figure A-04e. Ion density trend for AIO-EISCAT section of Rev 2975 (16 Jan 88). Detrender cutoff frequency was 0.046875 Hz.

A-19

Figure A-04f. Results of C_k analysis for AIO-EISCAT section of Rev 2975 (16 Jan 88).
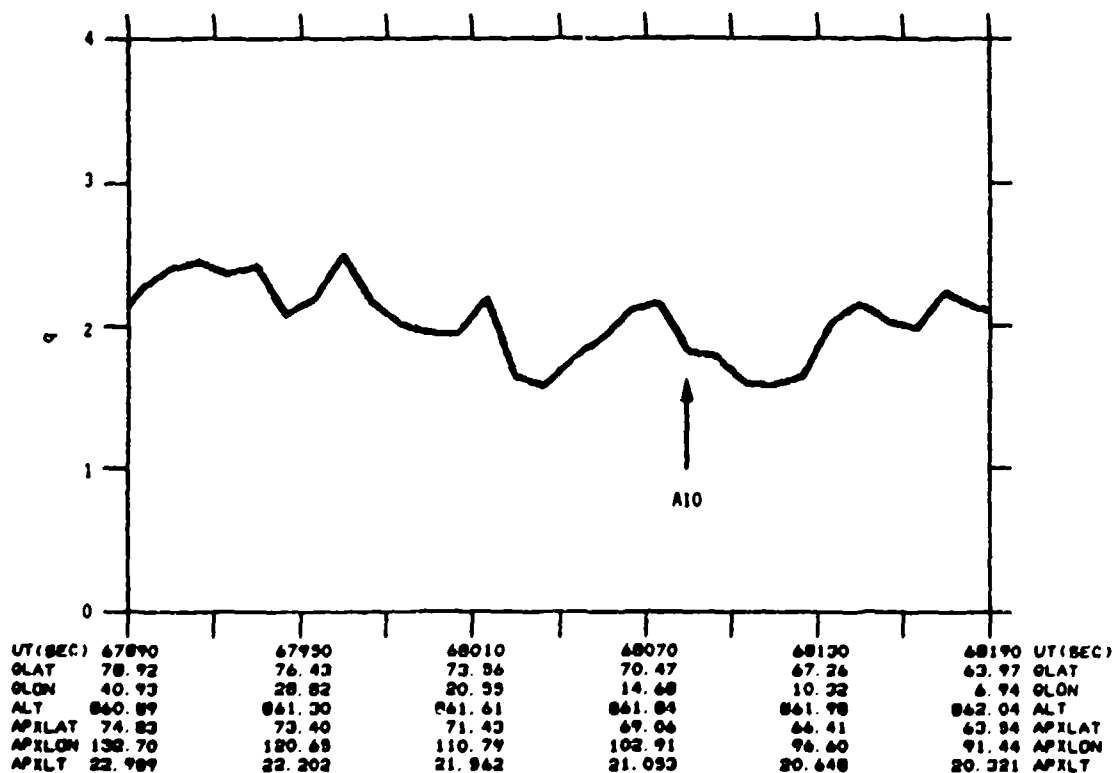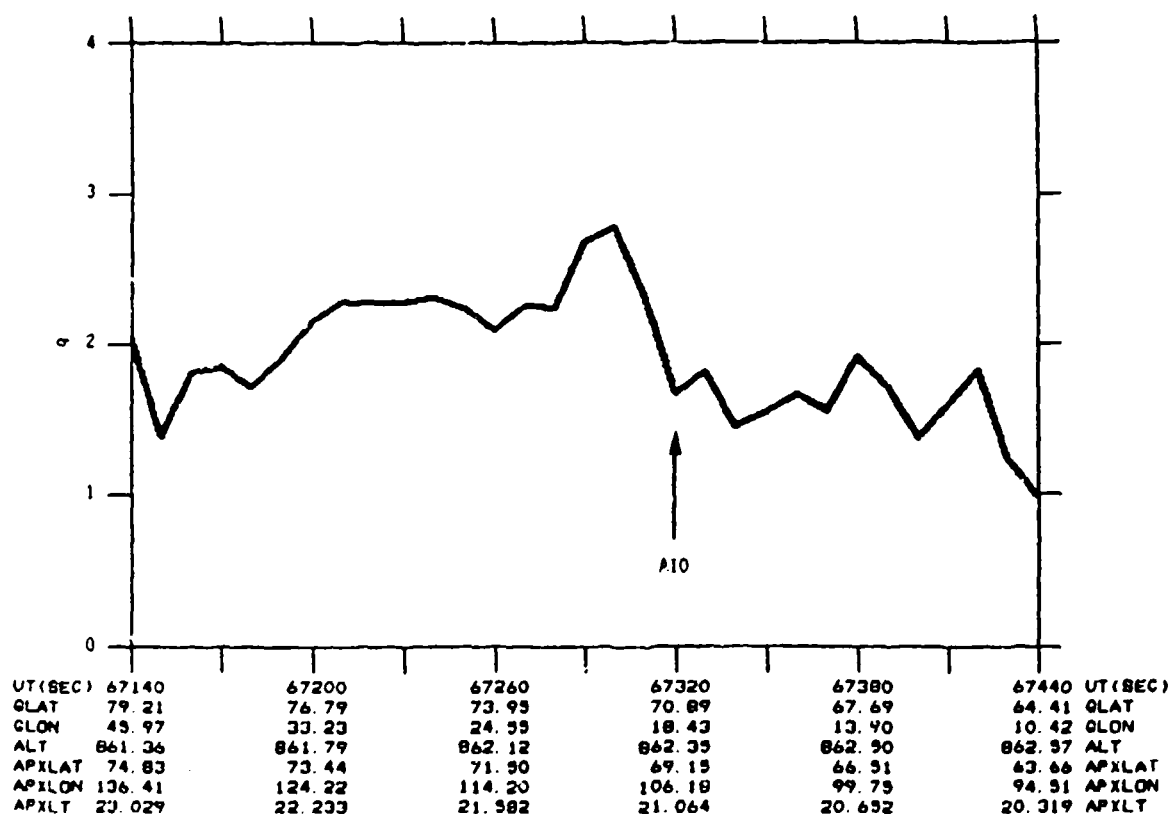

Figure A-04g. Spectral slope (q) for AIO-EISCAT section of Rev 2975 (16 Jan 88).
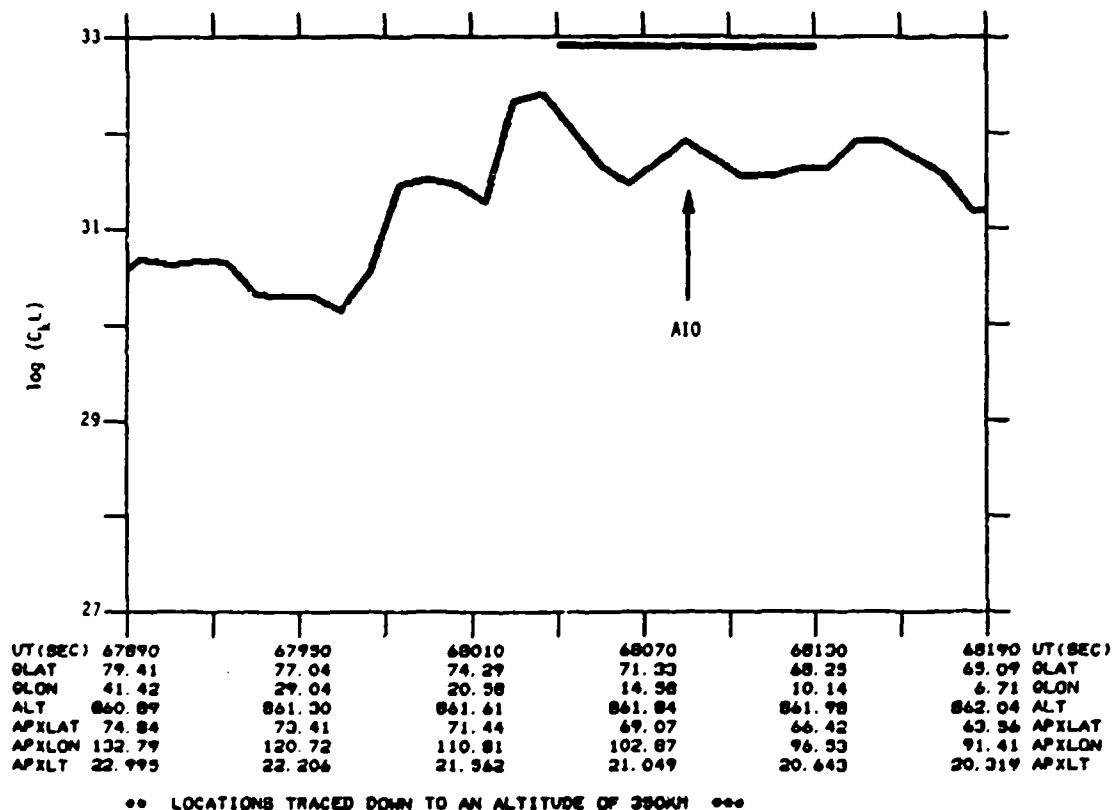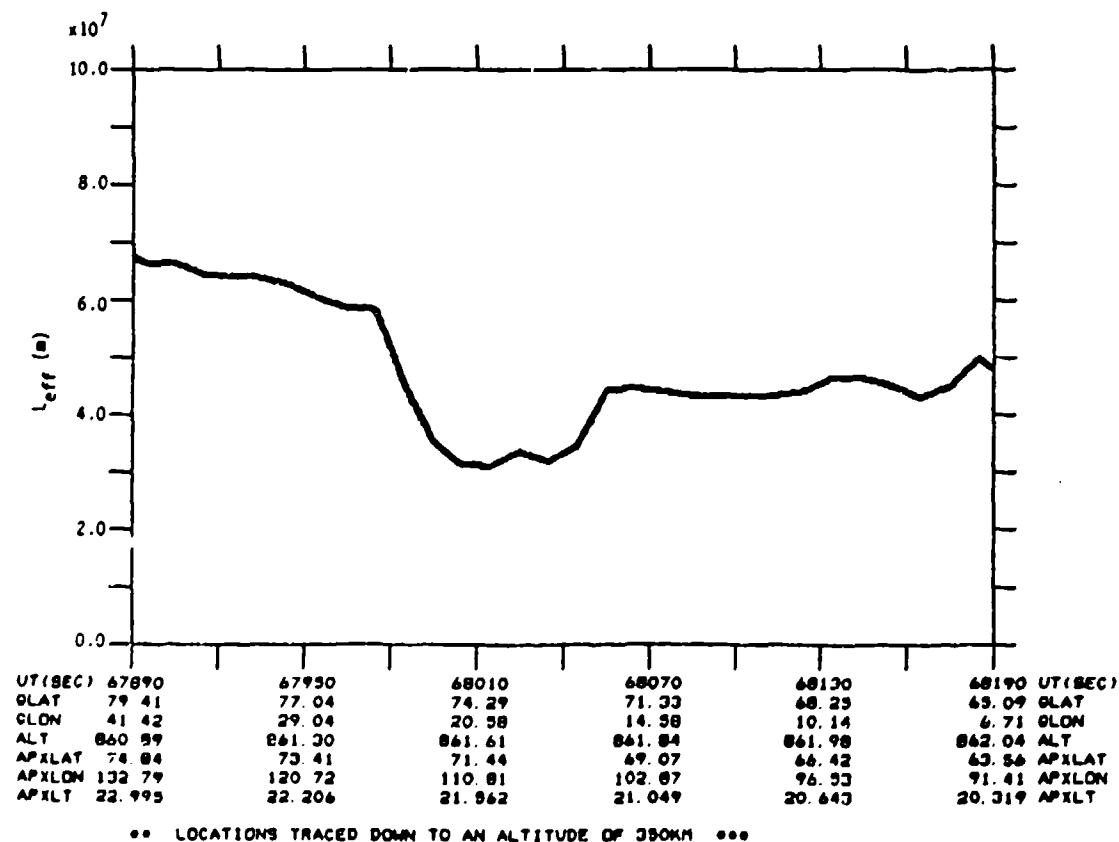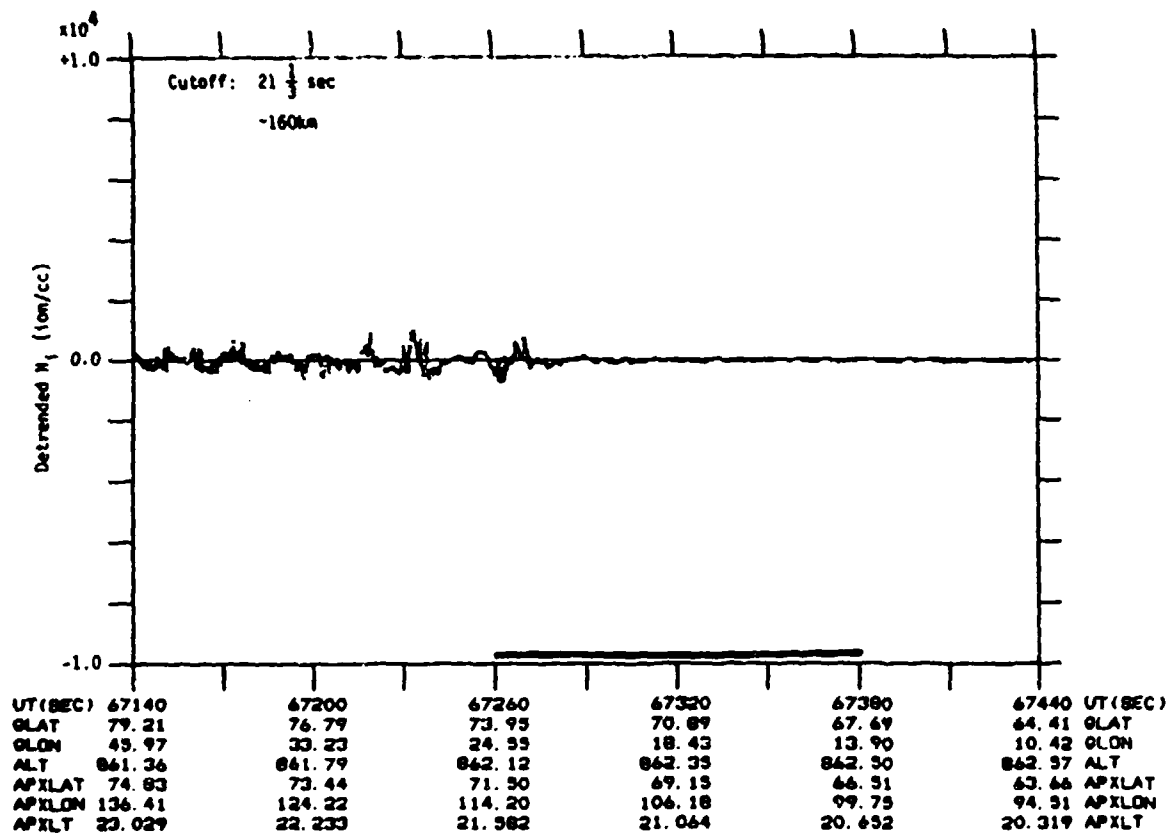
A-20
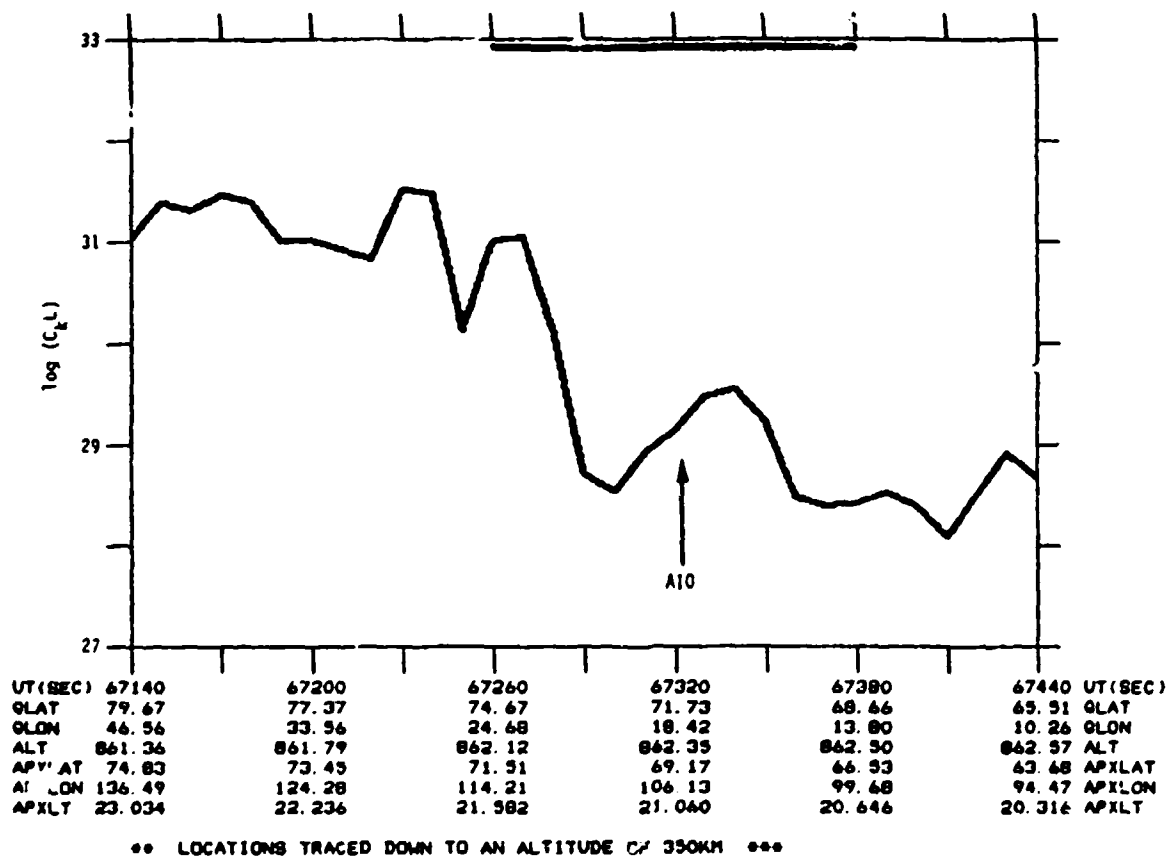
Figure A-04h. C_kL for AIO-EISCAT section of Rev 2975 (16 Jan 88).
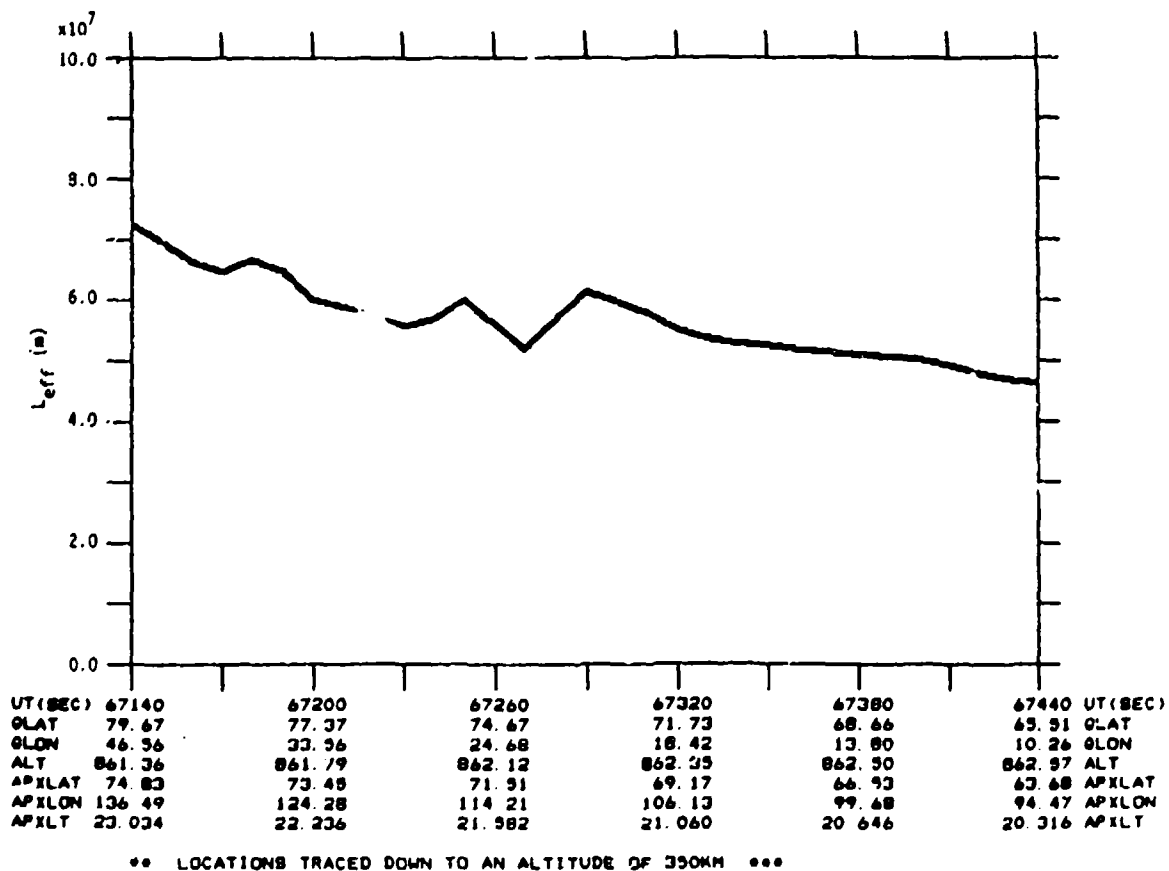
Figure A-04i. Effective layer thickness (L_{eff}) used to convert C_k to C_kL for AIO-EISCAT section of Rev 2975 (16 Jan 88).

A-21

EXPERIMENT GEOMETRY
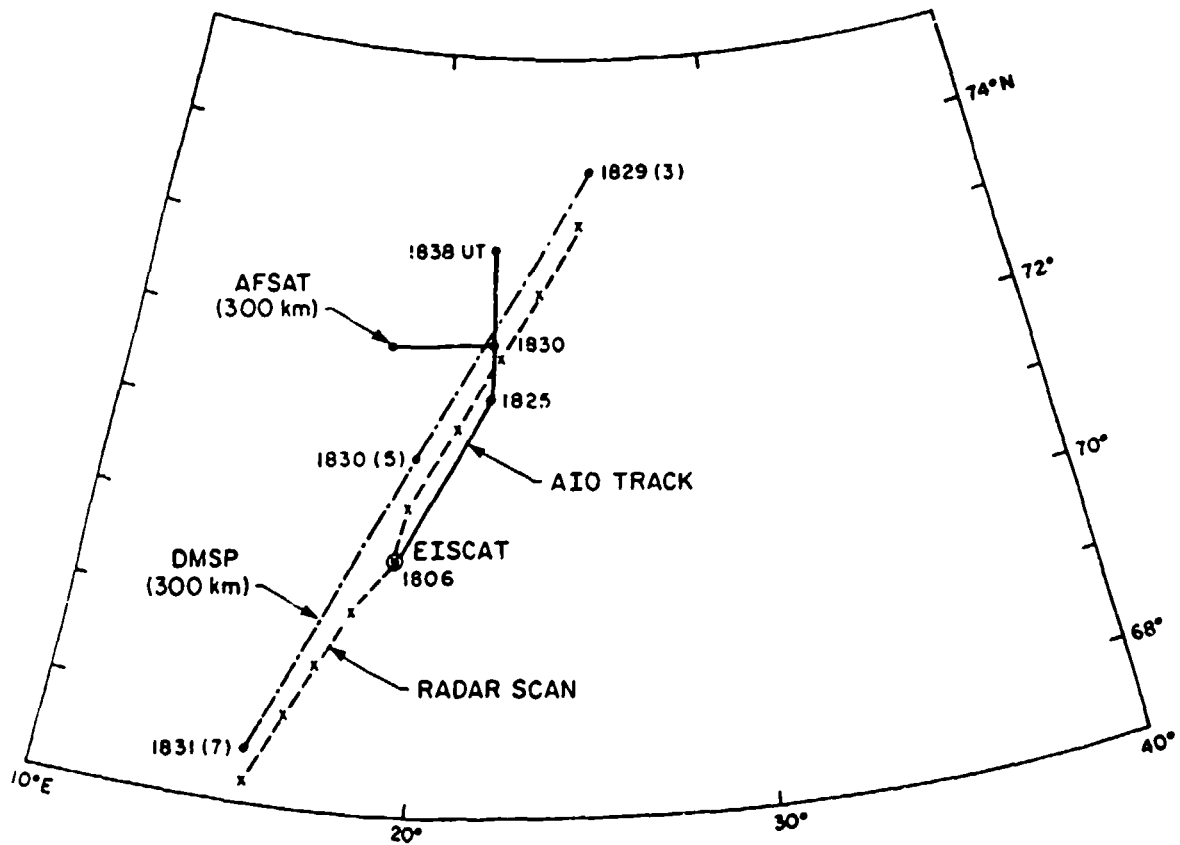
Figure A-05a. Experiment geometry for Rev 2989 on 17 January 1988. Solid line is the Airborne Ionospheric Observatory ai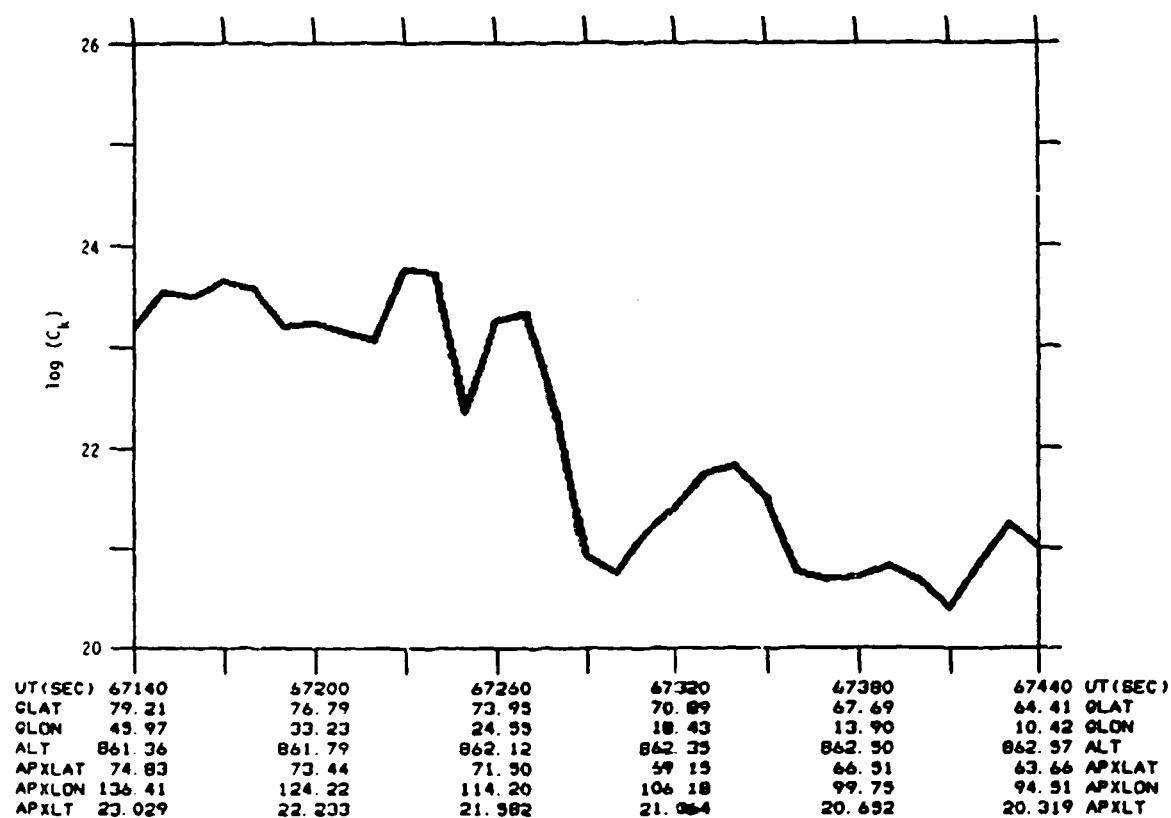rcraft ground track, dot-dashed line is the DMSP track mapped down to 300km, and the dash-x line is the EISCAT scan ground track. The location of the 300km penetration point of the AIO-AFSAT line-of-sight for 1830 UT is plotted. Locations are in geographic coordinates and all times are UT.

AIO Time Period: 18:27:00 to 18:32:00

K_p: 2+ ΣK_p: 13

SSN: 72

Average SSN: 79.1 (7-day)   43.8 (90-day)

UT(SEC)	65520		65820		66120		66420		66720		67020	UT(SEC)
OLAT	44.05		61.19		76.90		78.38		63.18		46.17	OLAT
OLON	171.47		162.64		136.67		43.76		12.40		2.76	OLON
ALT	846.92		853.09		858.61		862.07		863.10		862.40	ALT
APXLAT	42.17		57.24		71.36		74.24		62.31		45.95	APXLAT
APXLON	236.89		225.97		198.39		133.70		95.28		86.45	APXLON
APXLT	5.278		4.633		2.878		22.649		20.170		19.265	APXLT

Figure A-05b. Total ion density, entire polar cap section of Rev 2989 (17 Jan 88). The heavy line indicates AIO-EISCAT section of pass.

UT(SEC)	66420		66480		66540		66600		66660		66720	UT(SEC)
OLAT	78.38		75.78		72.84		69.72		66.49		63.18	OLAT
OLON	43.76		32.72		25.13		19.68		15.89		12.40	OLON
ALT	862.07		862.46		862.75		862.95		863.07		863.10	ALT
APXLAT	74.24		72.59		70.46		67.98		65.24		62.31	APXLAT
APXLON	133.70		122.44		113.31		104.02		100.12		95.28	APXLON
APXLT	22.649		21.914		21.323		20.893		20.477		20.170	APXLT

Figure A-05c. Total ion density, AIO-EISCAT section of Rev 2989 (17 Jan 88). The heavy line indicates section of pass shown in Figure A-05a; arrow indicates point of nearest spatial/temporal coincidence with AIO observations.

A-23

Figure A-05d. Detrended ion density for AIO-EISCAT section of Rev 2989 (17 Jan 88). Detrender cutoff frequency was 0.046875 Hz.

Figure A-05e. Ion density trend for AIO-EISCAT section of Rev 2989 (17 Jan 88). Detrender cutoff frequency was 0.046875 Hz.
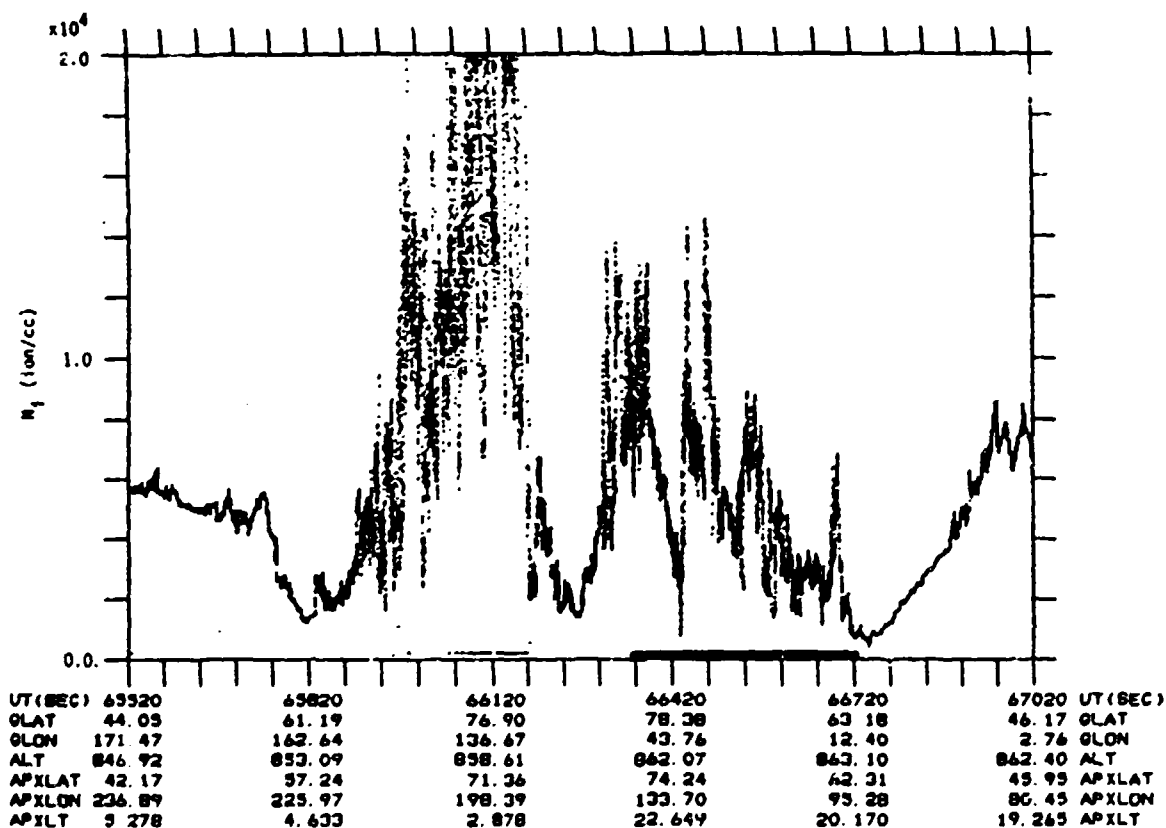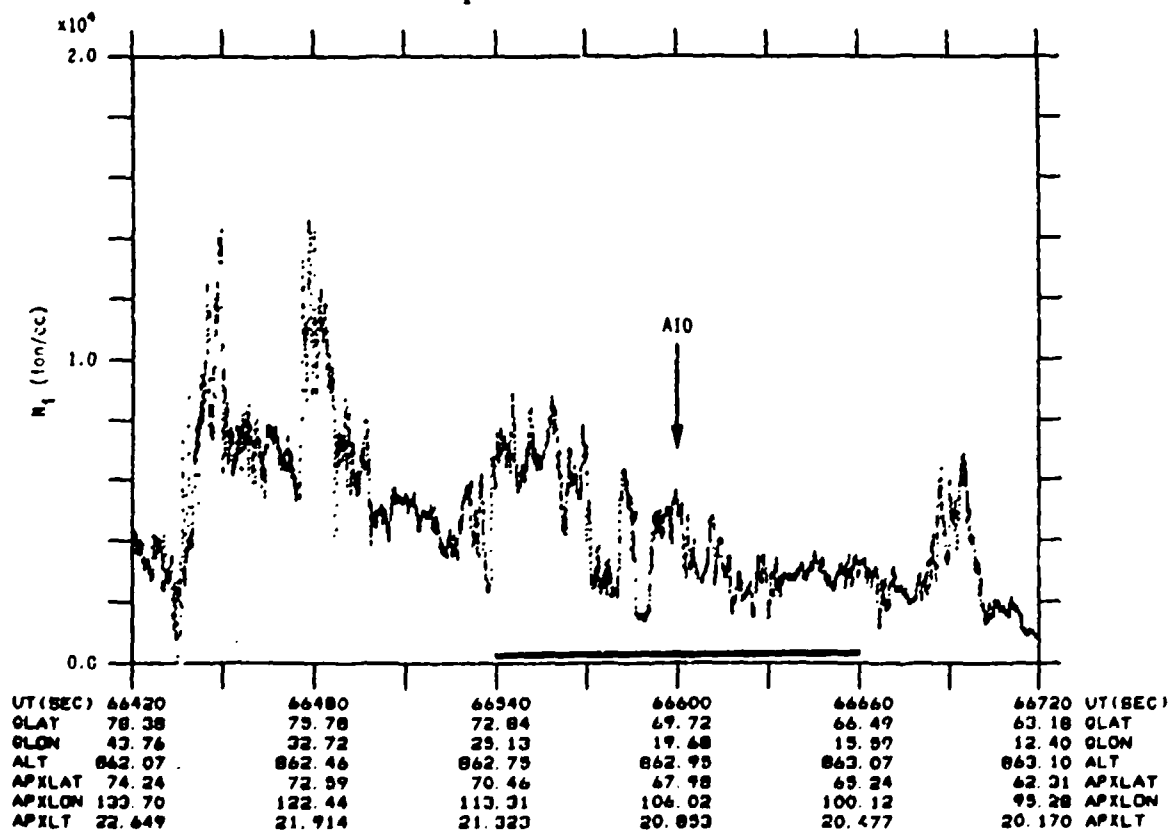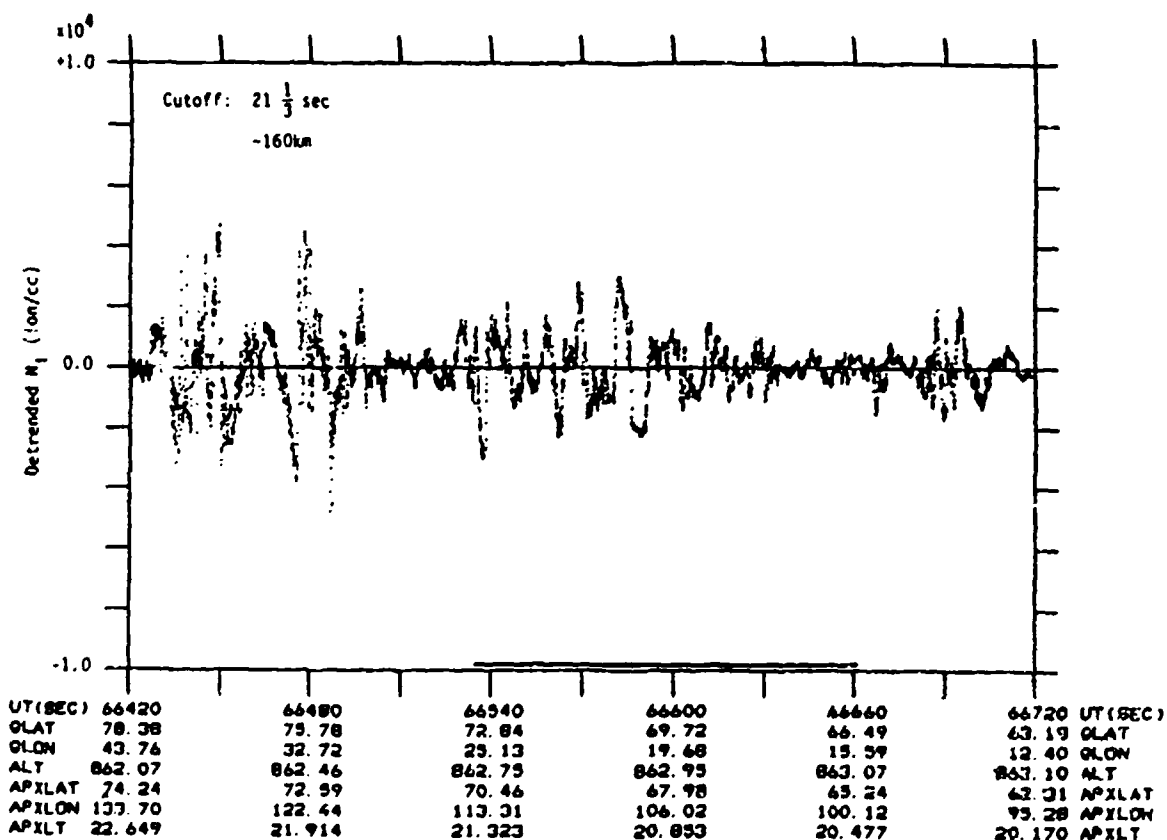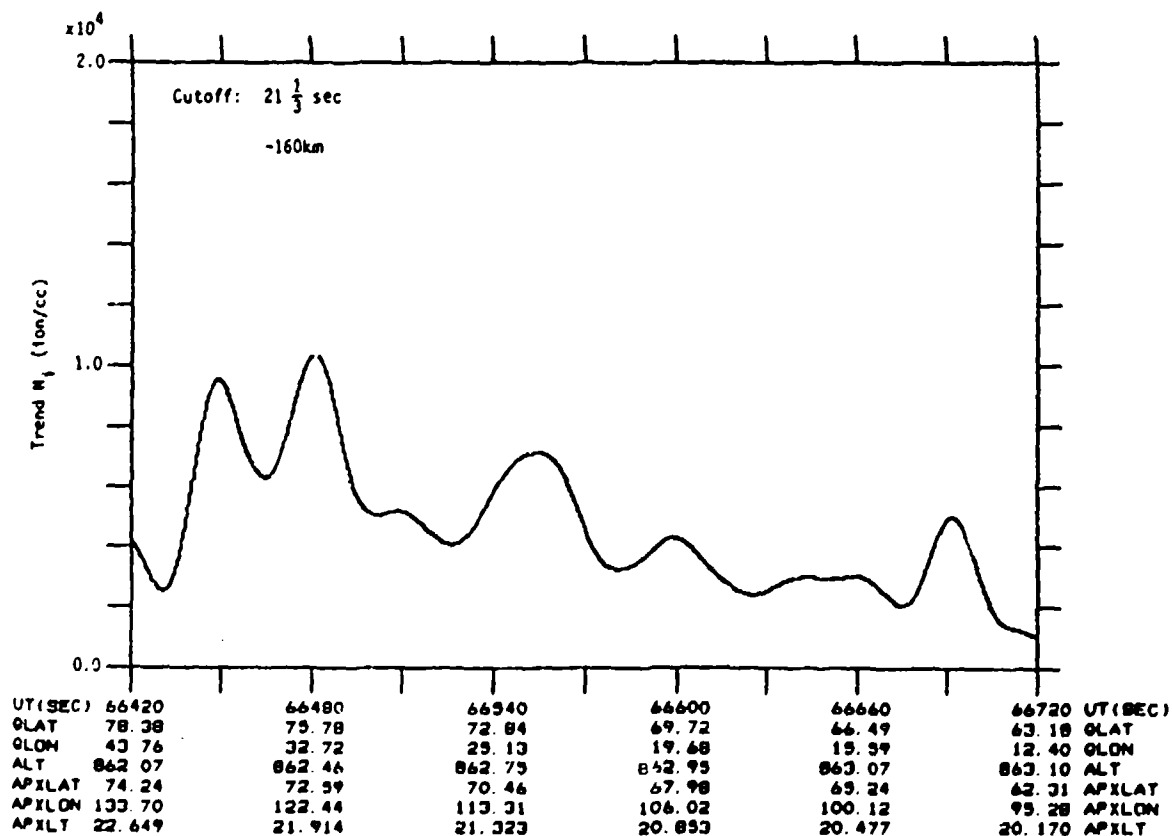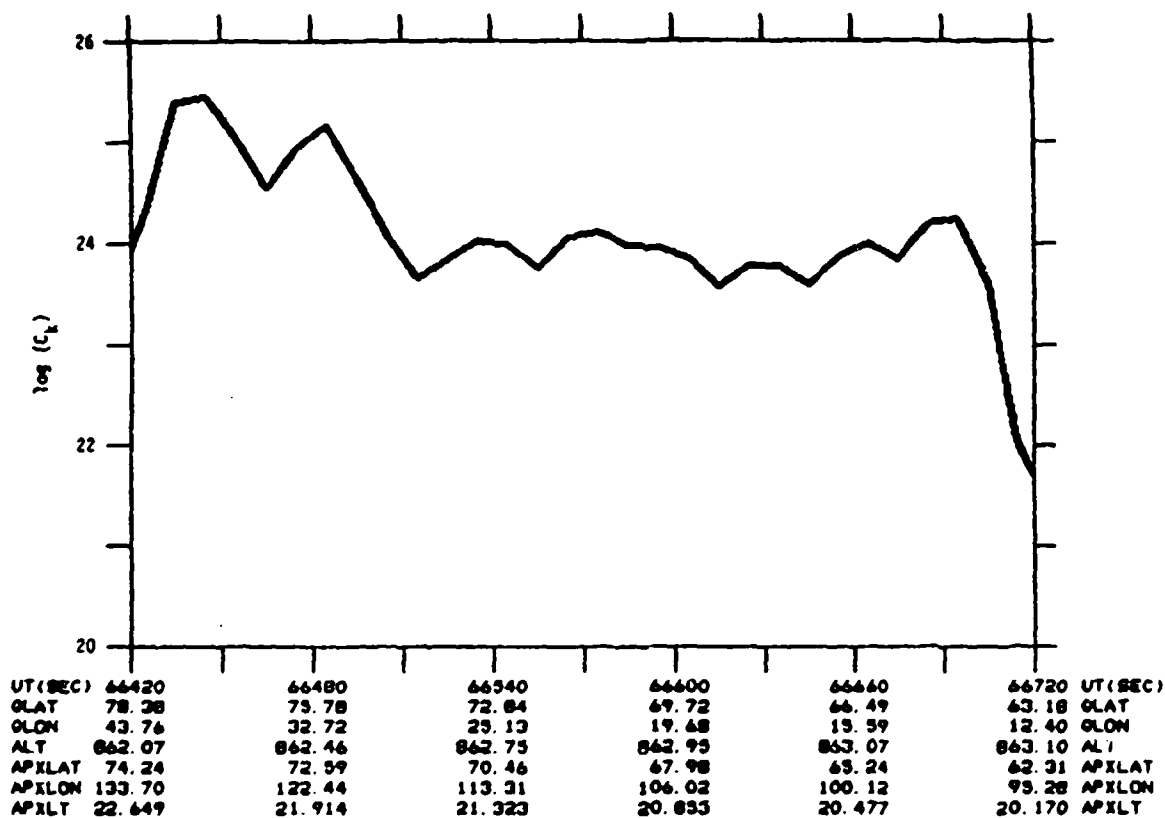
UT(SEC)	66420		66480		66540		66600		66660		66720	UT(SEC)
GLAT	78.38		75.78		72.84		69.72		66.49		63.18	GLAT
GLON	43.76		32.72		25.13		19.68		15.59		12.40	GLON
ALT	862.07		862.46		862.75		862.95		863.07		863.10	ALT
APXLAT	74.24		72.59		70.46		67.98		65.24		62.31	APXLAT
APXLON	133.70		122.44		113.31		106.02		100.12		95.28	APXLON
APXLT	22.649		21.914		21.323		20.853		20.477		20.170	APXLT

Figure A-05f. Results of C_k analysis for AIO-EISCAT section of Rev 2989 (17 Jan 88).

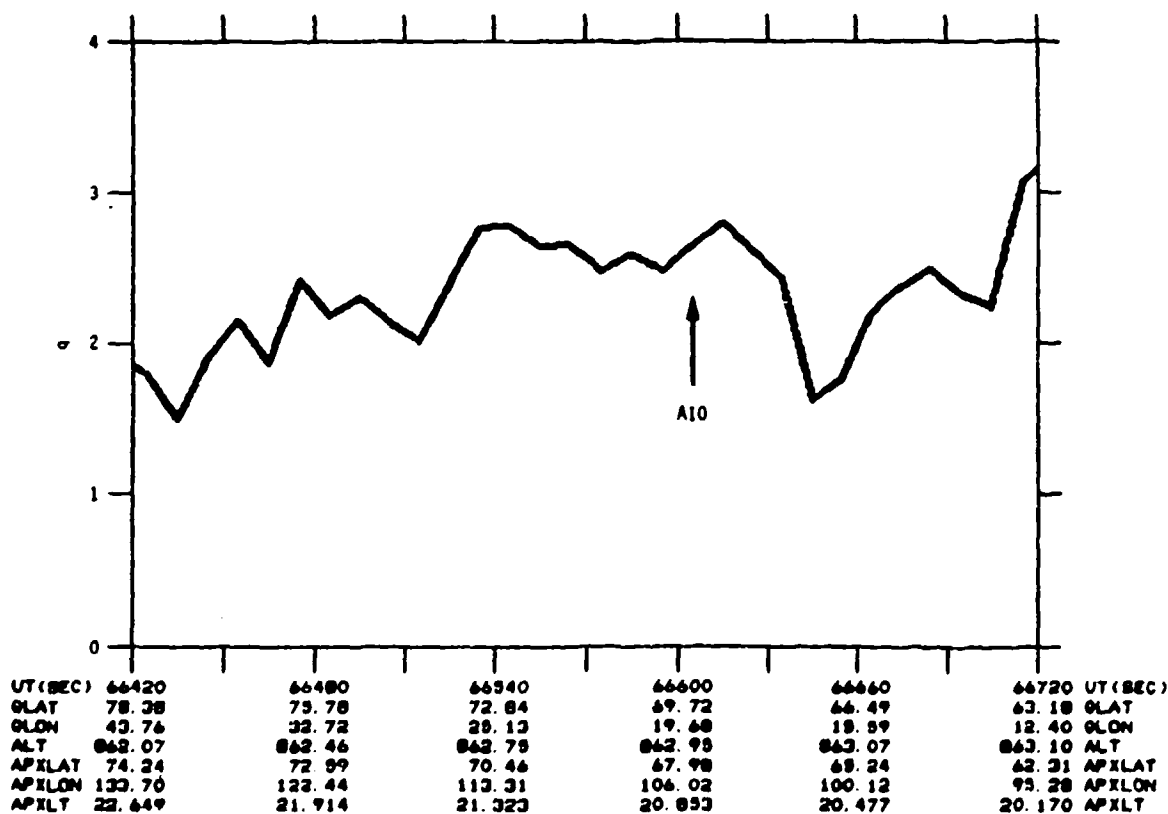| UT(SEC)	66420		66480		66540		66600		66660		66720	UT(SEC)
GLAT	78.38		75.78		72.84		69.72		66.49		63.18	GLAT
GLON	43.76		32.72		28.13		19.68		15.59		12.40	GLON
ALT	862.07		862.46		862.75		862.95		863.07		863.10	ALT
APXLAT	74.24		72.99		70.46		67.98		65.24		62.31	APXLAT
APXLON	133.70		122.44		113.31		106.02		100.12		95.28	APXLON
APXLT	22.649		21.914		21.323		20.853		20.477		20.170	APXLT

Figure A-05g. Spectral slope (q) for AIO-EISCAT section of Rev 2989 (17 Jan 88).
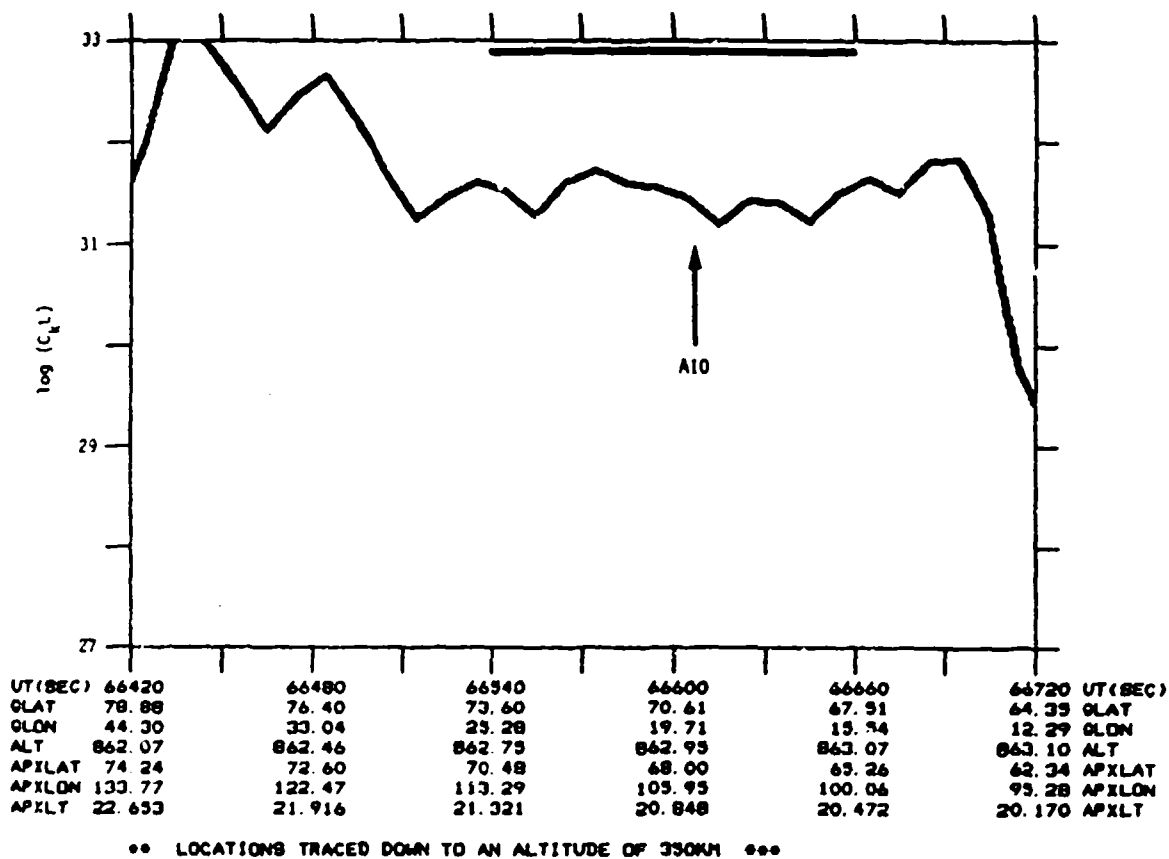
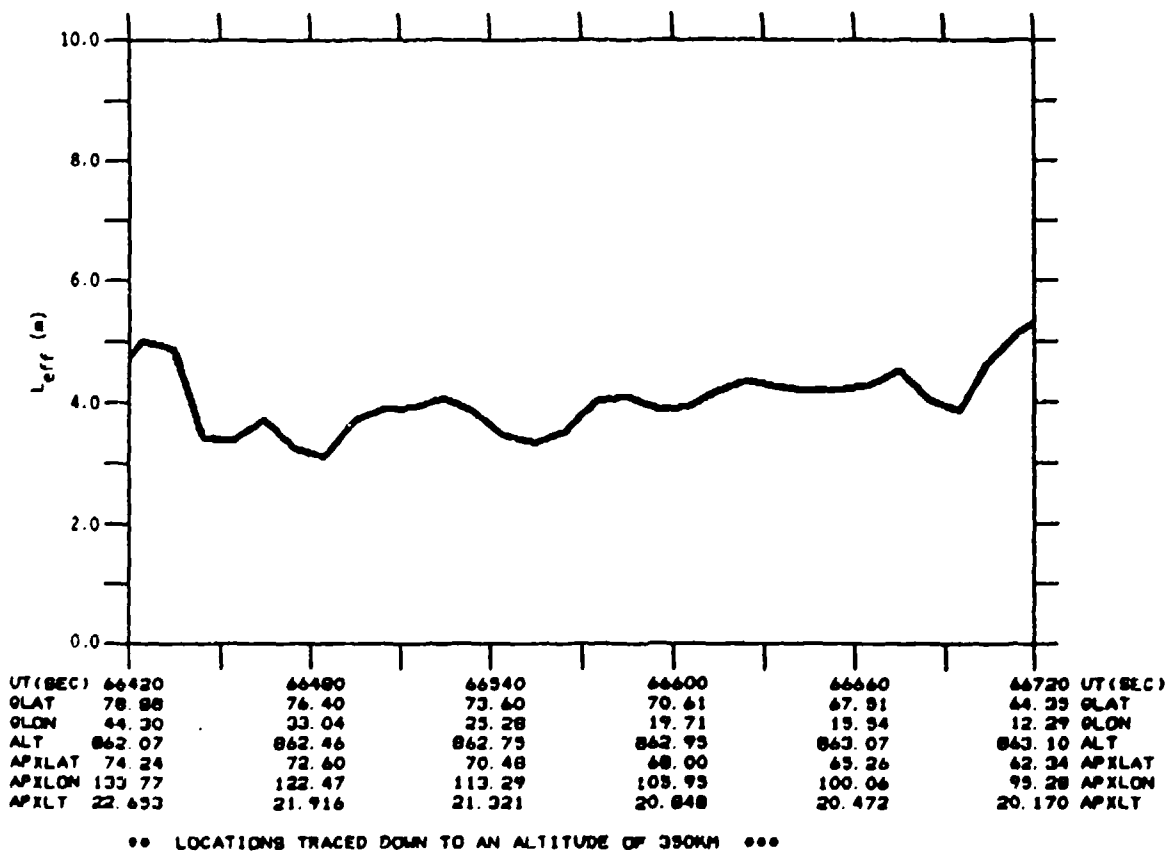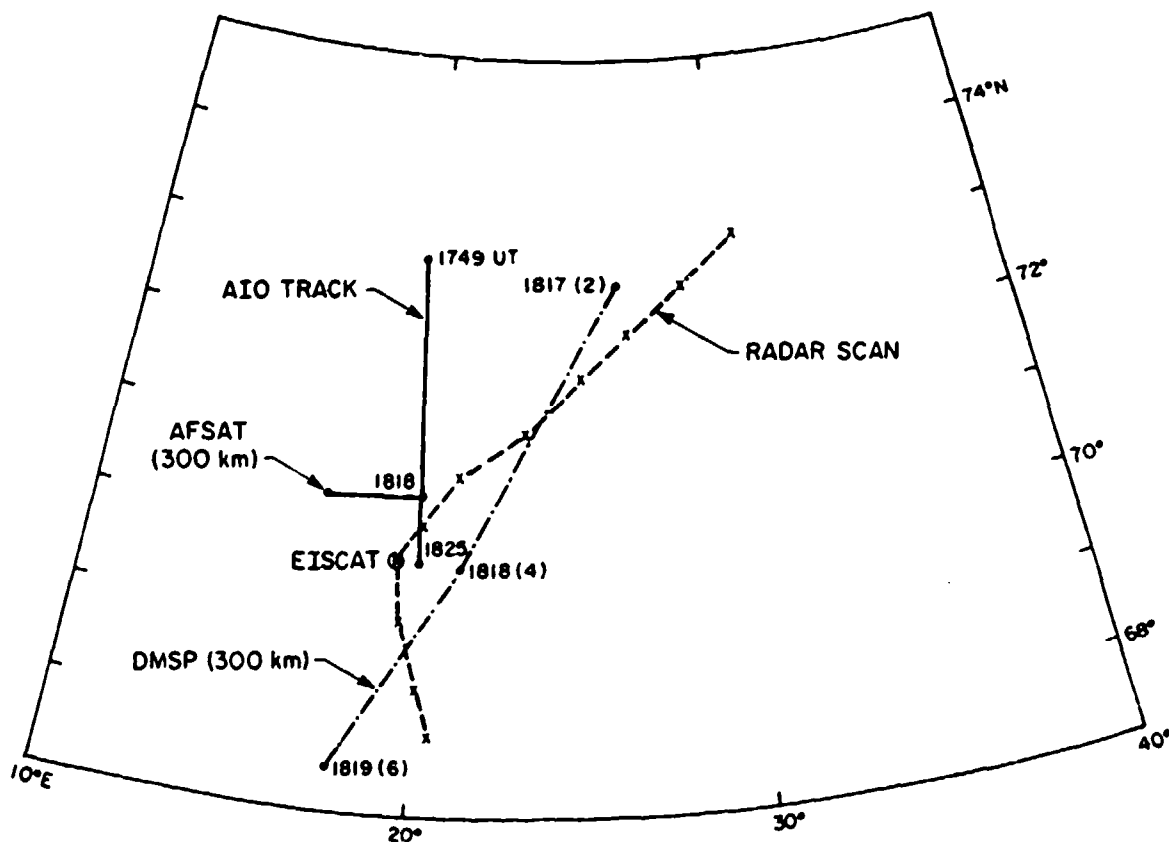Figure A-05h. C_kL for AIO-EISCAT section of Rev 2989 (17 Jan 88).

Figure A-05i. Effective layer thickness (L_{eff}) used to convert C_k to C_kL for AIO-EISCAT section of Rev 2989 (17 Jan 88).

A-26

EXPERIMENT GEOMETRY

Figure A-06a. Experiment geometry for Rev 3003 on 18 January 1988. Solid line is the Airborne Ionospheric Observatory aircraft ground track, dot-dashed line is the DMSP track mapped down to 300km, and the dash-x line is the EISCAT scan ground track. The location of the 300km penetration point of the AIO-AFSAT line-of-sight for 1818 UT is plotted. Locations are in geographic coordinates and all times are UT.

AIO Time Period: 18:15:30 to 18:20:30

K_p: 5- ΣK_p: 18+

SSN: 68

Average SSN: 78.1 (7-day) 44.1 (90-day)

UT(SEC)	64770	65070	65370	65670	65970	66270	UT(SEC)
GLAT	43.60	60.75	76.55	78.68	63.62	46.62	GLAT
GLON	174.70	166.03	141.09	48.63	19.85	6.02	GLON
ALT	847.09	853.36	859.00	862.55	863.62	862.88	ALT
APXLAT	42.10	57.01	71.12	74.27	62.48	46.19	APXLAT
APXLON	239.66	228.72	201.62	137.37	98.33	83.31	APXLON
APXLT	5.253	4.607	2.884	22.685	20.165	19.248	APXLT
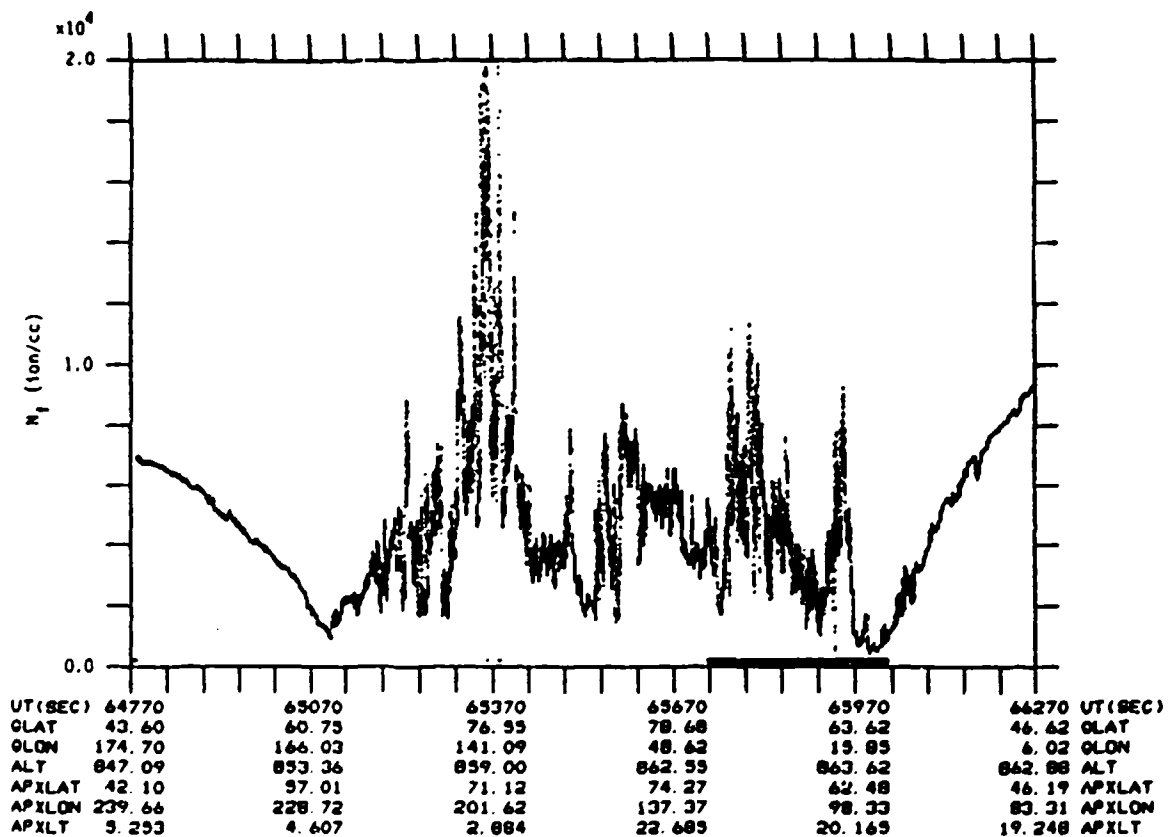
Figure A-06b. Total ion density, entire polar cap section of Rev 3003 (18 Jan 88). The heavy line indicates AIO-EISCAT section of pass.

UT(SEC)	65730	65790	65850	65910	65970	66030	UT(SEC)
GLAT	76.14	73.24	70.14	66.92	63.62	60.28	GLAT
GLON	37.01	29.05	23.38	19.14	15.85	13.19	GLON
ALT	862.96	863.26	863.47	863.58	863.62	853.57	ALT
APXLAT	72.67	70.57	68.11	65.39	62.48	59.42	APXLAT
APXLON	125.95	116.68	109.26	103.25	98.33	94.26	APXLON
APXLT	21.940	21.339	20.861	20.477	20.165	19.911	APXLT
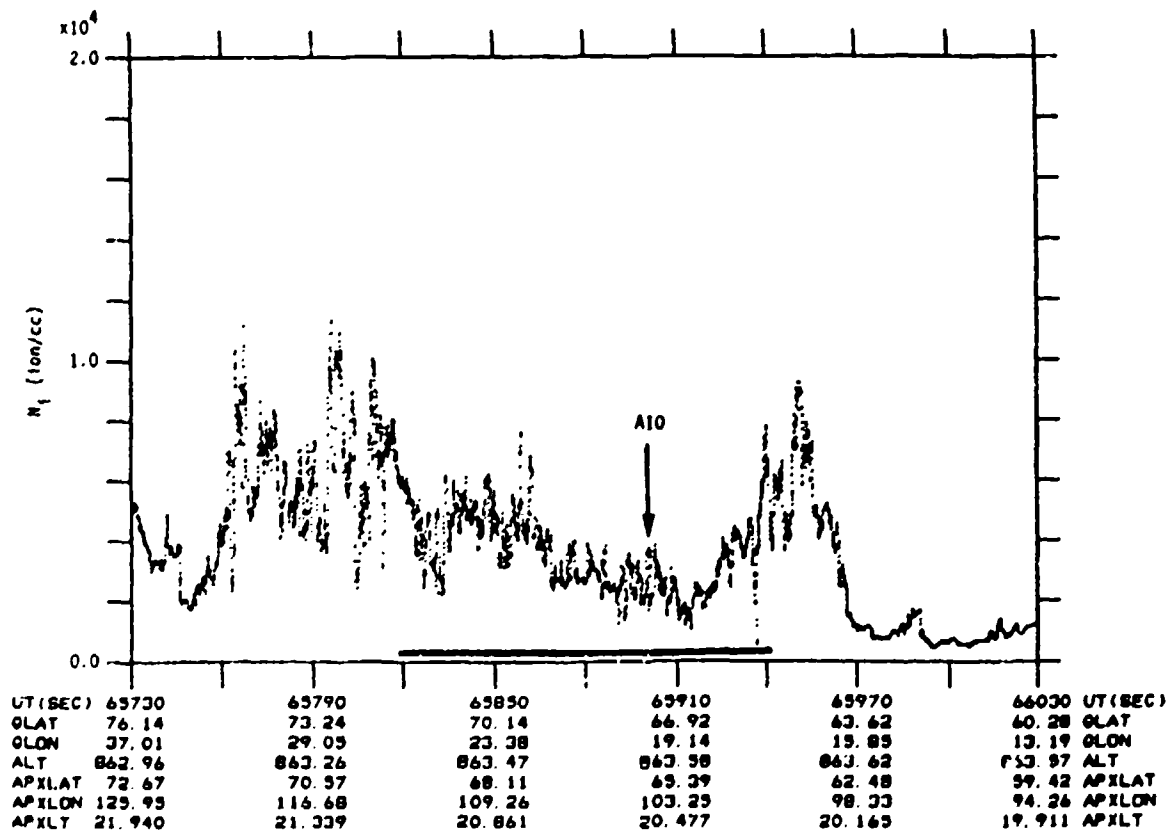
Figure A-06c. Total ion density, AIO-EISCAT section of Rev 3003 (18 Jan 88). The heavy line indicates section of pass shown in Figure A-06a; arrow indicates point of nearest spatial/temporal coincidence with AIO observations.
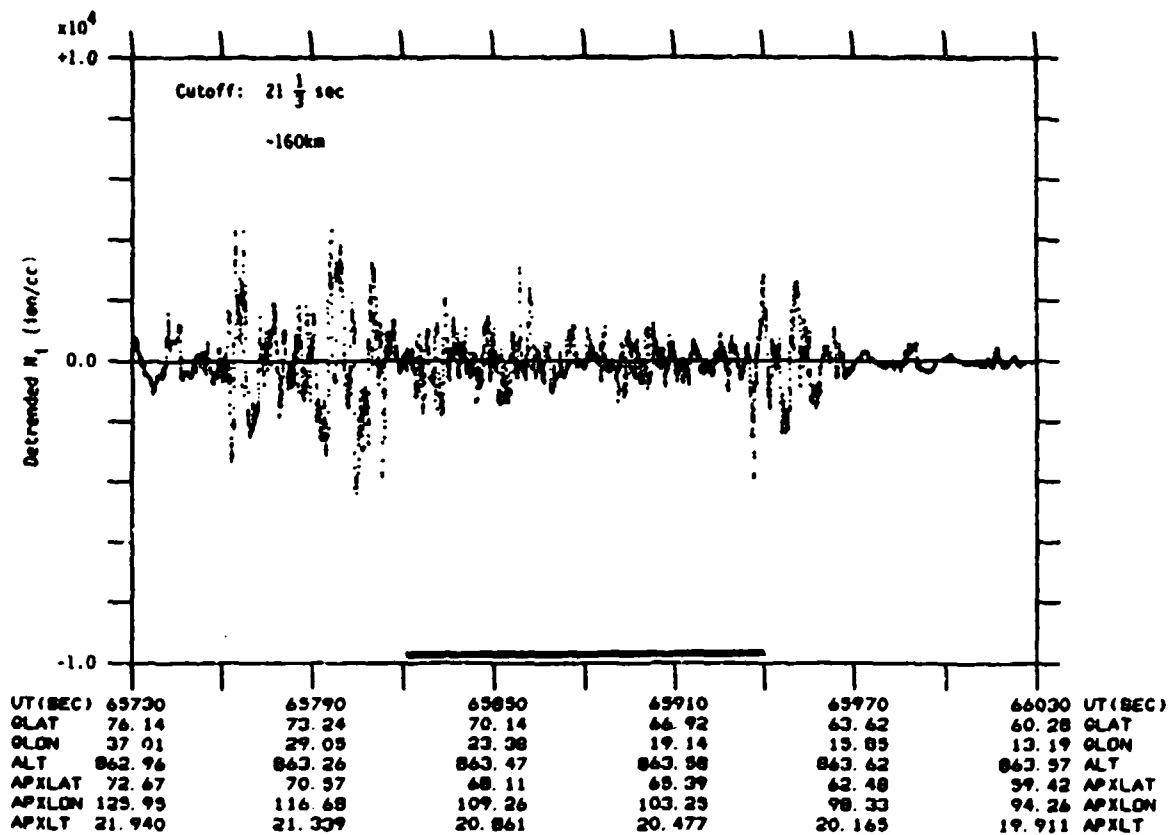
Figure A-06d. Detrended ion density for AIO-EISCAT section of Rev 3003 (18 Jan 88). Detrender cutoff frequency was 0.046875 Hz.
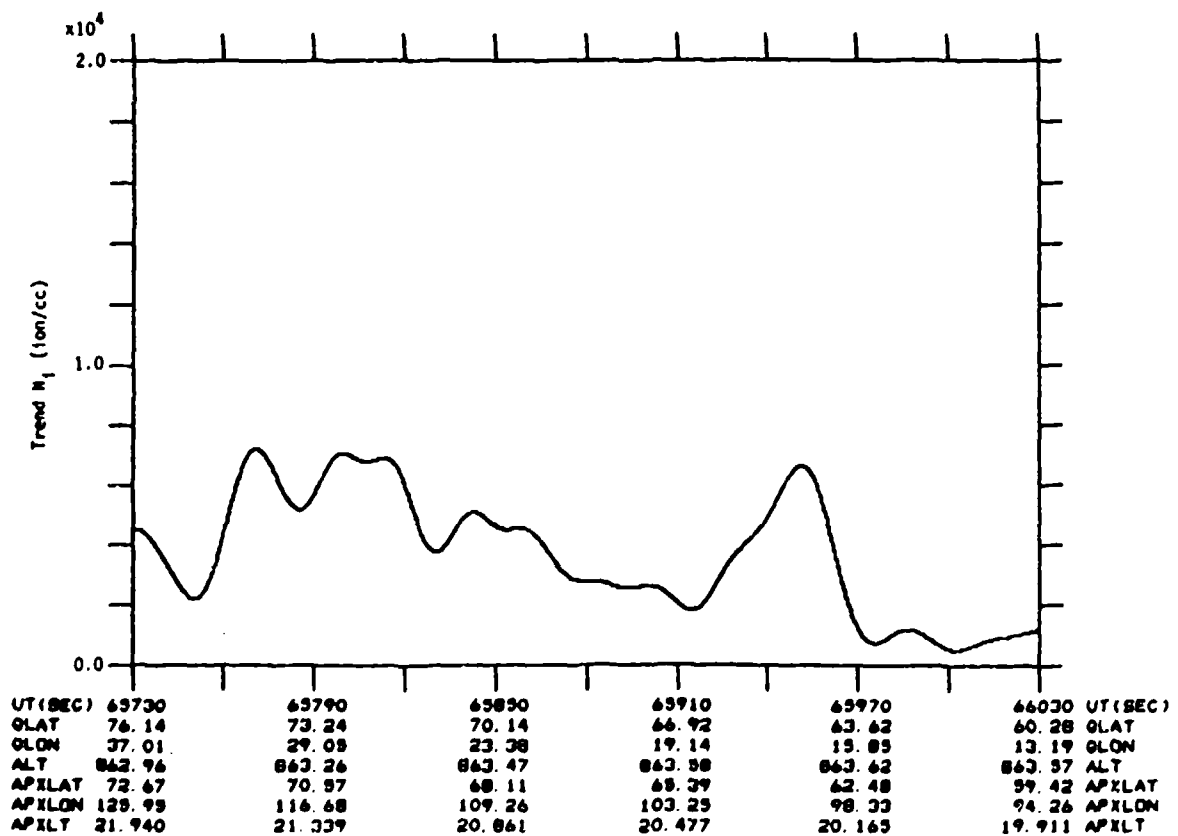

Figure A-06e. Ion density trend for AIO-EISCAT section of Rev 3003 (18 Jan 88). Detrender cutoff frequency was 0.046875 Hz.
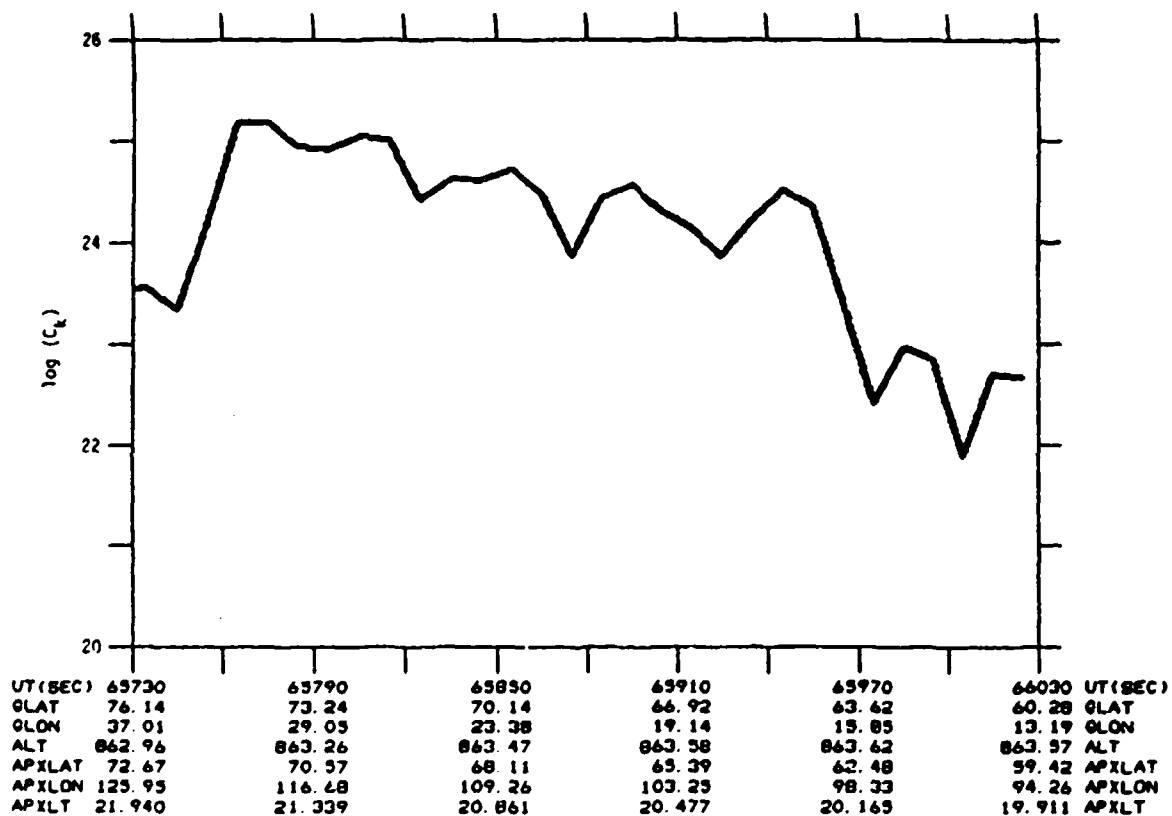
Figure A-06f. Results of C_k analysis for AIO-EISCAT section of Rev 3003 (18 Jan 88).
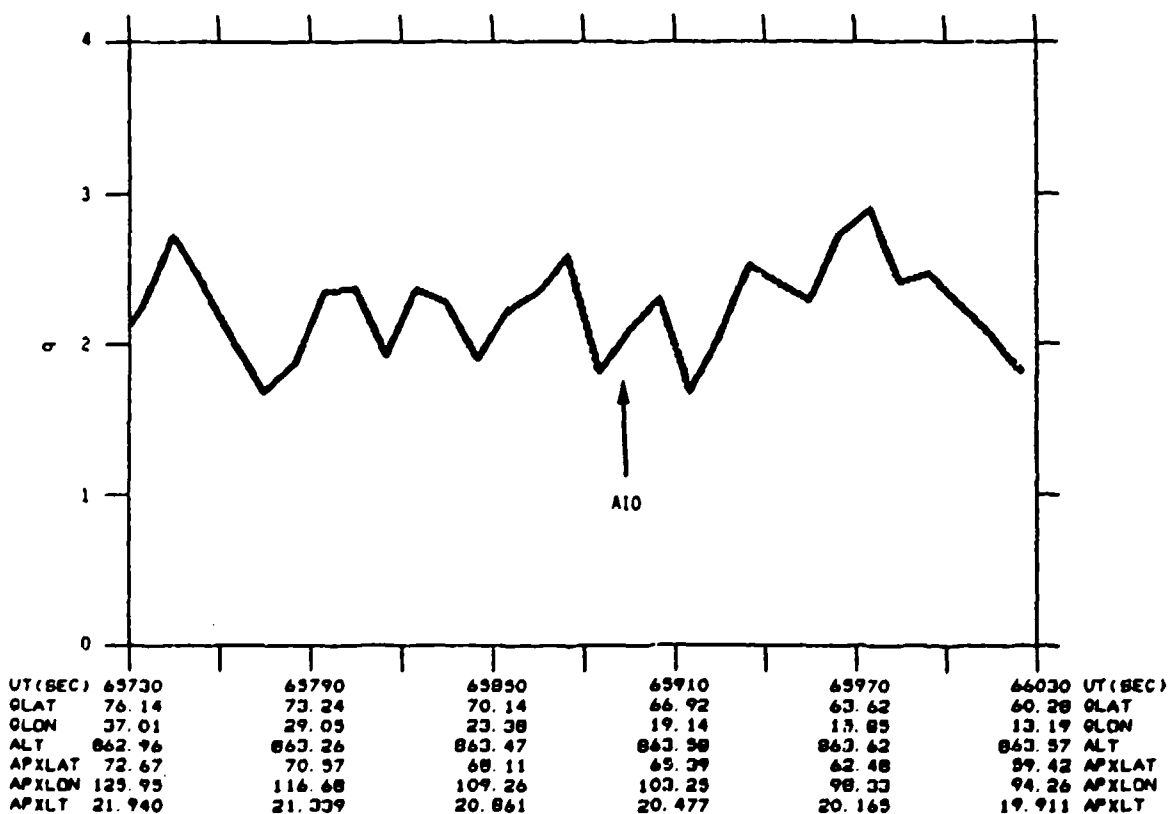

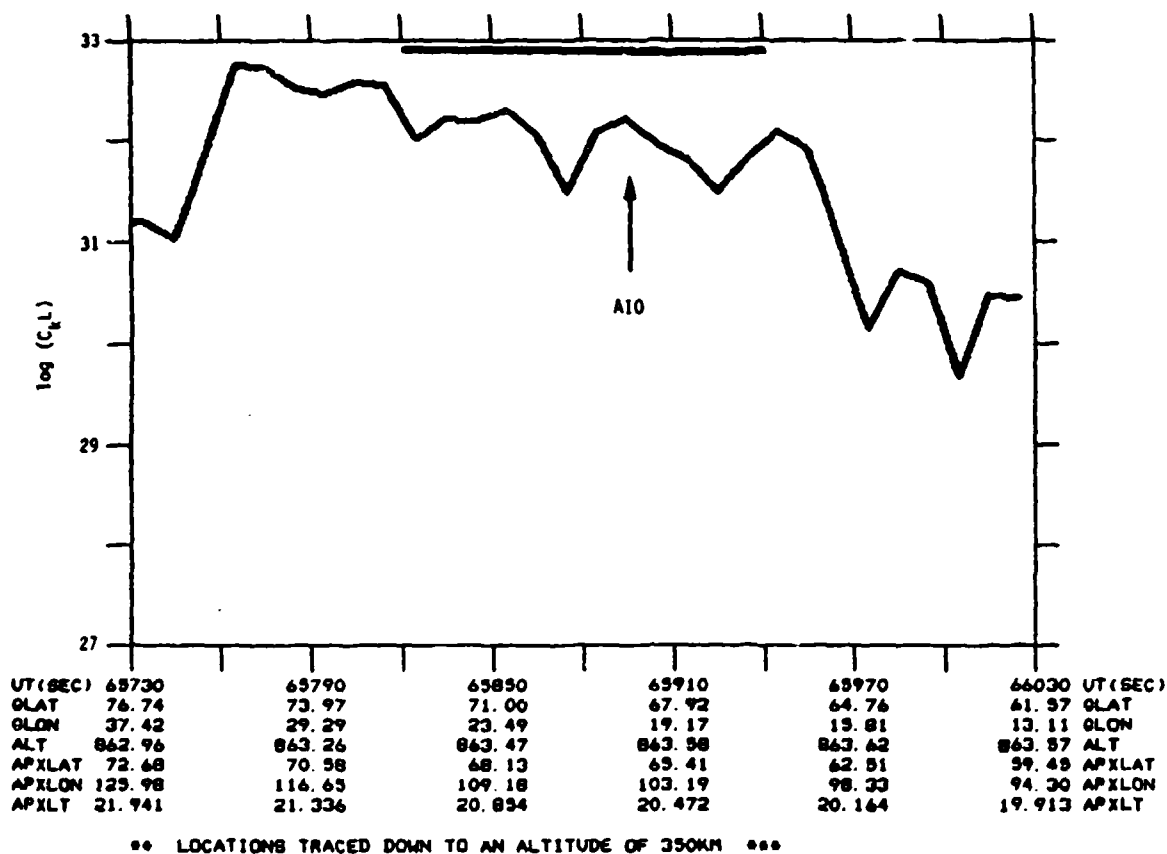Figure A-06g. Spectral slope (q) for AIO-EISCAT section of Rev 3003 (18 Jan 88).

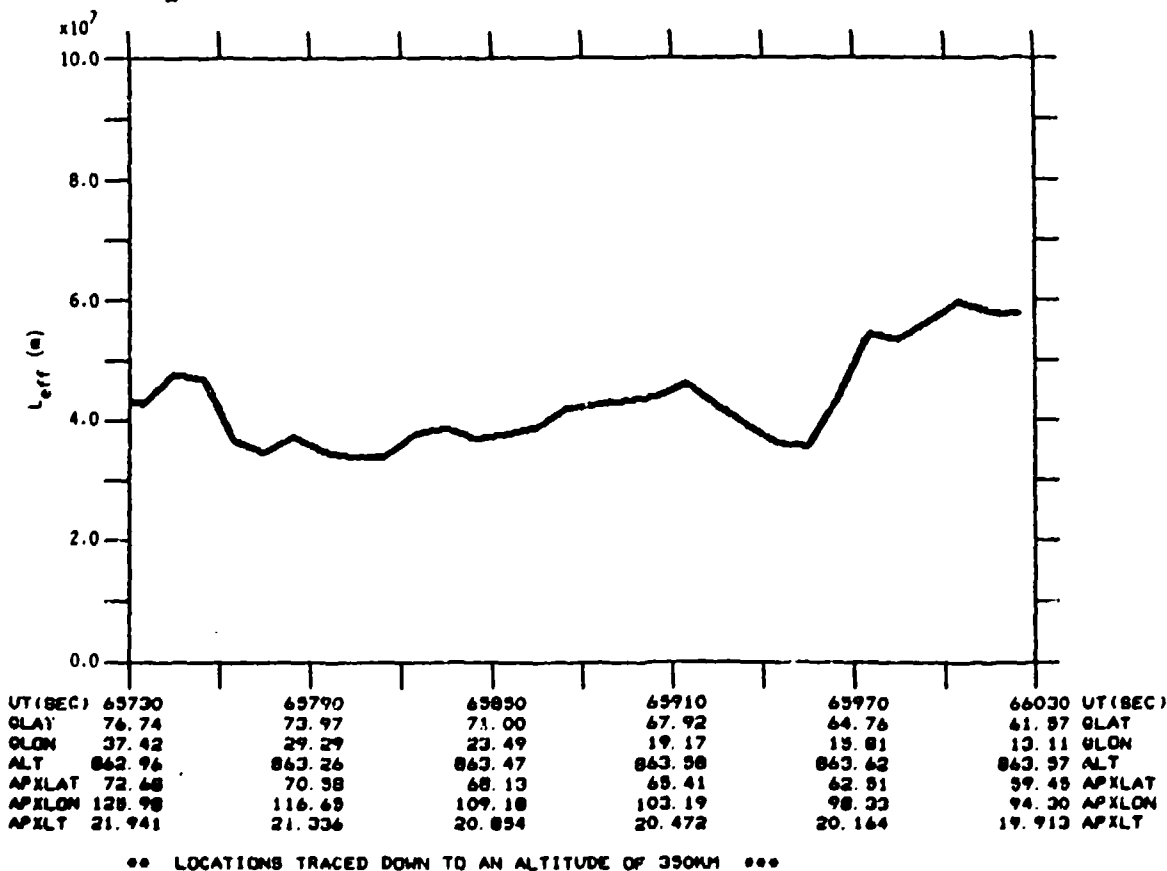**Figure A-06h.** C_kL for AIO-EISCAT section of Rev 3003 (18 Jan 88).

Figure A-06i. Effective layer thickness (L_{eff}) used to convert C_k to C_kL for AIO-EISCAT section of Rev 3003 (18 Jan 88).

A-31

Appendix B. Anomalous Behavior in the SSIES SM Data.

A number of problems have been encountered in processing data from the SM sensor on the DMSP F8 satellite, some of them associated with anomalous (or at least unexpected) behavior in the SM sensor and others caused by problems external to the SM sensor. These include (1) "floating" voltages for sensor status flags, (2) changes from the electrometer mode to the differencing-amplifier mode without a zero-point reading from the electrometer, (3) duplicate SSIES data frames from the DMSP OLS, (4) discontinuous offsets caused by changes in the ion sensor ground-plane voltage, and (5) miscellaneous odd behaviors. (Note: The following discussions will presuppose an understanding of the operation of the SM sensor. Full descriptions can be found in [3], [4], and Volume III of [7].)

B.1 "Floating" Status Flags.

The SM data stream includes status flags which indicate (1) whether the voltage data in the data frames are directly from the electrometer (EL data) or have been passed through a differencing amplifier (AMP data), and/or (2) the range setting of a ranging amplifier through which the EL/AMP data are passed prior to encoding and downlink. These status flags were designed to be at fixed voltage values outside the range within which the density-data values were constrained to lie. Unfortunately, the values being reported for these status flags and the limit-bands for the density data are "floating" from their nominal design values, so that occasionally it is almost impossible to determine whether a particular reading is a density value or a status flag. The processing code provided to AFGWC has been modified to deal with most of the cases we have encountered, but there are times when the data required manual review and editing to process it successfully.

B.2 Missing EL-mode Zero Point.

A second problem encountered with the status flags occurs primarily when the ionosphere is quite irregular and the sensor is frequently switching between the EL and AMP modes. In normal operation, when the sensor switches from the EL mode to the AMP mode, there is an EL reading just prior to the EL-to-AMP flag which establishes the zero point for the AMP data. On occasion, however, the sensor will switch from AMP to EL at the end of a data frame and then switch back at the start of the next frame with no intervening data point from EL mode to serve as a zero point for the AMP-mode data. While an automated code could undoubtedly be developed to deal with this situation, it was more cost-effective for us simply to flag these in the automated processing and then hand-correct them by inserting a bogus EL reading between the two sets of status flags using the raw-data editor and reprocessing.

B.3 Duplicate/Missing Data Frames.

The problem of duplicate SSIES data-frames in the telemetry stream was identified as a potential problem during ground checkout of the F8 spacecraft. The problem occurs at aperiodic intervals when the OLS telemetry formatter accesses the data buffer from the SSIES instruments for a one-second data frame prior to the data for this one-second period being loaded into the buffer by the SSIES microprocessor. The result is that the previous frame is duplicated in the telemetry stream, and the data from the current frame are lost. We have found that this occurs at a rate of roughly 35-40 duplicates per orbit (about 0.5%), with five to eight occurring in our periods of interest.

If there are no status changes in the SM sensor during one of the missing frames, this can be dealt with fairly simply by interpolating from the last data point in the previous frame to the first data point in the next frame. If a status flag is missed (and this is not always easy to determine), deciding what exactly has occurred and correcting/adjusting for this can often be difficult for a human, much less for an automated computer system. As with the missing EL-mode zero point problem, we have dealt with the duplicate frame problem by manually reviewing the telemetry data stream, making our best guess as to what has happened during the missing one second of data, and then entering a bogus data frame for the missing one. About 50% of the bogus frames we generated contained some sort of status change (range change or EL/AMP mode change).

B.4 Ground-Plane Voltage Offsets.

It appears that although the voltage on the ground plane of the three ion instruments should have been de-coupled from the microprocessor and connected to the SENPOT electronics, the microprocessor can affect the voltage on the ground-plane during the first three seconds of the 128-second EP/RPA sweep cycle. Figure B-01 is a plot of the SM ion density data from Rev 2989, and Figure B-02 is a plot of the voltage on the ground-plane ($V_{bias} + V_{IP}$) for the same Rev. The features labeled A-H on the voltage plot are three-second periods in which the voltage has been shifted away from the reading set by SENPOT to a voltage reading of 12.0-12.5 volts. These all occur during the first three seconds of the EP/RPA sweep cycle, and only when the SENPOT voltage setting is above roughly 12 volts. The effect of this on the density data can be seen in the upper plot, where the features are labeled corresponding to those in the lower plot.
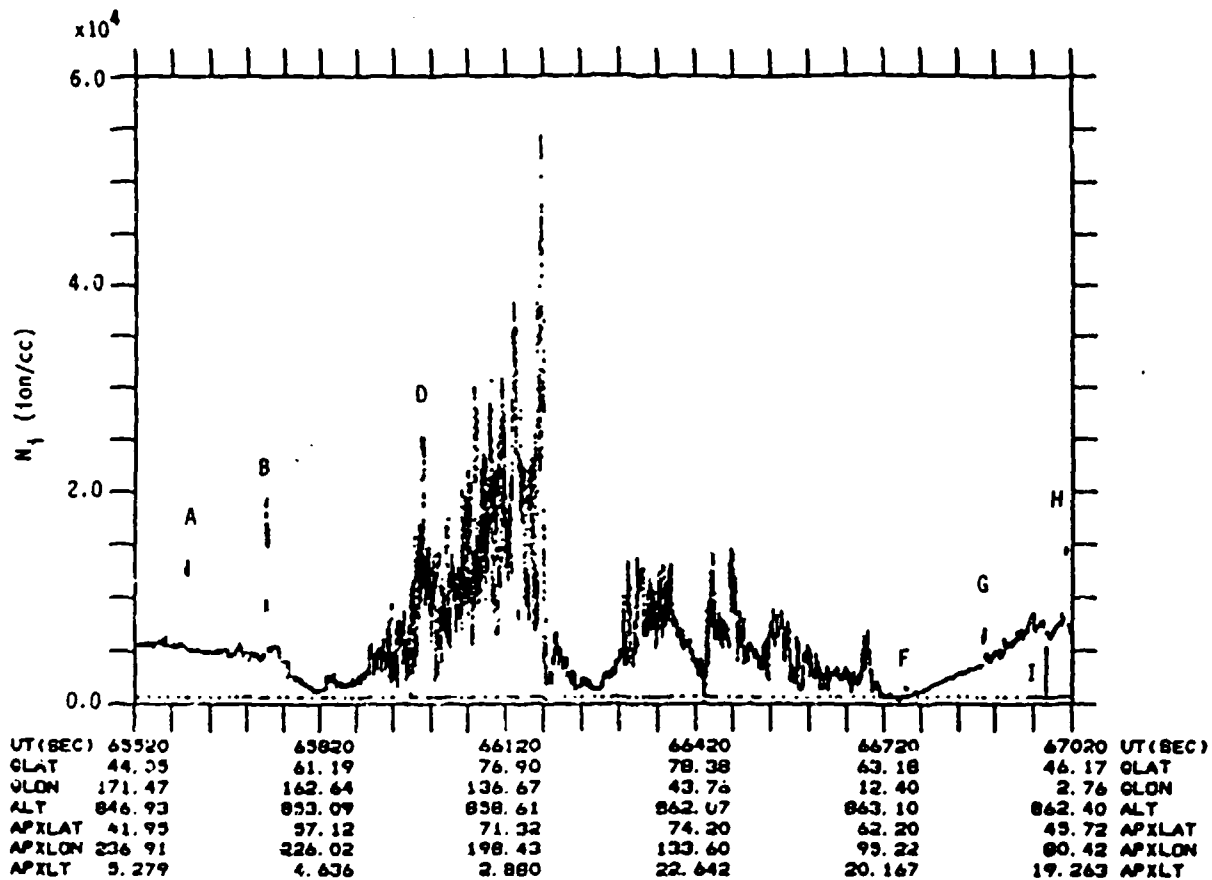
$\times 10^4$

N_i (ion/cc)

6.0 — 4.0 — 2.0 — 0.0

Features labeled A, B, C, D, E, F, G, H, I

UT(SEC)	65520	65820	66120	66420	66720	67020	UT(SEC)
GLAT	44.35	61.19	76.90	78.38	63.18	46.17	GLAT
GLON	171.47	162.64	136.67	43.76	12.40	2.76	GLON
ALT	846.93	853.09	858.61	862.07	863.10	862.40	ALT
APXLAT	41.95	97.12	71.32	74.20	62.20	49.72	APXLAT
APXLON	236.91	226.02	198.43	133.60	95.22	80.42	APXLON
APXLT	5.279	4.636	2.880	22.642	20.167	19.263	APXLT

Figure B-01. Ion density data record from Rev 2989, 17 Jan 88. Features labeled A, B, etc., correspond to features in Figure B-02.

Volts

25.0 — 20.5 — 15.0 — 10.0 — 5.0 — 0.0

Features marked A, B, C, D, E, F, G, H

UT(SEC)	65520	65820	66120	66420	66720	67020	UT(SEC)
GLAT	44.05	61.19	76.90	78.38	63.18	46.17	GLAT
GLON	171.47	162.64	136.67	43.76	12.40	2.76	GLON
ALT	845.93	853.09	858.61	862.07	863.10	862.40	ALT
APXLAT	41.95	97.12	71.32	74.20	62.20	49.72	APXLAT
APXLON	236.91	226.02	198.43	133.60	95.22	80.42	APXLON
APXLT	5.279	4.636	2.880	22.642	20.167	19.263	APXLT
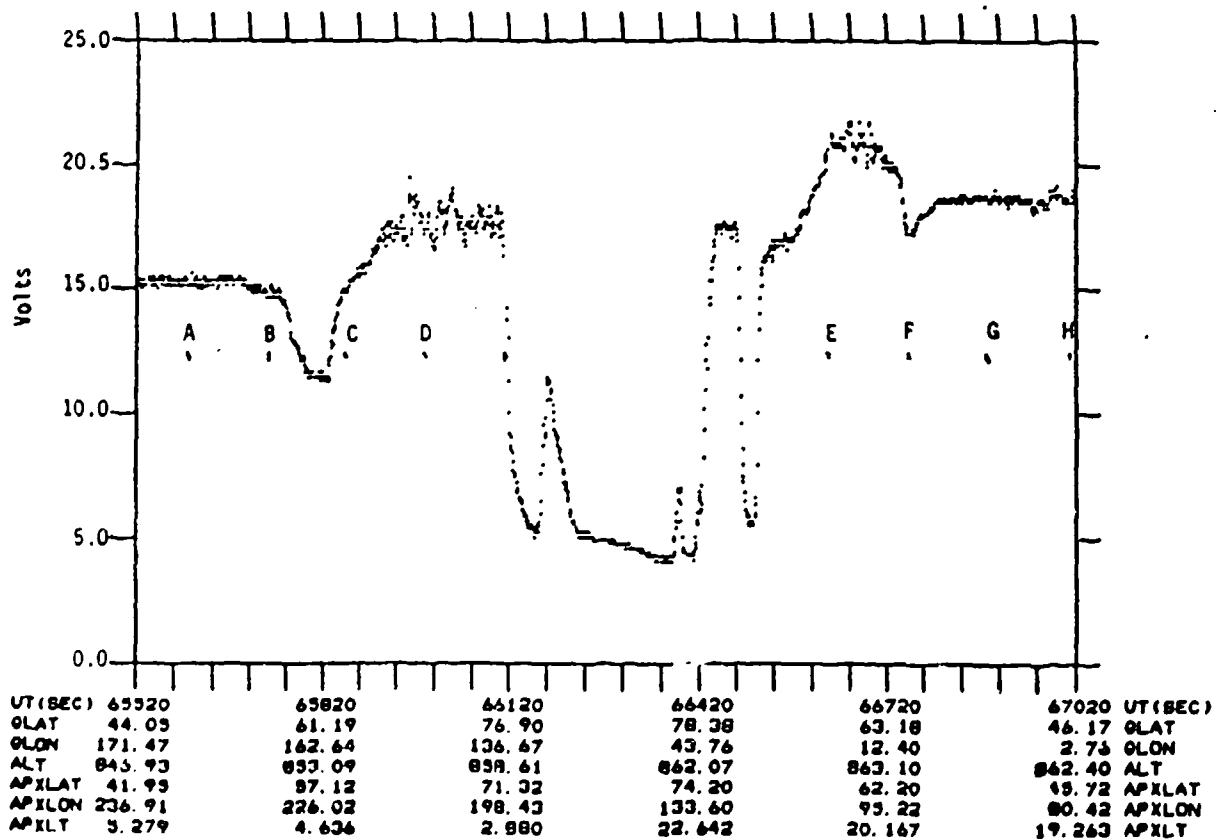
Figure B-02. Voltage on the ion sensor ground-plane as reported by the $V_{bias} + V_{IP}$ data word in the SSIES telemetry data frame. Features marked A, B, etc., are voltage offsets which occur in the first three seconds of the 128-second EP/RPA sweep cycle.

B-3

Expanded plots have been made of 10 seconds of density data for features A, B, and D (Figures B-03 through B-05). When the density is free of irregularities, as in Figures B-03 and B-04, the discontinuity is easy to spot and can be easily "corrected" by shifting the offset data to fit the ends of the non-offset data. When irregularities are present, as in Figure B-05, identifying the problem and then "correcting" it becomes more difficult. We have addressed each case individually, either shifting the data to fit in with the surrounding densities in cases similar to that in Figure B-03 and the first two seconds of the offset in Figure B-04, or removing the data and fitting with a linear interpolation in cases similar to the last second of the offset in Figure B-04 and the entire three-second period in Figure B-05. A list of the changes made is kept for tracking possible effects of the "corrections" on the values calculated for C_k and q.

B.5 Miscellaneous "Odd" Behaviors.

While we encountered a number of "odd" behaviors in the SM density data, only two of them were seen more than once and were odd enough that they appeared to be artifacts of the measurement process rather than a pathological ionospheric behavior. The feature labeled with an "I" in Figure B-01 is shown in an expanded plot in Figure B-06. This sudden drop in voltage from the SM sensor, covering a two-second period, did not correlate with any feature in t ground-plane voltage, nor did it correlate with anything else. Fortunately, this case occurred at a time when the ionosphere was fairly "flat" (i.e., no irregularities), and it was easily patched by a linear interpolation across the offending two-second period.

The raw data list in Figure B-07, however, is indicative of a much larger scale voltage dropout which occurred in a very structured density period. This list includes the time (seconds since midnight), voltage reported for the range data word, twenty-four EL/AMP voltages, and three range flags set by the processing code (RF from the range data, IF from the imbedded range flags, and WF for the wideband ranging amplifier for the SM filter data). The sudden drop starts in the data frame for time 67095 and continues through time 67138 with sporadic normal-appearing readings sprinkled throughout the last 11 seconds of the outage. Nothing can be done with dropouts of this magnitude other than to replace them with a linear interpolation segment so that the detrending process will not be seriously affected. We found three such dropouts in the six partial orbits we processed; none of them, fortunately, in one of the 5-minute analysis periods.
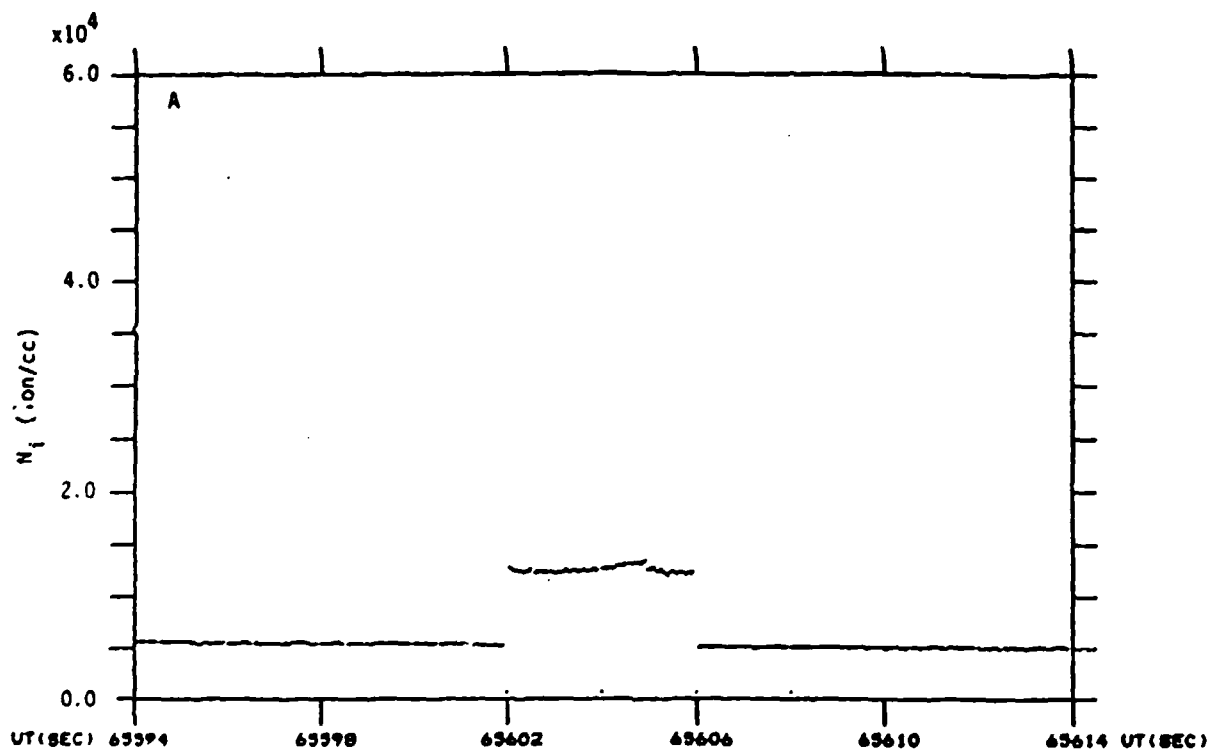
Figure B-03. Expanded plot of the ion density centered on the voltage offset feature labeled A in Figures B-01 and B-02.
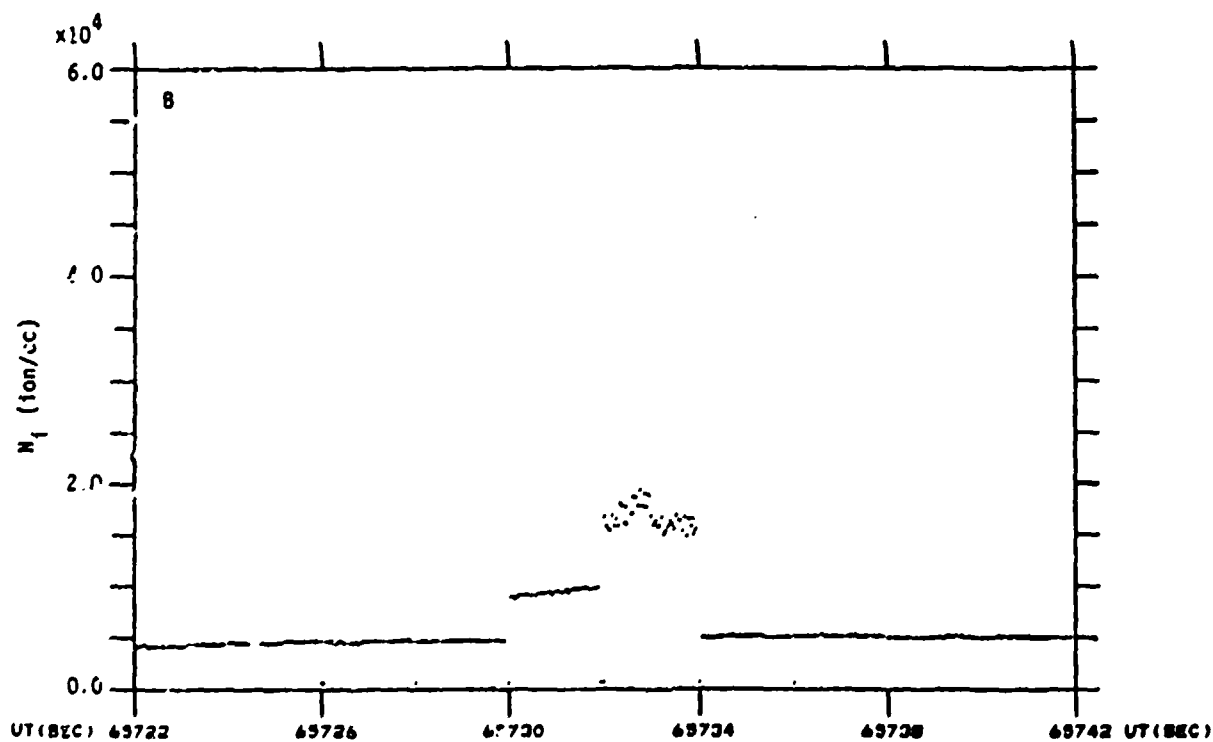

Figure B-04. Expanded plot of the ion density centered on the voltage offset feature labeled B in Figures B-01 and B-02.
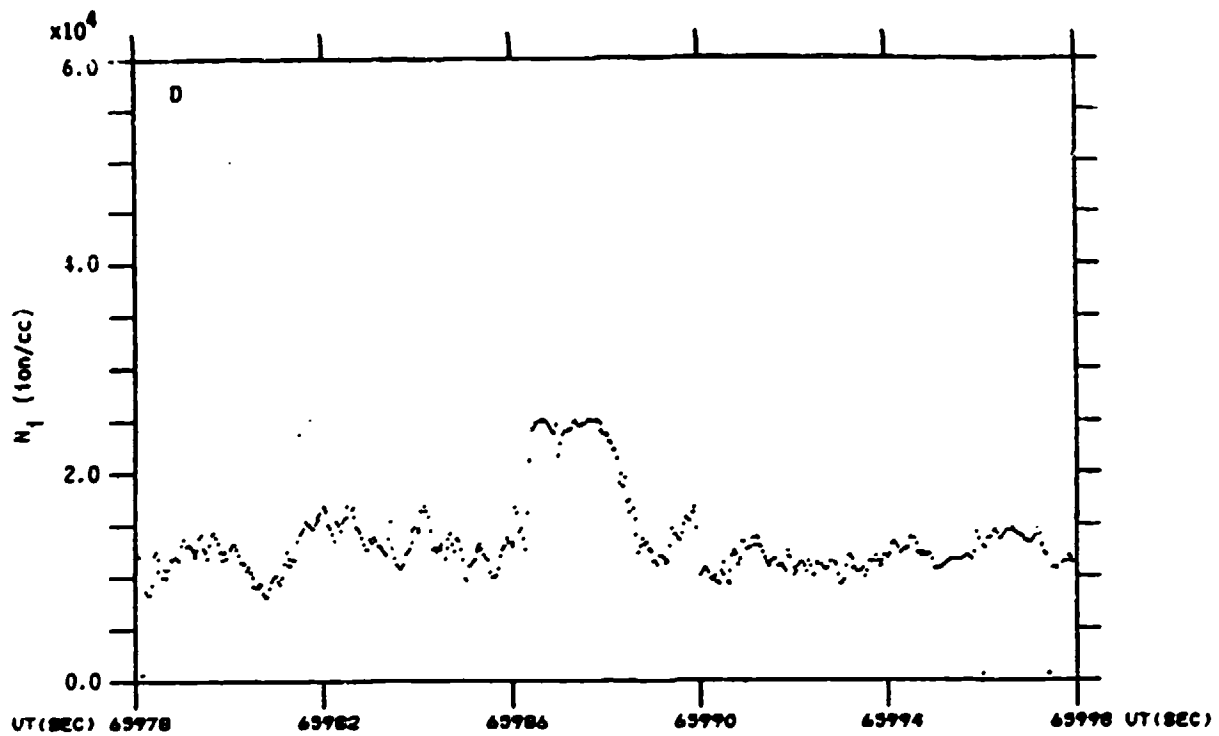
Figure B-05. Expanded plot of the ion density centered on the voltage offset feature labeled D in Figures B-01 and B-02.
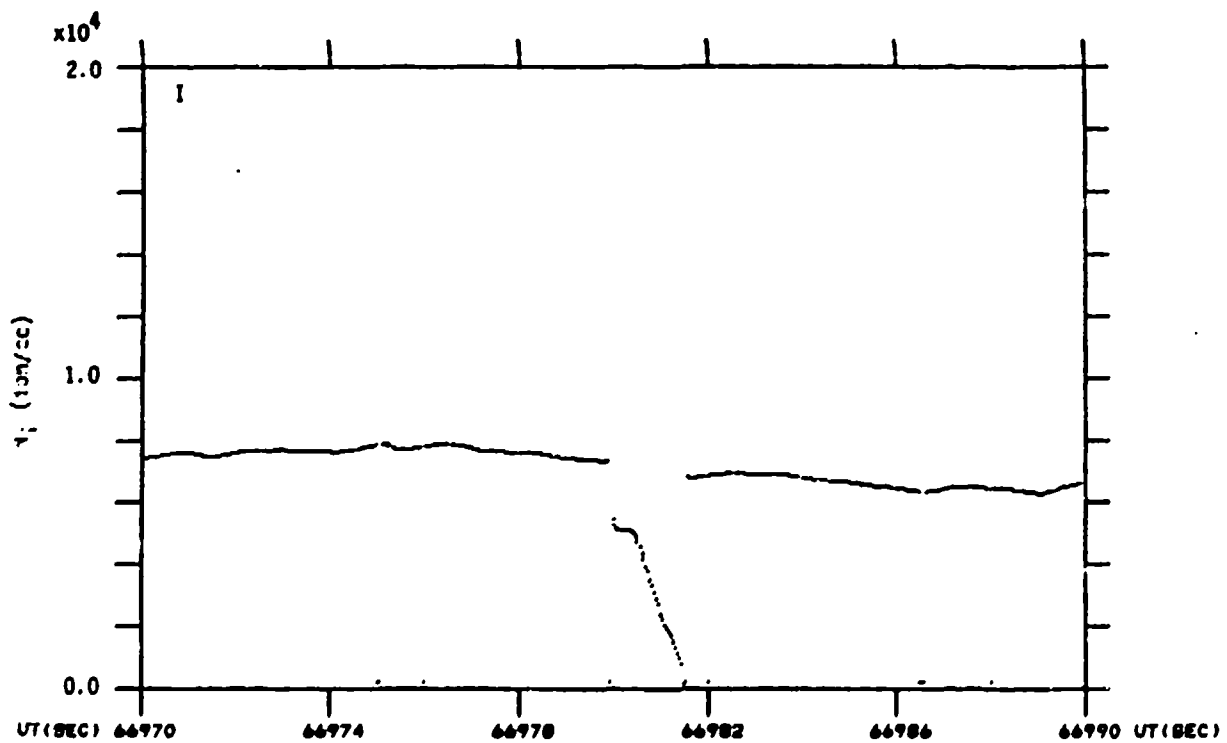

Figure B-06. Expanded plot of the ion density centered on the feature labeled I in Figure B-01.

Figure B-07. Raw SM telemetry data list showing an example of severe data dropout. The column labeled TIME is the time since midnight in seconds, RNG is the value of the range-data word, EL/AMP DATA are the 24 data samples, RF is the EL/AMP range derived from the range data, IF is a range derived from imbedded range flags, and WF is the WIDEBAND range derived from the range data.